JOURNAL OF MADENAT ALELEM COLLEGE

REFEREED SCIENTIFIC JOURNAL Published
by the University College of Madenat al-elem , Iraq , Baghdad , AlKadmyia

Vol:5 No:2 year: 2013 ISSN: 2073-2295

مجلة كلية مدينة العلم
العراق - بغداد - الكاظمية المقدسة
Journal of Madenat Al-elem College
(JMAC)

E-mail: Jmac2009m@yahoo.com
P.O,Box (9216) Tel:5238850
WWW.madenatalelem.com

INSTRUCTIONS to AUTHERS

Journal of Madinat Al-Elem University College publish articles in all fields related to the Academic Departments of the College (Biology, Law, programming Engineering Sciences, and Computer Techniques Engineering).

Written request for publication and signing a consent form to publish must be for articles which have not been published or submitted for publication to other journals. Three copies with CD are needed. Manuscripts should be typed on: A4 white paper, double spaced, written in Times New Roman font size 14. Margins should be 3cm from top, bottom, left and right. The main title should be in: bold Times New Roman font size 14. Author names should be written in the following sequence: first name, middle name, the family name, followed by the names of departments and institutions of work. A footnote accompanies the first page stating the full address of correspondence author.

Articles need to contain the following items:

- Abstract in English and Arabic not more than 300 words.
- Article includes the following items: Introduction, Materials and Methods, Results and Discussion, Conclusion and References.
- References should be numbered in the text according to the sequence appeared in the text and listed in order.
- Tables and figures should be appropriately titled with size not exceed an A4 page.

The editor reserves the right to reject or accept any article submitted.

Contents

Radar Absorbing Material (ram) and its Effects on the Radar Detection Range

Ismail M. Jaber[1] and Huda I. Hammed[2]

[1]University of Madenat AL-Elam

[2]Department of Electrical, College of Engineering, University of AL-Mustansiriya

ABSTRACT

The Radar Cross Section (RCS) has been reduced four techniques: Shaping, Radar Absorbing Material (RAM), Passive cancellation and Active cancellation. The RAM is a technology uses in camouflage application mainly in defense. The aim of this technology based on uses materials able upon absorbing the radar. The material consists of different composites consists of Polyaniline (PANI) Based on Nitrile Rubber (NBR) to produce RAMs. Permittivity of these materials is a fundamental to all other calculation. The calculation by used the cavity perturbation method in the X band (8−12 GHz), then, design four layers of the radar absorbing material backed with PEC (such a structure is typically Radar absorbing material RAS). Main goal of this design is tradeoff between low Reflection coefficients, structure thickness, the obtained results for the RC= −12.2 dB in the 12 GHz.

Keywords: Radar Cross Section (RCS), composites materials, Radar absorbing Material (RAM).

المواد الماصة لأشعة الرادار وتأثيرها على المدى الكشف الراداري

مقطع العرضي للرادار (RCS) يتقلل بالتقنياتِ الأربع: الشكل الهدف، المواد الماصة لأشعة الرادار، إلغاءَ سلبيَ ماديَ وإلغاءَ نشيطَ .المواد الماصة لأشعة الرادار(RAM) هي تقنية مستخدمة في التطبيقات التمويه في الدفاع ،تهدف هذه التقنية اساسا الى استخدام مواد قادرة على امتصاص اشعة الرادار المصطدمة بها. تتكون المواد من مركبات مختلفة تتكون من بولي انيلين (PANI) مستند على مطاط (NBR) التي تنتج المواد الماصة لأشعة الرادار . نفاذية هذه مواد تكون أساسية في كُلّ الحساباتِ الأخرى؛ ومَحْسُوبة بطريقةِ اضطراب التجويفَ للحزمة الترددية (8−12 GHz). التصميم اربع طبقات من المواد الماصة لأشعة الرادارِ دَعمتْ مَع PEC (يدعى تركيب المواد الماصة لأشعة الرادار RAS). الهدف الرئيسي من هذا التصميمِ موازنة بين اقل معامل الانعكاس و سُمك المركب والنَتائِج المكتسبة هي ان (معامل الانعكاس = −12,2 ديسيبل) في 12 GHz.

Introduction

The Radar Cross Section (RCS) is a measure of reflective behavior of a target defined as 4π times the ratio of the scattered power per soiled angle unit in an incident wave plane on the scatter from a specified direction. More precisely, it is the limit of the ratio as the distance from the scattered power is measured approaches infinity,the RCS is denoted by σ [1].

$$\sigma = 4\pi R^2 \frac{|E^{scat}|^2}{|E^{inc}|^2} \dots\dots\dots(1)$$

where E^{scat} is the scattered electric field and E^{inc} is the field incident at the target.

To reduce RCS by used the four techniques: shaping, radar absorbing material (RAM), passive cancellation and active cancellation. In this work, use RAM technique was used to reduce reflection from the target therefore use the composites materials have high dielectric constant is hard to achieve from one component to obtain on combination between the dielectric and mechanical properties.

The conducting polymer such as Polyaniline (PANI) uses as RAM because easy of synthesis, low cost and stability. The conductivity of PANI and low dielectric increases with blended with composites therefore combine with Nitrile rubber (NBR) to get high dielectric constant and improve the mechanical properties. The NBR Similar to natural rubber except for improved resistance to swelling in organic liquids and improved resistance to heat, light, and oxidative aging, Moderate cost [2]. The use of resins or rubber materials is more favorable than using sintered materials, due to flexibility and processiblity. In addition, conducting polymers are not susceptible to correction, like metallic coatings. Conducting blends of PANI with NBR due to the unique mechanical properties of the rubber. The conducting elastomer composites uses as RAM because of the light of weight, anti-correction and flexibility.

$$\varepsilon_r = \varepsilon' - j\,\varepsilon'' \dots\dots\dots\dots\dots(2)$$

The complex permittivity ε_r consists of real part of permittivity (ε'_r) is a measure of how much energy from an external electric field is stored in a material. The imaginary part of permittivity (ε''_r)is called the loss factor and is a measure of how dissipative or lossy a material is to an external electric field. The imaginary part of permittivity is always greater than zero and usually smaller than real part of permittivity. The complex permittivity of theses composites calculation

by means the cavity perturbation method in the X- band (8- 12 GHz). The complex permittivity is a fundamental to the calculation impedance of the composite then calculation the reflection coefficient (RC) from these composites.

Techniques to Reduce RCS

There are four techniques to reduce RCS: shaping, radar absorbing material (RAM), Passive cancellation and active cancellation.

The Shaping involve modifying the external features of the target to reduce the radar returns in a specified (usually the backscatter) direction. In the shaping technique to reduce RCS by the form target is a faceted configuration with flat surfaces to minimize normal reflection return to the radar or the form target must be smooth blended with external geometry to achieve a continuously varying curvature (e.g. Northrop B-2).

Radar absorbing materials (RAM) is to absorb the incident radar energy to minimize the energy scattered back to the radar by absorption. Radar energy is converted the energy incident into heat energy. The RAM can be reducing the radar cross section of other kinds such as ships, and other of the targets. The RAM is the three kinds of materials such as dielectric materials, magnetic materials and hybrid materials uses in the stealth technology. These materials have ability to the absorption energy incident.

Passive cancellation is the basic concept is to design the target surface so that the reflected radar signal from parts of the target cancels the reflected radar signal from another part of the target [3].

Active cancellation- also called active loading, active cancellation is even more ambitious than impedance loading. The basic concept is the target must emit radiation in the same time with incoming pulse whose amplitude and phase cancels the reflected signal. This implies that the target must be smart enough to sense these data are the angle of arrival, intensity, wave from and frequency of the received wave [4].

Composites Preparation

Polyaniline preparation

The PANI was prepared using ammonium peroxydisulfate according to the procedure described [5].

Formulation of the Preparation

The formulation of the preparation Nitrile Rubber/Polyaniline composites in Table (1),

NP series represent PANI with NBR. NP merely symbols represent of the weights of PANI based on 100g of NBR. Phr represent parts of weights to the parts of rubber.

Table (1):- Formulation of the NBR/PANI

phr	NP0	NP1	NP2	NP3
NBR	100	100	100	100
PANI	0	50	100	150

Cavity Perturbation Method

The cavity perturbation method is one of the several methods to calculate complex permittivity of the composites materials at microwave frequency. The cavity perturbation method offers the advantage of relative simplicity, high sensitivity, and requires only a small quantity of the sample [6]. The resonant cavity used for the measurement of the complex permittivity is a rectangular wave-guide cavity with dimensions of 11.5 cm in length, 1.9 cm in width, and 1 cm in the height as shown in fig (1).

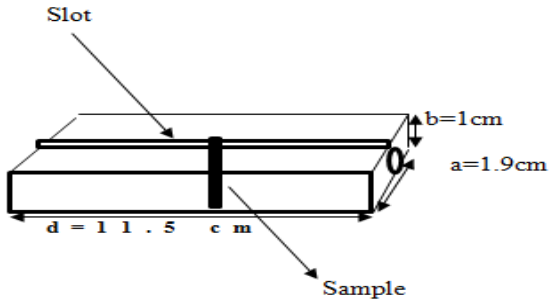

Figure 1. Design layout of the Rectangular cavity, at dimension of the X-band.

For the rectangular cavity, the Transvers Electrical modes (TE_{10N}) (N is an integer) [6] are widely used for the complex permittivity calculation. The sample placed in the position of the maximum electric field when N is odd modes usually to get the maximum electric fields [7]. The specimen position will have to be move with different TE_{10N}modes. The samples in the form of thin rectangular rods, assume the length of which equals the height of the cavity, so that both the ends of the specimen are in contact with the cavity walls, were used. The samples were inserted into the cavity through a slot and positioned at the maximum electric field. Could be excited for operation in four modes (TE_{101} to TE_{107}) and accordingly, four resonant peaks corresponding to theoretical frequencies around 8, 8.8, 10.24, 12 GHz. The real and imaginary parts of the relative complex permittivity are calculated by [7,5].

$$\varepsilon' = \left(\frac{V_C(f_C - f_S)}{2V_C f_S}\right) + 1 \ldots\ldots\ldots\ldots (3)$$

$$\varepsilon'' = \frac{V_C}{4V_S}\left(\frac{1}{Q_S} - \frac{1}{Q_C}\right) \ldots\ldots\ldots\ldots (4)$$

Where f_c and Q_c are resonant frequency and the quality factor of the empty cavity and f_s and Q_s are corresponding for the perturbed case. V_c

is the region enclosed by the cavity, and V_s is the volume of the sample, respectively.

Results and Discussion

Electrical Permittivity

In figures 2 and 3 real and imaginary part of the permittivity of the different loading of the PANI based on NBR is calculated by the cavity perturbation method at various weights of PANI are shown in Table (1). The ε' and ε" increase with increase frequencies and increase with loading of PANI are shown in the same figures. Comparison between this results of the ε' and ε" of the PANI based on Natural Rubber (NR) exits the ε' and ε" of NBR/PANI is higher than the results of the PANI based on NR [8].

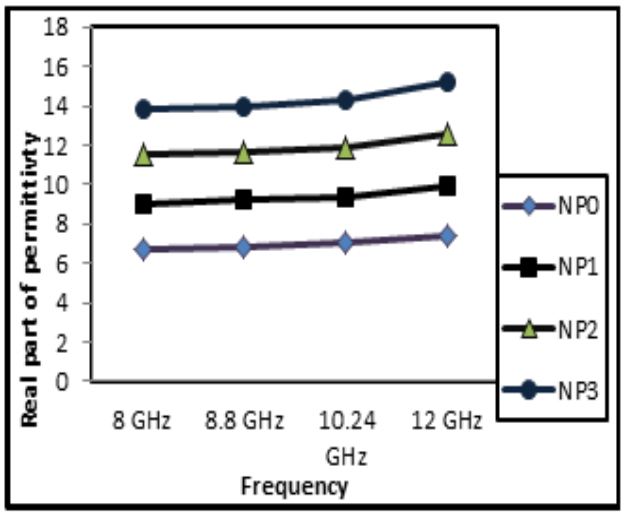

Figure 2. Real part of the NBR/PANI CPCs.

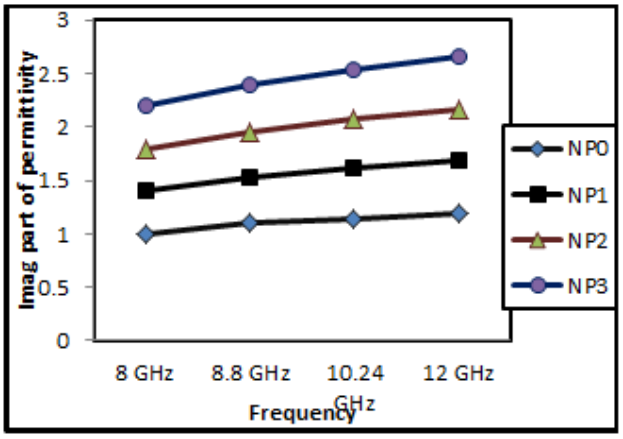

Figure 3. Imaginary part of the NBR/PANI CPCs.

Composite intrinsic wave impedance

For the transversal electromagnetic (TEM) wave propagating in a dielectric material, denoted with k index, the wave impedance η is express by the equation [9, 10].

$$\eta_k = \sqrt{\frac{\mu_k}{\varepsilon_k}} = \sqrt{\frac{\mu_\circ \mu_r}{\varepsilon_\circ \varepsilon_r}} = \sqrt{\frac{\mu_\circ}{\varepsilon_\circ}} \sqrt{\frac{\mu_r}{\varepsilon' - j\varepsilon''}} \dots\dots\dots (5)$$

Where $\mu_\circ$ is the permeability of free space $(4\pi * 10^{-7}\ H/m)$ [9] and μ_r is the relative permeability of the material and equal 1 for the dielectric materials. $\varepsilon_\circ$ is the free space permittivity $(8.854 \times 10^{-12}$ F/Hz) and ε_r is the relative permittivity of the material. Since dielectric permittivity is a function of frequency, the microwave intrinsic impedance of the composites material depends on frequency, and its value is in general complex number. In figure (4) PANI based NBR composites

intrinsic X-band microwave impedance modules are shown. It is evident that PANI based NBR show the lowest wave impedance values. The intrinsic wave impedance decreases with increases frequencies and increase the complex permittivity of the NBR/PANI composite.

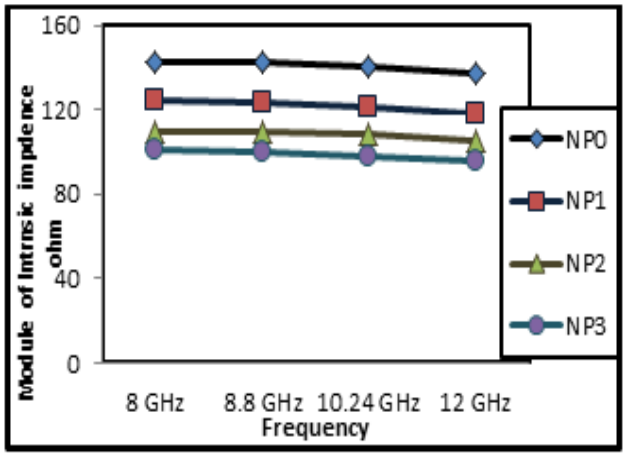

Figure 4. Microwave impedance module of for different loading of NBR/PANI in the X-band.

Numerical analysis for obtaining design solutions

Where the mathematical model to use in the subsequent, the results obtained for the real and imaginary parts of NBR/PANI CPCs and the microwave characteristic impedance will be used in order to design a multilayer system capable to minimize the reflection of an incident electromagnetic wave.

Single layer microwave absorbing structure simulation

A normal incident electromagnetic field; has been assumed, then design single layer of the NBR/PANI composites is attached on a PEC plate, as depicted in figure 5. In order to neglect border effects and the calculated Reflection Coefficient (RC) at the air-composite material layer interface by use the transmission line theory.

$$RC = 20\log_{10}\left|\frac{Z_i - Z_\circ}{Z_i + Z_\circ}\right| \ldots (6)$$

RC is the reflection coefficient (dB) at the single layer, $Z_\circ = \sqrt{\frac{\mu_\circ}{\varepsilon_\circ}} \cong 377\Omega$ is the free space impedance, and Z_i is the input impedance at the air- absorber interface. This latter can be expressed by:

$$Z_i = \eta_k \frac{Z_L \cos(\beta t) + j\eta_k \sin(\beta t)}{\eta_k \cos(\beta t) + jZ_L \sin(\beta t)} \ldots\ldots (7)$$

Where t is the thickness of the absorber layer in **m**, and the propagation number β is given by:

$$\beta = 2\pi f\sqrt{\mu_\circ \varepsilon_\circ}\sqrt{\mu_r \varepsilon_r} = \sqrt{\varepsilon' - j\varepsilon''} \ldots (8)$$

Where f is the frequency of the incident electromagnetic wave in Hz and η_k is the

intrinsic wave impedances of the **xth** material have been compute using the equation (5).

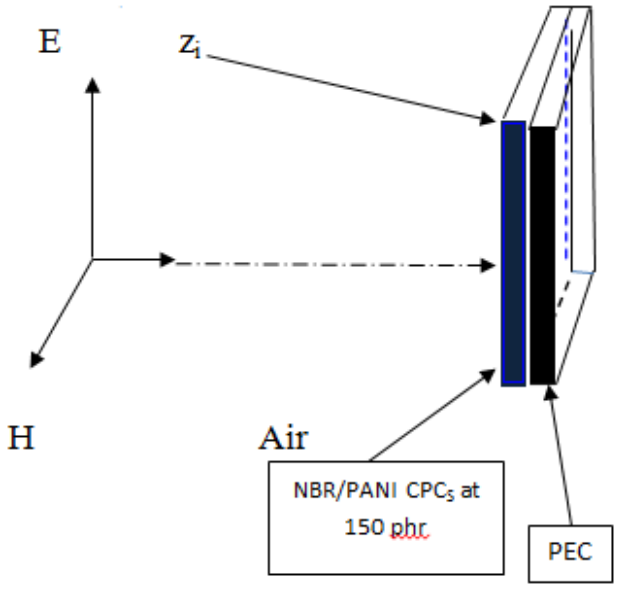

Figure 5. Microwave single layer absorber scheme.

The absorption capability of a "thin" layer is mainly due to both dielectric losses within the material and impedance matching condition. The dielectric losses are mainly function of the imaginary part of the permittivity, while the matching conditions are to be study by taking into account the microwave wavelength. From the Eq. (7) it is possible to observe that the imaginary part of Z_i vanishes for certain multiple values of the quantity βt. This route can evaluate the RC module: from figure 6 show the reflection coefficient of the NBR/PANI composite structure reaches when reflection coefficient −2.2 dB of frequency 12 GHz.

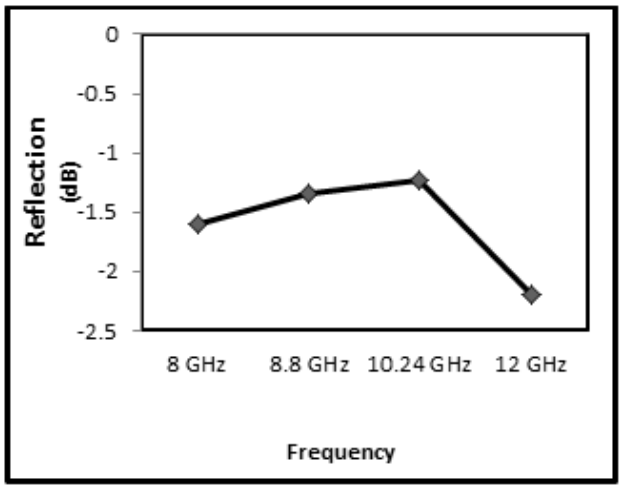

Figure 6. Module of single layer RAM structure reflection coefficient when the thickness layer =4mm.

Four Microwave Absorbing layers structure

Let us suppose a multilayer RAM structure made of four layers of composite material backed with a PEC layer, as depicted in figure 7. Using Eq. (7) iteratively, we can find the corresponding input impedance at each layer interface; by this way, we contemporary take into account of the other layers, which in turn become the new load impedances. The several input impedances are then expressed by:

$$Zi_1 = \eta_1 \frac{Z_{PEC}\cos(\beta_1 t_1)+j\eta_1 \sin(\beta_1 t_1)}{\eta_1 \cos(\beta_1 t_1)+jZ_{PEC}\sin(\beta_1 t_1)}$$

$$Zi_2 = \eta_2 \frac{Zi_1 \cos(\beta_2 t_2) + j\eta_2 \sin(\beta_2 t_2)}{\eta_2 \cos(\beta_2 t_2) + j\, zi_1 \sin(\beta_2 t_2)}$$

$$Zi_3 = \eta_3 \frac{Zi_2 \cos(\beta_3 t_3) + j\eta_3 \sin(\beta_3 t_3)}{\eta_3 \cos(\beta_3 t_3) + j\, zi_2 \sin(\beta_3 t_3)} \quad \ldots . (9)$$

$$Zi_4 = \eta_4 \frac{Zi_3 \cos(\beta_4 t_4) + j\eta_4 \sin(\beta_4 t_4)}{\eta_4 \cos(\beta_4 t_4) + jzi_3 \sin(\beta_4 t_4)}$$

In addition, the resulting impedance matching condition between free space and RAM structure is RC at the four layers.

$$RC = 20\log_{10}\left|\frac{Zi_4 - Z_\circ}{Zi_4 + Z_\circ}\right| \ldots \ldots . (10)$$

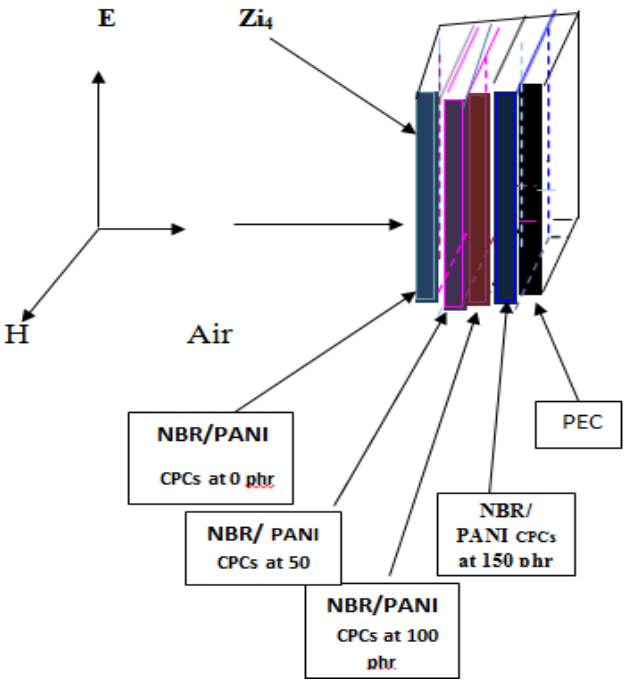

Figure 7. Four microwave absorbers layers scheme.

Let us suppose the following materials and thickness, as shown in figure 7.

-layer one: NBR/PANI 0phr 1mm.

-layer two: NBR/PANI 50phr 2mm.

-layer three: NBR/PANI 100phr 2mm.

-layer four: NBR/PANI 150phr 4mm.

The final RAM reflection coefficient is plotted in figure 8. It can be noticed that the lower RC of the NBR/PANI composites at low loading and thickness.

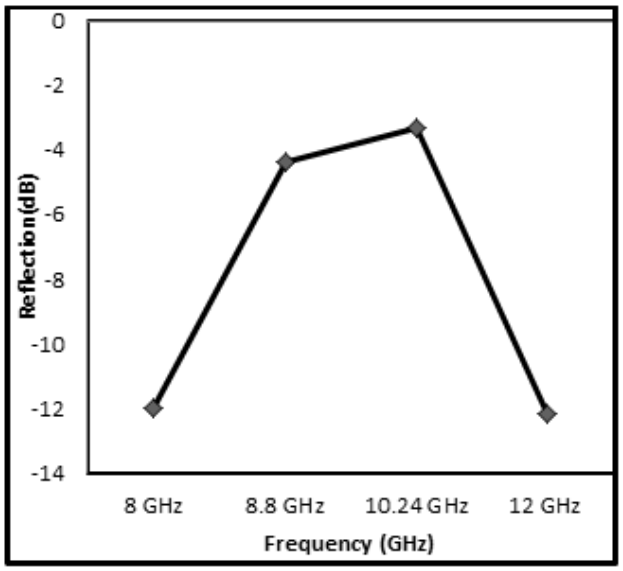

Figure 7. Module of four-layer RAM structure reflection coefficient at the X-band.

Conclusion

The uses NBR/PANI composites as radar absorbing materials (RAM) analysis in the X-band with simulation of RAM structure based on the calculated quantities. The complex permittivity of NBR/PANI computed by used the cavity perturbation method at (8-12 GHz). The results obtained the real and imaginary parts of the NBR/PANI composites increases with increased frequency and loading of PANI. At **12** GHz it is obtained (**ε'=7.4**) when 0phr then (**ε'=15.2**) at 150phr at the same frequency. The intrinsic wave impedance of NBR/PANI is calculated in the X-band and it is evident the intrinsic wave decrease with increase complex permittivity of NBR/PANI. In order to design a microwave RAM structure composed of four layers of conducting composite backed with a PEC. The absorption properties have been evaluated using the microwave reflection coefficient at the air- four layers RAM interface. The results obtained show the low **RC** (- **12.2 dB**) at the **12** GHz in the four layers is better from **RC**=- **2.2 dB** in the single layer RAM structure at the same frequency.

References

1. R.S. Biscaro, E. L. Nohara, G. G. Peixoto, R. Faez, M.C. Rezende. (2003). performance Evaluation of Conducting Polymer Paints as Radar Absorbing Materials (RAM)", Proceedings SBMO/IEEE MTT-S IMOC PP. 355-358.

2. A. K. Sen, M. Tech, Ph.D. thesis. (2001). Coated Textiles: Principles and Applications. Technomic Publishing Company.

3. I.Nicolaescu. (2006). Radar Absorbing Materials used for Target Camouflage. Journal of optoelectronics and advanced materials, vol.8, No. 1, PP. 333-338.

4. Eugene. F. Knott, (2004). Radar Cross Section. 2nd edition, SciTech Publishing, Inc.

5. R. B.Yang, W.F. Liang, W. S. Lin, H. M. Lin, C. Y. Tsay, C. K. Lin. (2011). Microwave absorbing properties of iron nanowires at x-band frequencies. Journal of Applied Physics, No. 109, PP.507-527.

6. J. Sheen. (2007). Amendment of cavity perturbation technique for loss tangent measurement at microwave frequencies. Journal of Applied Physics, No. 102, PP. 014102.

7. R. B. Yang, C.Y. Tsay, D. S. Hung, W. F. Liang, Y. D. Yao, C. K. Lin. (2009). Complex permittivity and permeability of iron-based composite absorbers measured by cavity

perturbation method in x-band frequency range. Journal of Applied Physics, 105, 07A528.

8. H. John, R. Joseph. K. T. Mathew. (2007). Dielectric Behavior of Natural Rubber Composites in Microwave Fields. Journal of Applied Polymer Science, Vol. 103, PP. 2682-2686.

9. D. Micheli, C. Apollo, R. Pastore, M. Marchetti. (2010). X-band microwave characterization of carbon-based nanocomposite material, absorption capability comparison and RAS design simulation. Composites Science and Technolgy, No. 70, PP. 400-409.

10. D. Micheli, R. Pastore, C. Apollo, M. Marchetti, G. Gradoni, F. Moglie, V. M. Primiani. (2009). Carbon based nanomaterial composites in RAM and microwave shielding applications. 9th IEEE Conference on Nanotechnology , 978-981-08-3694-8 (RPS), PP. 226- 235.

Study Performance of the Fiber Bragg Grating as a Dispersion Compensator an Optical Transmission System Using Optisystem Software

Ali Mahdi Hummadi
College of Electrical and Electronic Techniques
E.mail: dralioptic@gmail.com

Abstract

This paper presents the design and simulation of an optical transmission system in optical fiber. Optical fiber is one of the most important communications media in communication system. Due to its versatile advantages and negligible transmission loss it is used in high speed data transmission. Although optical fiber communication has a lot of advantages, dispersion is the main performance limiting factor. There are various types of optical fiber, the Fiber Bragg Grating (FBG) is commonly chosen as important components to compensate the dispersion in optical communication system. Because the low cost of filter for wavelength selection and low insertion loss, it has also customized reflection spectrum and wide bandwidth. The simulation of transmission system will be analyzed based on different parameters by using OptiSystem simulator. By simulating a model of communication system and using the most suitable settings of the system which include input power (dBm), fiber cable length (km) and attenuation coefficient (dB/km) at cable section, there are three different parameters will be investigated, which are Signal power (dBm), Noise power (dBm), output power (Watt), at receiver.

Keywords: Optisystem simulator, parameters, Optical Transmission System Fiber Bragg Grating (FBG).

دراسة وضائف FBG كمعوض للتشتت في نظام الاتصالات الضوئية باستخدام برنامج Optisystem

د. علي مهدي حمادي

مدرس في كلية التقنيات الكهربائية والاليكترونية

الخلاصة

تم في هذا البحث تصميم محاكاة لنظام البث البصري في الألياف البصرية . ان الألياف البصرية هي واحدة من وسائل الاتصال الأكثر أهمية في نظام الاتصالات.وذلك لمتلاك الألياف البصرية مزايا عديدة ومنها خسارة الإرسال ضئيلة لذلك يتم استخدامه في نقل البيانات عالية السرعة. ، والتشتت هو العامل الرئيسي الذي يحد الأداء. هناك أنواع مختلفة من الألياف البصرية، ومنها المشابك براج الألياف (FBG) يتم اختيارة عادة لكونة احد العناصر المهمة لتعويض التشتت في نظام الاتصالات البصرية.واهم مزاياة لديه مرشح منخفض التكلفة لاختيار الطول الموجي وانخفاض خسارة الإدراج، وله طيف منعكس وعرض النطاق الترددي واسع وسوف يتم تحليل محاكاة لنظام الاتصالات استنادا إلى معايير مختلفة باستخدام Optisystem simulator. من خلال محاكاة نموذج لنظام الاتصالات البصرية وباستخدام الإعدادات الأنسب للنظام والتي تشمل مدخلات الطاقة (ديسيبل)، وطول الكيبل البصري (كم) ومعامل التوهين (ديسيبل / كم) الخاص بالليف البصري، وتم في هذا البحث حساب ثلاث معلمات مختلفة وتشمل كلا من طاقة إلاشارة (ديسيبل)، طاقة الضوضاء (ديسيبل) والطاقة الخارجة (واط) عند المستلم.

Introduction

Fiber optics is a medium for carrying information from one point to another in the form of light. Unlike, the copper form of transmission, fiber optics is not electrical in nature. A basic fiber optic system consists of a transmitting device that converts an electrical signal into a light signal, an optical fiber cable that carries the light, and a receiver that accepts the light signal and converts it back into an electrical signal [1]. Fiber Bragg Gratings (FBG) is added for the design of Optical Transmission System. Fiber Bragg gratings have many applications in fiber optical telecommunication systems such as dispersion compensation, gain flattering for EFDAs, Raman amplifiers and add/drop multiplexers and in fiber grating sensors and pulse shaping in fiber lasers. Combining, controlling and routing light are three main uses of FBGs in the optical communications [2]. They are also stimulating growth in fiber optic applications outside of telecommunications, such as nonlinear frequency conversion, spectroscopy, and remote sensing [3].

Optisystem is an innovative optical communication system simulation package that designs tests, and optimizes virtually any type of optical link in the physical layer of a broad spectrum of optical networks, from analog video broadcasting systems to intercontinental backbones. Optisystem is a stand-alone product that does not rely on other simulation frameworks. It is a system level simulator based on the realistic modeling of fiber-optic communication systems. It possesses a powerful new simulation environment and a truly hierarchical definition of components and systems. Its capabilities can be extended easily with the addition of user components, and can be seamlessly interfaced to a wide range of tools [4].

In this study, the simulation of the optical transmission system in optical fiber has been discussed by analyzing the effect of the components in data receiver by using different parameters setting. The value of parameters has been investigated such as Signal power (dBm), Noise power (dBm), output power (Watt), at receiver.

Background theory

Fiber optics is a medium for carrying information from one point to another in the form of light. Unlike the copper form of transmission, fiber optics is not electrical in nature. A basic fiber optic system consists of a transmitting device, which generates the light signal; an optical fiber cable, which carries the light; and a receiver, which accepts the light signal transmitted. The fiber itself is passive and does not contain any active, generative properties. This principle is shown in figure 1 [5].

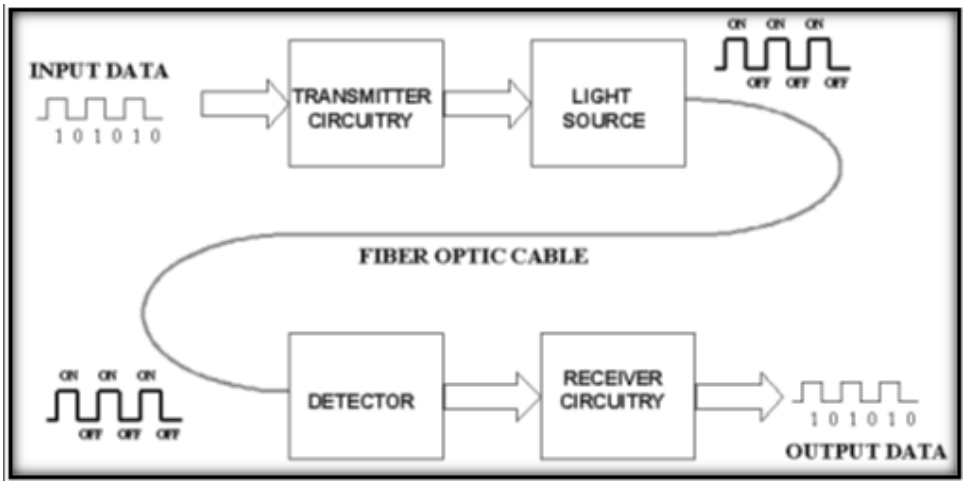

Figure 1. Basic fiber optic communication system [1].

A. Fiber Bragg Grating (FBG)

Fiber Bragg Grating (FBG) has the advantages of a simple structure, low insertion loss, high wavelength selectivity, polarization insensitivity and full compatibility with general single mode communication optical fibers [6]. Fiber Bragg gratings reflect a narrow spectral part of light that is guided in the optical fiber core at the Bragg wavelength, which is dependent on the fiber grating period and the refractive index of the optical fiber. FBG is one mode that will be presented basic periodic pattern intense UV. This leads to increased exposure of the refractive index, and thus the refractive index is increased permanently. Then the exposure pattern formation will be created called fixed index grating. When a light source is supplied to the FBG, only a narrow range of light wavelengths corresponding to the Bragg wavelength will be reflected, transmitting this spectral data to the attached FBG spectrum analyzer. All other wavelengths will partially reflect at tiny index variations and interfere destructively, causing those wavelengths to be transmitted. This principle is shown in figure 2 [7].

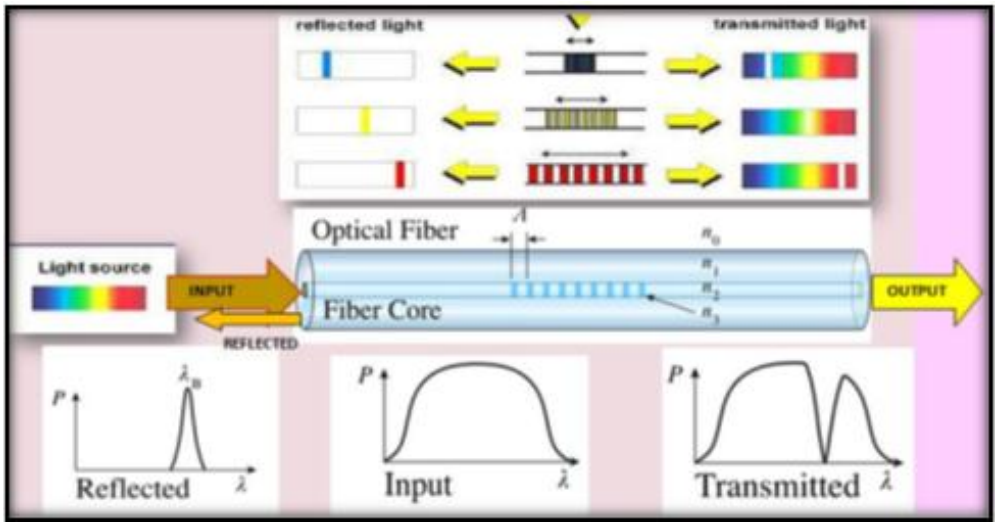

Figure 2. The principle of Bragg's light.

B. Description of Components and consideration

The system is operated with the basic optical communication which consists of a transmitter, transmission link and a receiver. The system transmits information using optical carrier wave from transmitter to receiver via optical fiber.

Figure 3 shows the layout parameters. From Optisystem 7.0, the components used in it are shown in below.

1. Pseudo–Random Bit to generate sequence random bits (0 or 1).
2. NRZ pulse generator has an advantage on controlling bandwidth. This is due to the characteristic of the generator that the returning signals to zero between bits. Pseudo–random bit sequence generator is used to scramble data signal in terms of bit rates [8].
3. Mach Zender– Modulator (MZ) has two inputs (optical signal and electrical signal) and one output (optical). Then the input signal is modulated with semiconductor laser that is represented by Continuous Wave (CW) laser through Mach–Zehnder modulator.
4. Continues laser diode (CW) to generate optical signals supplies input signal with 1550 nm wavelength and input power of 5dBm which is externally modulated at 10 Gbits/s. with a non–return–zero (NRZ) pseudorandom binary sequence in a Mach–Zehnder modulator with 30 dB of extinction ratio.

5. The optical fiber used is single mode fiber because single mode fiber has higher data rate, less dispersion therefore operate in long haul distance, so it is suitable to be used as transmission link.
6. The fiber Bragg grating which use as the dispersion compensator. The length grating that will be used is 6 mm since the most proper length for proposed model is equal to l = 6 mm by try and error method [9].
7. Fiber amplifier (EDFA). Optical amplification is required to overcome the fiber loss and also to amplify the signal before receive by Photo detector PIN at the receiver part.
8. Photodetector Diode Positive Intrinsic Negative (PIN) to translate the optical signal into an electrical signal. One photon yields one electron [10].
9. Optical Spectrum Analyzer (OSA), to monitoring output signals after each component.

The initial settings for the design are shown in Figure 3 order to operate as the optical transmission system: Input power 5dBm, frequency at transmitter 1550nm, fiber length 5km, Attenuation coefficient at cable section 0.2dB/km.

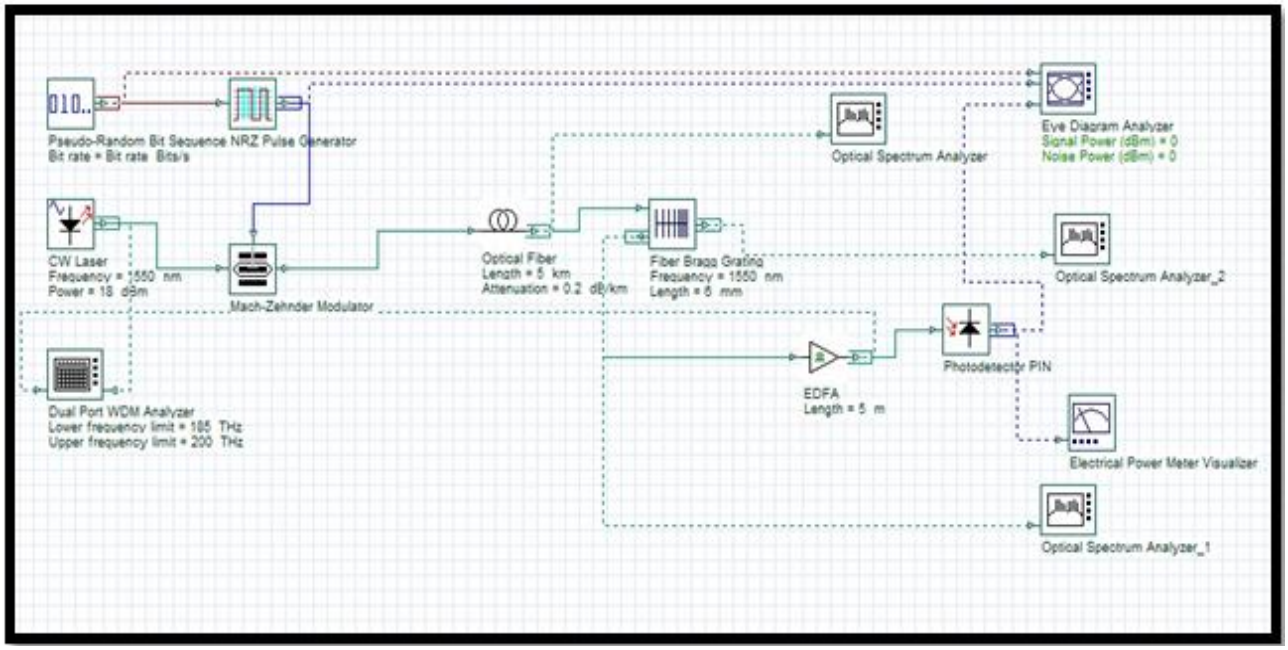

Figure 3. The designed model of simulated system with Optisystem software.

Results and Discussion

The simulation and optimization of the design is done by Optisystem 7.0 simulation software. The eye diagrams and results of output power, Signal power (dBm) at receiver, noise power are tabulated into figure 4 until figure 11 by using different values of input power (dBm), attenuation coefficient (dB/km), and variable length of FBG (mm). The related graphs are also plotted as shown in figures 6, 9 and 11.

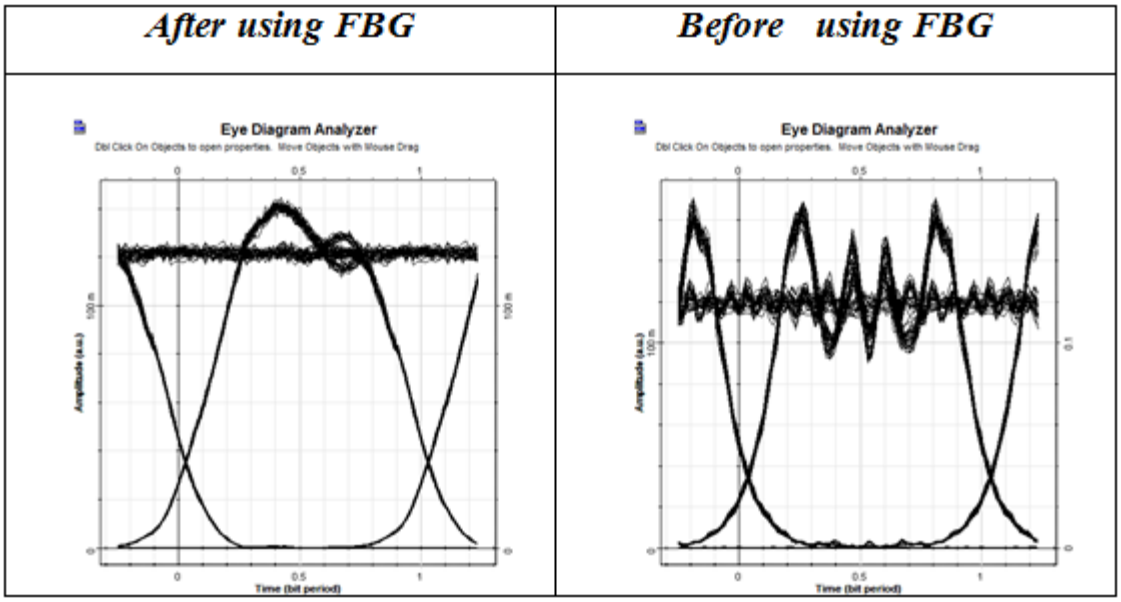

Figure 4. The differences of the eye diagram for the design with and without using Fiber Bragg Grating.

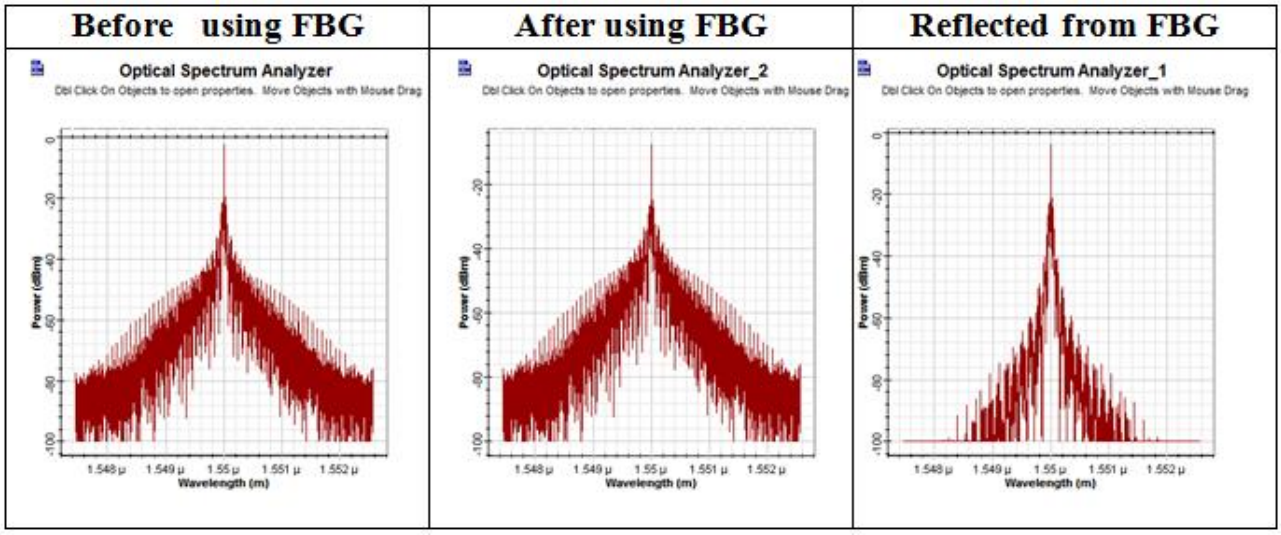

Figure 5. The output readings are measured by Optical power meter with(Transmitted and Reflected) and without using Fiber Bragg Grating.

Table 1. The output readings are measured by varying the fiber bragg grating.

Length (mm)	Signal Power (dBm)	Noise Power (dBm)	Output power (mw)
1	5.73945	-21.6174	3.775
2	7.35215	-25.8324	5.438
3	7.74958	-28.3721	5.957
4	7.93449	-29.9351	6.216
5	8.04336	-30.9361	6.374
6	8.11548	-31.5858	6.48

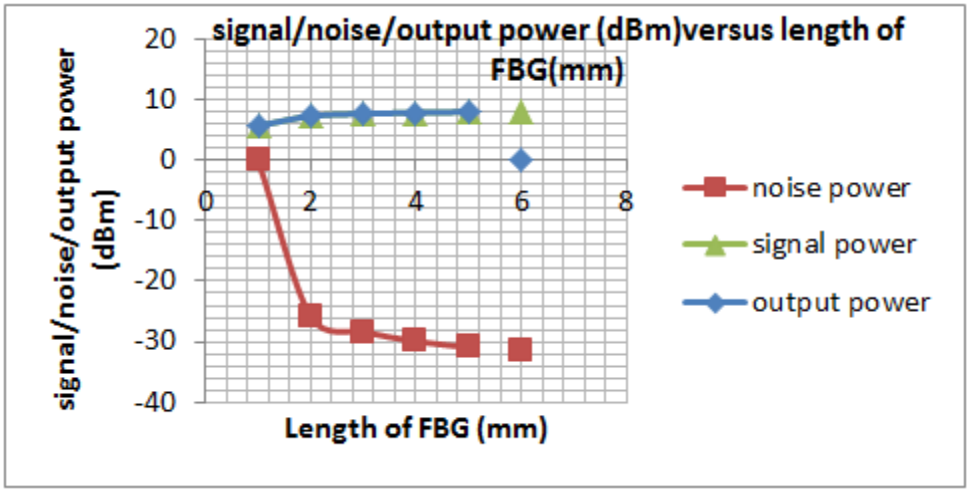

Figure 6. Graph of Signal/noise/output power figure versus length of FBG.

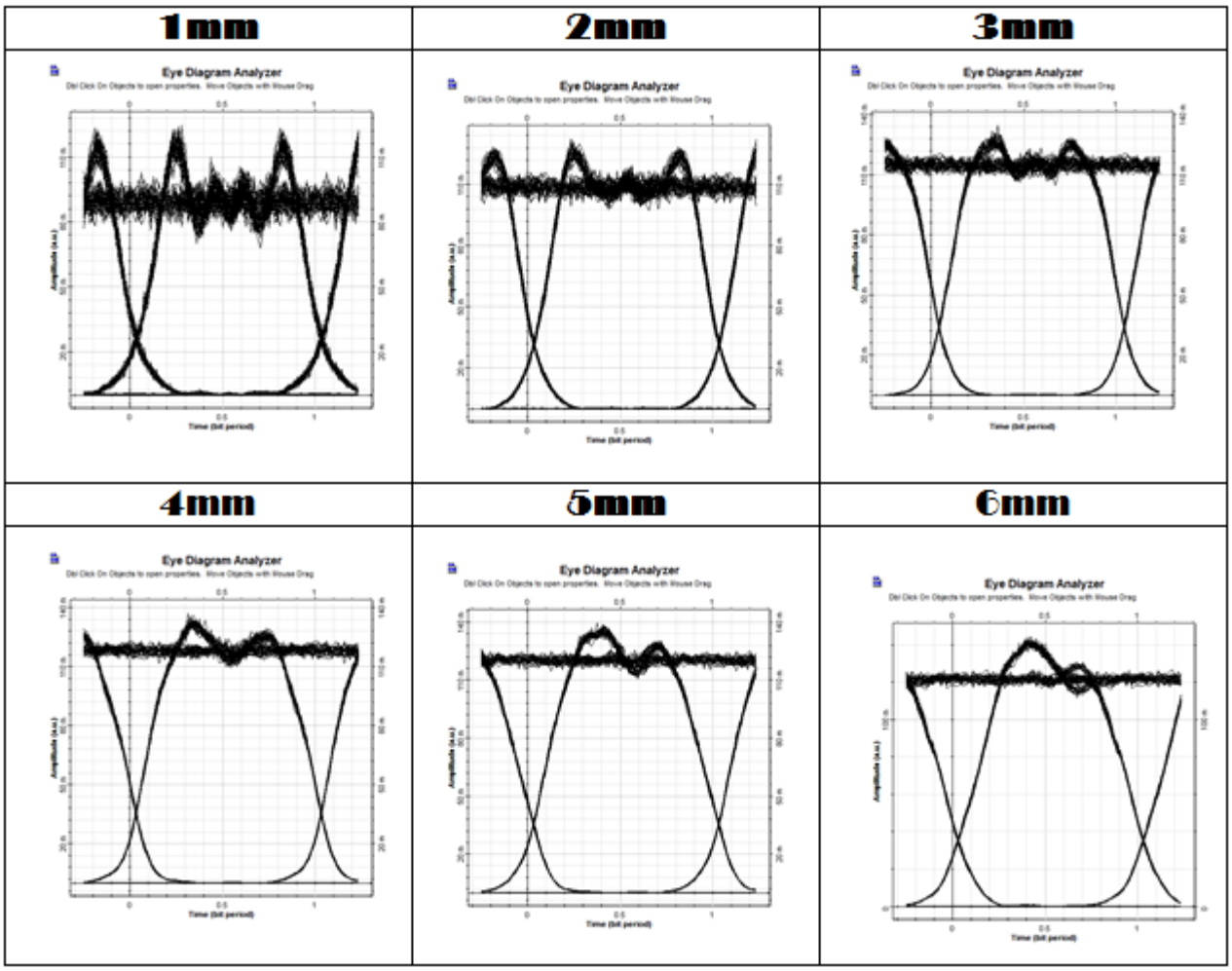

Figure 7. Eye diagrams are analyzed by using different values of fiber bragg grating.

Table 2: The output readings are tabulated by varying the input power.

Input Power (dBm)	Signal Power (dBm)	Noise Power (dBm)	Output power (mw)
1	7.7409	-28.123	5.945
5	8.11548	-31.5858	6.48
10	8.58785	-35.5157	7.224
15	9.48629	-38.3241	8.885
20	11.6114	-39.276	14.493

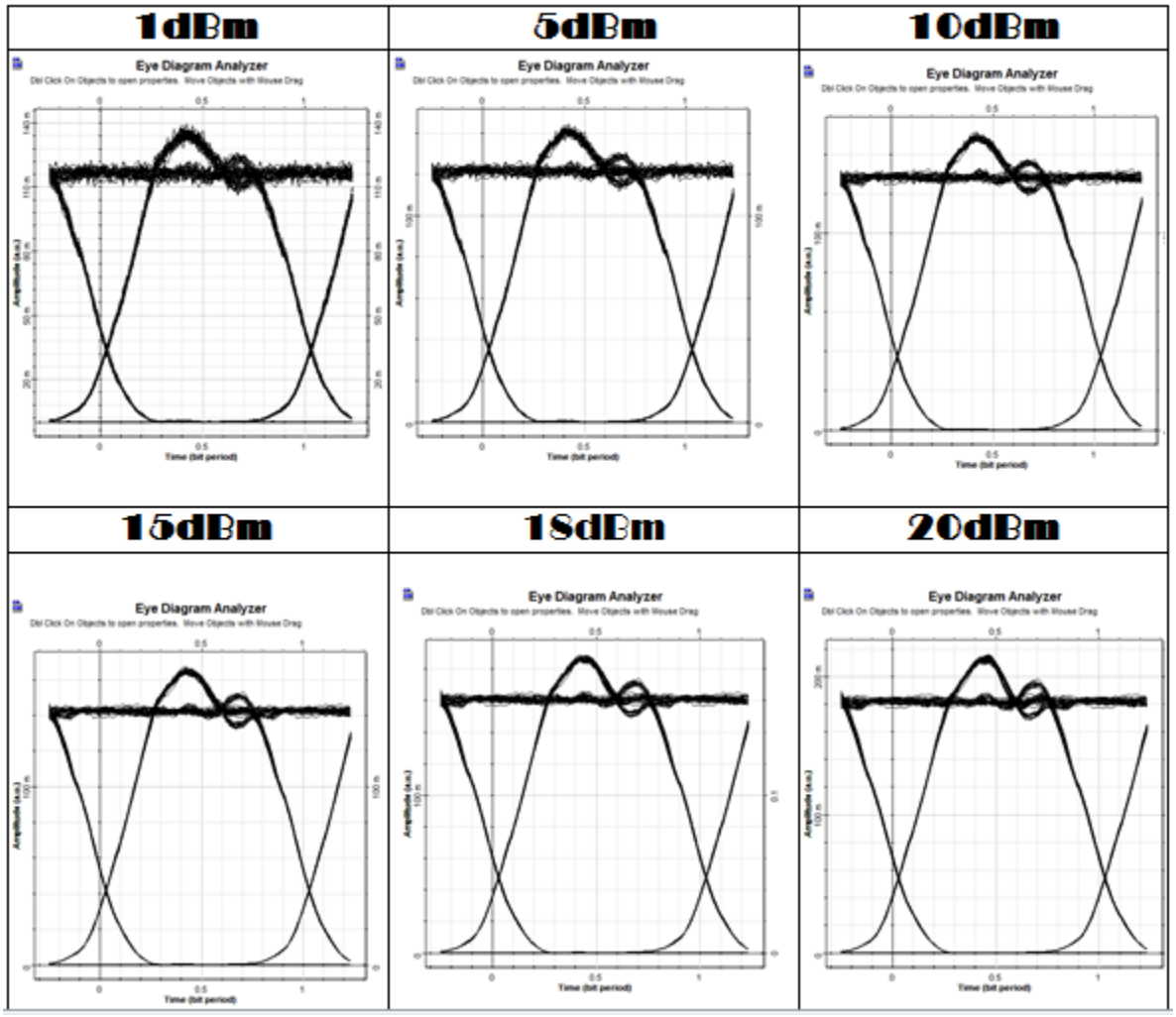

Figure 8. Eye diagrams are analyzed by using different values of input power.

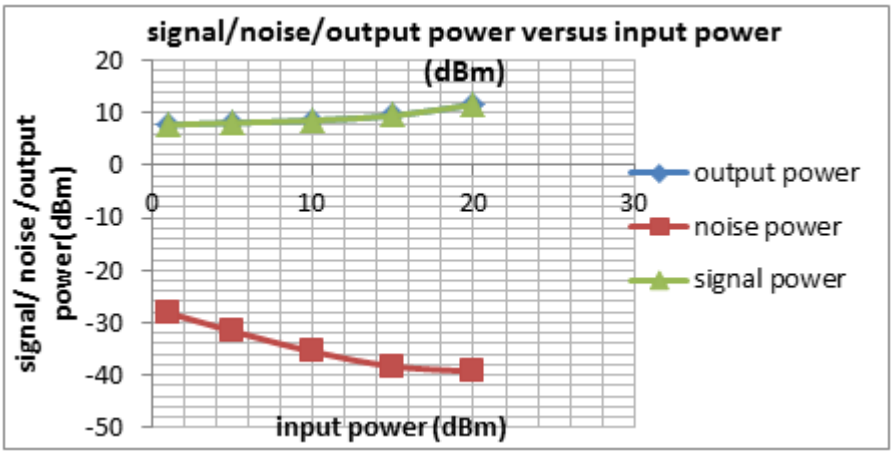

Figure 9. Graph of signal/noise and output power figure versus input power.

Table 3. The output readings are obtained by varying the attenuation coefficient at cable section.

Attenuation Coefficient (dB/Km)	Signal Power (dBm)	Noise Power (dBm)	Output power (mw)
1	7.74082	-28.1233	5.945
3	4.85972	-20.704	3.070
5	-6.5435	-21.1503	0.229
7	-24.987	-26.7976	0.00526

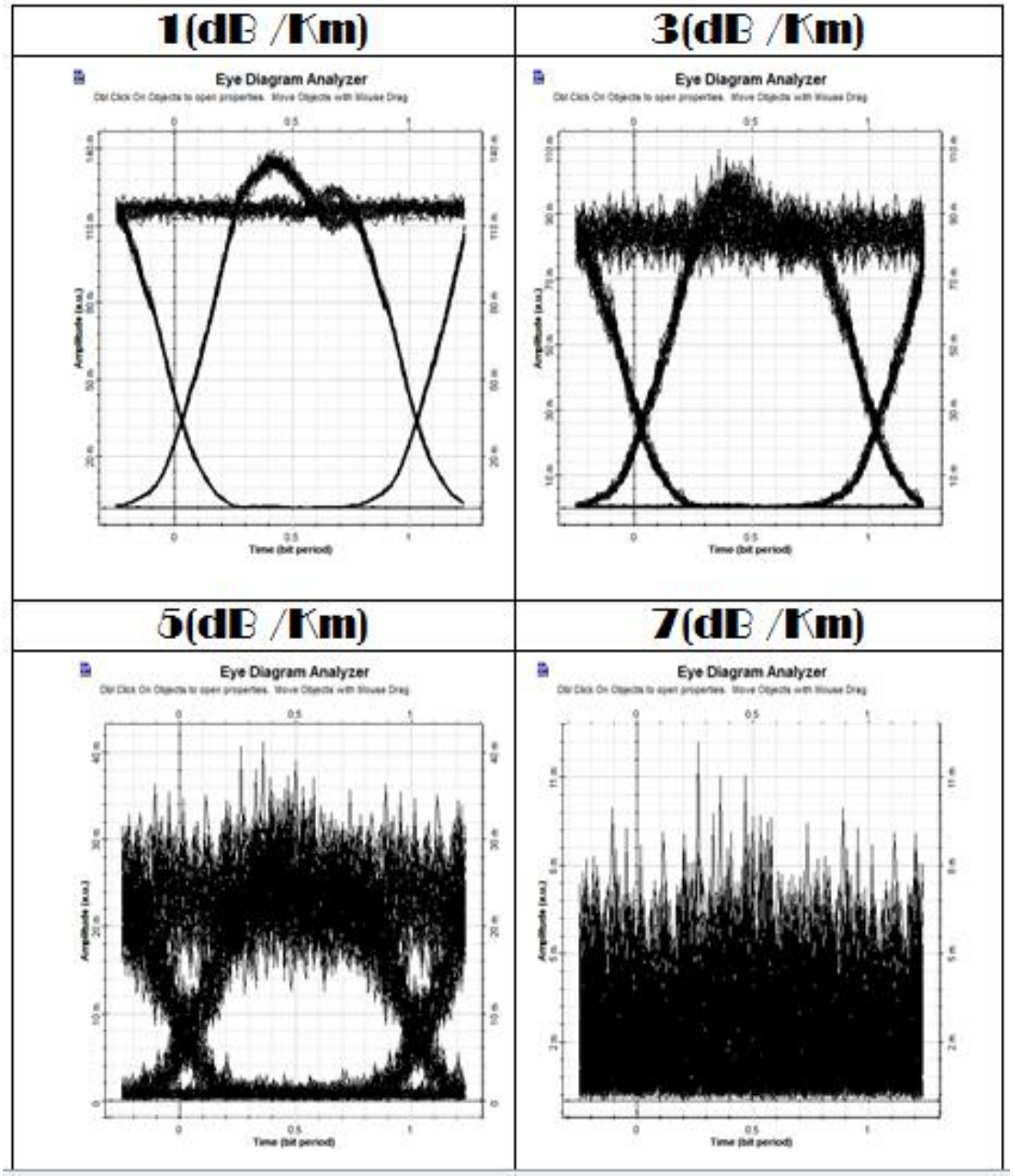

Figure 10. Eye diagrams are analyzed by using different values of attenuation coefficient at cable section.

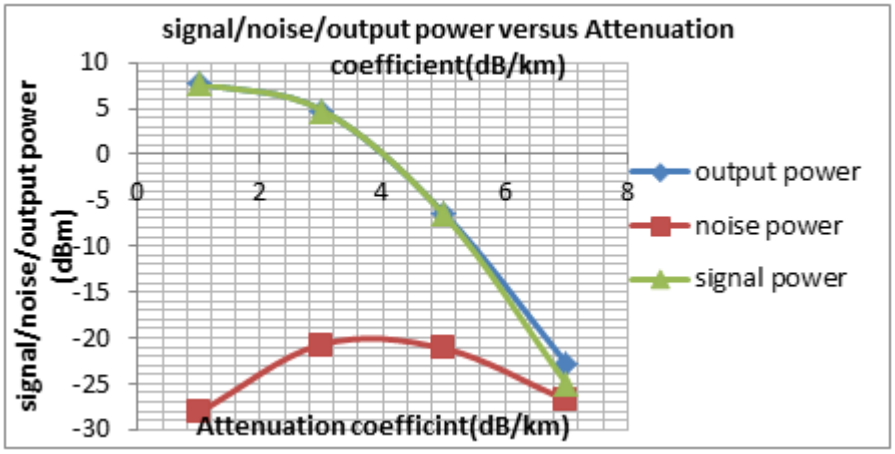

Figure 11. Signal/noise / output power versus attenuation coefficient

In this project, the transmission system has good performance and a characteristic is designed from the design, the optical fiber transmission system can be combined with the modulator which can modulate the output signals. Then, the transmission system consists of Fiber Bragg Grating (FBG) acts as to compensate the dispersion, optical amplifier which can be used to reduce the fiber loss and amplify the signal before being received by photo detector PIN at the receiver [7]. There are different parameters which include output power (mw), attenuation coefficient (dB/km) at cable section and Signal power (dBm) at receiver will be investigated to determine the most suitable setting for a high performance optical transmitter. By analyzing data on Table 1, it shows that the length of fiber bragg grating is directly proportional to the value of noise signal. Figure 6 shows that with increasing FBG length, the Noise power decreases with further increasing length while the signal power and output power reading by electrical power meter increase linearly as increasing length.

Table 2 shows the varying of input power as verse as data of signal/noise and output power, figure versus input power is plotted in figure 9 showed when increasing of input power the noise was decreased with increasing input power, while the signal power and output power increase when the output power increase. Since EDFA is used as the optical amplifier, output power will indicate that the optical amplifier will saturate or the gain has been compressed. The reason is that the power source of the amplifier.

Table 3 shows the output readings are obtained by varying the attenuation coefficient at cable section. From the table, it

is obvious that when the attenuation coefficient is increased, the noise power will increase as well while the signal and output power is decreasing when the attenuation coefficient is increased.

Conclusion

From the design and simulation of optical transmission system, the system will transmit information using optical carrier wave from transmitter to receiver via optical fiber, the transmission system block diagram Figure1 has been designed which consists of laser light as the source, modulator, single mode optical fiber as the channel, fiber Bragg grating (FBG) as the dispersion compensator, optical amplifier and the photo detector as the light detector. The optical transmission system has been modeled by using Optisystem7.0 simulator as shown in Figure 3 in order to investigate different parameters of the system. From the simulation result, it can conclude that the fiber Bragg grating length and the input power are directly proportional to the signal power. While the noise is getting lower with the increasing length, on the other hand, the output power is decreased although the attenuation coefficient increased.

References

1. Fundamentals of Photonics, Fiber Optics in Telecommunication, Nick Massa Springfield Technical Community College Springfield, Massachusetts, University of Connecticut 2000.
2. Phing, H. S., Ali, J., Rahman, R. A., Tahir, B., A., (2007). "Fiber Bragg grating modeling, simulation and characteristics with different gating length," Journal of Fundamental Sciences 3, 167-175.
3. Navneet Singh Aulakh, " Investigations on fiber bragg gratings for fiber optic communication systems, " , department ofelectronics & communication engineering thapar university 2010.
4. OptiSystem Getting Started, Optical Communication System Design Software, Version 3.0 for Windows® 2000/XP, Optiwave Corporation 2003.
5. Sawsan A. Abdul- Majid. 2011" Software Simulation FWM in WDM Optical Communication Systems," College of Information Technology-University of Koya Journal of Kirkuk University – Scientific Studies, vol.6, No.1,.
6. M.A. Othman1, M.M. Ismail2, H.A. Sulaiman3, M.H. Misran4, M.A. Meor Said5, Y.A. Rahim6, A.N. Che Pee7, M.R. Motsidi8, "An Analysis of 10 Gbits/s Optical Transmission System using Fiber Bragg Grating (FBG) ,"IOSR Journal of Engineering (IOSRJEN) ISSN: 2250-3021 Volume 2, Issue 7(July 2012).

7. E. Gemzický a, J. Müllerová (2009) Numerical analysis of reflection characteristics of cascaded non-uniform fiber Bragg gratings," Department of Engineering Fundamentals, Faculty of Electrical Engineering, University of Žilina, Optical Sensors, Proc. of SPIE Vol. 7356, 73561R.
8. MohamadHasrulAriffin Bin MohdBadri, "A Cost Effective Broadband ASE Light Source Based FTTH", thesis, page 20-26.
9. S. O. Mohammadi, Saeed Mozzaffari and M. Mahdi Shahidi, (2011). "Simulation of a transmission system to compensate dispersion in an optical fiber by chirp gratings." International Journal of the Physical Sciences, Vol. 6(32), pp. 7354 - 7360, 2 December.
10. Chong Wing Keong, K R Subramanian, V K Dubey, "Optical Fiber System for Video and Telemetry Signal." Singapore Polytechnic, Electronics and Comm Engineering, School of Electrical and Electronic Engineering, Nanyang Technology University, Singapore.

Effects of Driving ForceEnergy$\Delta V^{\circ}(eV)$ on the Rates of Electron–Transfer Reactions at Metal/LiquidInterface

Hadi, J.M. AL–Agealy[1]; Waleed Bdaiwi Salih[2] and Taif, S. Murdhi[2]

[1]Department of Physics, College of Education for Pure Science Ibn–ALHaitham, University of Baghdad.

[2]Department of Physics, College of Education for Pure Science, University of Anbar.

ABSTRACT

Electron transfer (ET) in metal/liquid interface exhibits dependence on the driving free–energyΔV°. It has been studied depending on the quantum theory. The driving force energies ΔV° for the electron transfer reaction are calculated as a function of the reorganization $\mathbf{E}_{\mathbf{met}}^{\mathbf{liq}}$, and absorption energy $E_{abs}$when a light is incident on the donor–acceptor system. The results show that the driving force energy $\Delta V^{\circ}$for electrons increase with increases absorption energy and decreasing with wave length and reorganization energy$\mathbf{E}_{\mathbf{met}}^{\mathbf{liq}}$. A MATLAP program has been used to calculate the reorganization energy$\mathbf{E}_{\mathbf{met}}^{\mathbf{liq}}$, driving free energy$\Delta V^{\circ}$, and the rate constant of electron transfer$\mathfrak{R}_{ET}$. The present results show that the rate constant $\mathfrak{R}_{ET}$increases with the increasing of the reorganization energy $\mathbf{E}_{\mathbf{met}}^{\mathbf{liq}}$, and with the decreasing of the driving force energyΔV°. Probability of electron transfer occurs in most polar solvent $f(\mathbf{n},\varepsilon)$ system and has low driving force energy.

Keywords: Driving Force, Electron transfer, Metal/Liquid Interface

تأثيرطاقة القوة الدافعة $\Delta V^{\circ}(eV)$على ثابت معدل الانتقال الالكتروني لوصلة سطح معدن /سائل

الخلاصة

أن الانتقال الالكتروني في وصلة معدن /سائل أعتمد على القوة الدافعة للكترونات وقد درس أعتمادا على أنموذج نظري . طاقة القوة الدافعة للالكترونات حسبت كدالة لطاقة اعادة الترتيب و الطاقة الممتصة عندما يسقط الضوء على نظام مانح–مستقبل. قيم طاقة القوة الدافعة للالكترونات تزداد مع زيادة الطاقة الممتصة وتناقص الطول وطاقة أعادة الترتيب. برنامج الMATLAP استعمل لحساب طاقة القوة الدافعة للالكترونات و وطاقة اعادة الترتيب ومعدل الانتقال الالكتروني.لقد اظهرت النتائج ان معدل الانتقال الالكتروني يزداد مع زيادة طاقة اعادة الترتيب وتناقص طاقة القوة الدافعة للكترونات. أن أحتمالية الانتقال الالكتروني تحدث لنظام له استقطابية عالية وطاقة قوة دافعة للالكترونات قليلة.

Introduction

Electron transfer reactions represent a simple process which occurs in donor-acceptor system molecules. The transfer of a single electron from an atom or a molecule to another is considered to be the most elementary reactions.It is one of the most important reaction in physical chemistry and biology involves an oxidation of donor state $|D\rangle$ and reduction of an acceptor state $|A\rangle$ [1].

The electron transfer reaction rate could be as fast as 1PecoSec^{-1} and as slow as 1 Year^{-1}, depending on reactions environmental conditions. An electron transfer reaction may occur between an electrode and molecule or ion (heterogeneous) or between two molecule or ions (homogeneous and bimolecular) or between the two constituents of the same molecule or ion (homogenous and unimolecular) [2]. Electron transport at the Nano scale is remarkably essential to many processes in nature and is therefore an important subject in scientific disciplines such as biology, chemistry, and physics. Electron transfer processes are also essential in electrochemistry which concerns the reactions taking place at the interface between electronic conductors and ionic conductors [3]. It should be noted that the particle that is actually transferred in redox reactions need not always be just a single electron [4]. Rudolph Marcus described electron transfer between two states, a model which was the basis for the classical theory of electron transfer. Latter, this model was extended to describe electron transfer from a single donating state to a continuum of accepting state [5]. Understanding transport across the interface between the active organic molecule and the metallic electrode has proved particular challenging, especially in the single molecule limit. Electron transfer between a

molecular and a metal surface is a ubiquitous process in many chemical disciplines, ranging from molecular electronics to surface photochemistry. Subsequent evolution of the excited electronic wave function is probed in energy, momentum, and time domains by the absorption of a photon. These experiments studies reveal the important roles of molecule/metal wave function mixing, intermolecular band formation, polarization, and localization in interfacial electron transfer [6].

The field of electron transfer has been greatly advanced by the detailed analytical theory in the past half century ago depending on the standards theory and also by introduction a new technology, such as photochemical initiation [7]. The aim of this work is the study of the effect the driving force energy on the electron transfer rate constant at Cu metal with 1,4,5,8-naphthalene tetra carboxylicdiimide molecule interface system; that is calculated theoretically depending on the reorganization energy.

Theory

The rate of the electron transfer from a discrete donor state to continuum acceptor state is the time derivative of the probability which is given by [8].

$$\Re_{ET} = \frac{2\pi}{\hbar}\int_{-\infty}^{\infty}|\mathcal{H}_{DA}(E)|^2(4\pi E_{met}^{liq}k_B T)^{\frac{-1}{2}} exp\frac{-(E_{met}^{liq}+\Delta V)^2}{4E_{met}^{liq}k_B T})\,F_{(E)}\delta(E_m - E_n)dE \quad \ldots\ldots\ldots\ldots\ldots\ldots 1$$

where $\hbar$ is the Planck constant divided by 2π, $|\mathcal{H}_{DA}(E)|^2$ is the coupling matrix element between the electronic state of the metal and the molecule of liquid ,E_{met}^{liq} is the reorganization energy ,$k_B$is the Boltzmann constant , T is absolute temperature ,and $F_{(E)}$ is the Fermi-Dirac probability distribution of the electrons in the electron metal-liquid interface and given by [9].

$$F_{(E)} = \frac{1}{1+exp\frac{E}{k_B T}} \quad \ldots\ldots\ldots\ldots\ldots\ldots\ldots\ldots(2)$$

For electron transfer in metal/liquid interface system, the rate constant of electron transfer at metal/liquid interface can be got by substituting Eq.(2) in Eq.(1),and solving the integration Eq.(1) ,one gets [10].

$$\Re_{ET} = \frac{2\pi}{\hbar}(4\pi E_{met}^{liq}k_B T)^{\frac{-1}{2}}\exp - \frac{E_{met}^{liq}}{4k_B T}|\overline{\mathcal{H}_{DA}(0)}|^2\left[1 - \frac{1}{4E_{met}^{liq}k_B T}\left(\frac{(\pi k_B T)^2}{4}\right) + \frac{1}{32E_{met}^{liq\,2}k_B{}^2T^2}\left(\frac{5(\pi k_B T)^4}{16}\right) - \frac{1}{384E_{met}^{liq\,3}k_B{}^3T^3}\left(\frac{61(\pi k_B T)^6}{64}\right)\ldots\ldots\ldots\ldots + \frac{1}{n!\left(4E_{met}^{liq}k_B T\right)^n}(\propto(\pi k_B T)^{2n})\right]$$

$\ldots\ldots\ldots\ldots\ldots\ldots\ldots\ldots(3)$

The reorganization energy E_{met}^{liq} due to the electron transfer reaction for metal/liquid interface is given by [11].

$$E_{met}^{liq} = \frac{e^2}{8\pi\varepsilon_o}f(n,\varepsilon)\left(\frac{1}{R} - \frac{1}{2D}\right)\ldots\ldots(4)$$

where e is the electron charge, ε_o is the vacuum permittivity, D is the distance between the complex and electrode, R is the radius of the molecule and $f(n,\varepsilon)$ is the polarity function $f(n,\varepsilon)$ that given by.

$$f(n,\varepsilon) = \left(\frac{1}{n^2} - \frac{1}{\varepsilon}\right) \quad \text{.....(5)}$$

Whereε is the staticdielectric constant of the solvent, n is the refractive index of the solvent.

The radius of the molecule can be estimated from the apparent molar volume using spherical approach [12].

$$R = \left(\frac{3M}{4\pi N\rho}\right)^{\frac{1}{3}} \quad \text{..... (6)}$$

Where M is the molecular weight, N is Avogadro's number, and ρ is the mass density.

The driving force energy $\Delta V^{\circ}$of the electron transfer reaction is a function for the absorption energy $E_{abs}$and the reorganization energy E_{met}^{liq} is given by [13].

$$\Delta V^{\circ} = E_{abs} - E_{met}^{liq} = hf - E_{met}^{liq} \quad \text{.....(7)}$$

Where h is the Planck constant, f is the frequency, $f = \frac{c}{\lambda}$ where c is the velocity of light, and λ is the wave length.

Results

One of the most important parameter for the Studies of the electron transfer rate constant at metal/liquid interface is the driving force energy $\Delta V^{\circ}(eV)$ that can be calculated theoretically using Eq. (7).

The absorption energy $E_{abs} = hf$

can be roughly taking from the wave length $\lambda$for thespectrum region (350nm-800nm) and transform energy equation $\frac{hc}{\lambda}$, where h= 4.135667334$\times 10^{-15}$ $eV.sec$,C is the velocity of light $3 \times 10^{8}(^{m}/_{sec})$.

The reorganization energies $E_{met}^{liq}(eV)$ for the electron transfer have been evaluated using Eq.(4-5) with the values of the static dielectric constant , and optical dielectric constantϵ_{op} ,for solvents from table (1).

The radius for donor and acceptor system are estimated using approach in Eq.(6) with the values of Avogadro's constant $N = 6.02 \times 10^{23}\ \frac{Molecule}{mol}$, molecular weight M=302.24 [15], density ρis1.751 g/cm3 [16] for 1,4,5,8- naphthalene tetra carboxylicdiimide molecules and molecule weight

M=$63.546 g.mol^{-1}$, and ρ=$8.92 g.cm^{-3}$ for Cu metal [**14**] in Eq.(6). The estimation of the values of radii are 1.41343A and 4.089977A for Cu metals and of 1,4;5,8-

naphthalene-tetracarboxylic diimide molecules respectively.

The driving force energies $\Delta V^{\circ}(\mathrm{eV})$is provided the electrons to transfer cross interface. It is related to the difference between the reorganization energy from table 1 and the absorption energy spectra (350nm-800nm), results are summarized in table 2.

The rate constant of the electron transfer at semiconductor/liquid interface was calculated using Eq.(3) with a Matlab designed program and inserting the result of the reorganization energy fromtable (1) , the matrix element coupling coefficient [17], driving force energy from table (2) ,and temperature is taken T=300K ,results are shown in table (3).

Table 3 shows the results of the rate constant for electron transfer at Cu metal/ 1,4,5,8-naphthalene tetra carboxylicdiimide molecule liquid interface with variety coupling coefficient $\mathcal{H}_{DA}$.

Discussion

Electron transfer interactions at metal/molecule interface system should be effected by polarity parameter for the solvent molecules. The reorganization energy $\mathrm{E}_{\mathrm{met}}^{\mathrm{liq}}$(eV) is large for large polarity function and vice versa, this indicates that the reorganization energy $\mathrm{E}_{\mathrm{met}}^{\mathrm{liq}}$(eV) is a function of the polarity of the solvent. The probability of electron transfer $\Re_{ET}(Sec^{-1})$across the interface created between metal and molecule in solvent system depends on the reorganization energy $\mathrm{E}_{\mathrm{met}}^{\mathrm{liq}}$(eV), driving force energy$\Delta V^{\circ}(\mathrm{eV})$ and the coupling coefficient $|\mathcal{H}_{DA}(E)|$(eV). The probabilities of rate constant $\Re_{ET}(Sec^{-1})$at metal/molecule system are depending on the organization energy $\mathrm{E}_{\mathrm{met}}^{\mathrm{liq}}$(eV) of the electron transfer. It is calculated depending on continuum Marcus theorywith thephysical concepts such as a refractive index, and static dielectric constant for donor/ acceptor system.

Results of the driving force energy$\Delta V^{\circ}(\mathrm{eV})$ in table 2 for electron transfer is take term accounting for the drive more electron to transfer across interface, that describe the interactions between of the donor state wave function and acceptor state wave function. Results of the driving force energy show that the drive energies $\Delta V^{\circ}(\mathrm{eV})$ for electrons as a function of the reorganization energy and the absorption energy at region (350-800) nm. Table 2 of the driving force$\Delta V^{\circ}(\mathrm{eV})$, show that its energies that take to bring the donor and acceptor together and is the part of the work broken to derive the electrons to transfer from donor to acceptor. The driving force energy $\Delta V^{\circ}(\mathrm{eV})$to drive the electron increases with increases absorption energy and decreasing in wave length and reorganization energies for system.Furthermore, the reorganization energy$\mathrm{E}_{\mathrm{met}}^{\mathrm{liq}}$(eV) and the driving force energy

$\Delta V^{\circ}(\mathrm{eV})$ and the coupling coefficient energy are the base of electron transfer in system. Data of rate constant depending on these parameters enable to understand the idea of the behavior of electron transfer in metal/molecule

Data of ET rate constant $\Re_{ET}(Sec^{-1})$ that occur in metal/molecule system with lest polarity function solvents,that's view from comparing between tables 1 and 2.

On the other hand, the rate constant $\Re_{ET}(Sec^{-1})$ values are large for system with lest polarity function and low values of reorganization energy, this indicates that Ethyleneolamine and Dimethylsulfoxid l are more reactive towards metal than others and ET occur activity with less polar solvents. Table 3 gave the theoretical results for rate constant of electron transfer and show that rates are increasing with increasing of the driving force energy. This because of when the system have low reorganization energies make the driving force energy become large and finally more electrons that transfer the interface between metal and molecules and vice versa .On the other hand, the absorption energy divided to reorientation the system to transfer and the other enable to drive the electron to transfer due to tunneling height from donor to acceptor and the rates are increasing.

Another controlling of electron transfer is the coupling coefficient $|\mathcal{H}_{DA}(E)|$(eV) that can be assume in the range $(0.000111- 0.000186)\ (\mathrm{eV})^2$ for metal/molecule system according the experimental data [17]. At interface between metal and molecule, the wave functions for metal and molecule overlapping and electron can be transfer due tunneling. However, if the electron tunneling occurs, the initial and final electronic states should have approximated equal energies that happen under the considering continuum of electronic states for the metal/molecule system interfaces. These electronic states are brought into resonance by fluctuations of polar medium surrounding metal and molecule system and this resonance is the transition state of electron transfer reaction.

Conclusions

In conclusion the probability of electrontransfer $\Re_{ET}(Sec^{-1})$across the interface created between metal and molecule in solvent system depends on the reorganization energy E_{met}^{liq}(eV), driving force energy$\Delta V^{\circ}(\mathrm{eV})$ and the coupling coefficient $|\mathcal{H}_{DA}(E)|$(eV).

Driving force energy$\Delta V^{\circ}(\mathrm{eV})$for electron transfer is a function of the reorganization energy and the absorption energy take term accounting for the drive more electrons to transfer across interface, and describe the interactions between of the donor state wave function and acceptor state wave function. The driving force energy $\Delta V^{\circ}(\mathrm{eV})$to drive the electron increases with increases absorption energy and decreasing in wave length and reorganization energies for system.

Electron transfer rate constant $\Re_{ET}(Sec^{-1})$ that occur in metal/molecule system with lest polarity function and low values of reorganization energy and show that rates are increasing with increasing of the driving force energy due to tunneling height from donor to acceptor and the rates are increasing. At interface between metal and molecule, the wave functions for metal and molecule overlapping and electron

can be transfer due tunneling and electronic states are brought into resonance by fluctuations of polar medium surrounding metal and molecule system and this resonance is the transition state of electron transfer reaction.

Table 1. The results of the reorganization energy $E_{met}^{liq}(eV)$ for electron transfer at Cu/ for 1,4,5,8− naphthalene tetra carboxylicdiimide molecule interface system.

Solvent	$f(n,\varepsilon)$	Refractive index[14]	Dielectric constant[14]	Reorganization energy
Methanol	0.5377	1.3265	32.70	0.594
Acetonitrile	0.5289	1.3416	37.50	0.585
Ethylenimine	0.4467	1.4123	18.30	0.494
Fornicacid	0.5161	1.3694	58.50	0.571
Propionitnile	0.5010	1.3636	27.20	0.554
Ethyleneolamine	0.3972	1.4513	12.90	0.439
Propanol-1	0.4731	1.3837	20.33	0.523
Benzen	0.00519	1.5011	2.28	0.005
Dimethylsulfoxidl	0.4367	1.4773	46.68	0.483
Vale-onirile	o.4601	1.3991	19.71	0.509

Table 2. The results of the calculated driving free energy $\Delta V^{\circ}(eV)$for the electron transfer in Cu/1,4,5,8− naphthalene tetra carboxylicdiimide systems with ten solvents.

Solvent Type	ΔV°(eV) Wave length									
	350nm	400nm	450nm	500nm	550nm	600nm	650nm	700nm	750nm	800nm
Methanol	2.95034	2.50719	2.16251	1.88677	1.66117	1.47317	1.31409	1.17773	1.05956	0.95616
Acetonitrile	2.96008	2.51693	2.17226	1.89652	1.67091	1.48291	1.32383	1.18747	1.06930	0.96590
Ethylenimine	3.05103	2.60788	2.26320	1.98746	1.76186	1.57386	1.41478	1.27842	1.16025	1.05685
Fornicacid	2.97419	2.53104	2.18637	1.91063	1.68502	1.49702	1.33794	1.20159	1.08341	0.98001
Propionitnile	2.99092	2.54777	2.20310	1.92736	1.70176	1.51375	1.35467	1.21832	1.10014	0.99674
Ethyleneolamine	3.10574	2.66259	2.31792	2.04218	1.81657	1.62857	1.46949	1.33314	1.21496	1.11156
Propanol-1	3.02183	2.57868	2.23400	1.95826	1.73266	1.54466	1.38558	1.24922	1.13105	1.02765
Benzen	3.53946	3.09631	2.75163	2.47589	2.25029	2.06229	1.90321	1.76685	1.64868	1.54528
Dimethylsulfoxidl	3.06201	2.61886	2.27418	1.99844	1.77284	1.58484	1.42576	1.28940	1.17123	1.06783
Vale-onirile	3.03619	2.59304	2.24836	1.97262	1.74702	1.55902	1.39994	1.26358	1.14541	1.04201

Table 3. The results of the rate constant for electron transfer at Cu metal/ 1,4,5,8-naphthalene tetra carboxylicdiimide molecule liquid interface with variety coupling coefficient $\mathcal{H}_{DA}$.

Solvent Type	The electron transfer rate constant $\Re_{ET}(Sec^{-1})$			
	$\mathcal{H}_{DA}(0)$ = 0.01115 eV	$\mathcal{H}_{DA}(0)$ = 0.01177eV	$\mathcal{H}_{DA}(0)$ = 0.01239eV	$\mathcal{H}_{DA}(0)$ = 0.01363eV
Methanol	1.627E+09	1.814E+09	2.010E+09	2.432E+09
Acetonitrile	1.773E+09	1.975E+09	2.189E+09	2.649E+09
Ethylenimine	3.904E+09	4.350E+09	4.820E+09	5.833E+09
Fornicacid	2.006E+09	2.235E+09	2.477E+09	2.997E+09
Propionitnile	2.321E+09	2.586E+09	2.866E+09	3.468E+09
Ethyleneolamine	6.222E+09	6.933E+09	7.683E+09	9.298E+09
Propanol-1	3.035E+09	3.382E+09	3.748E+09	4.535E+09
Benzene	-9.726E+12	-1.083E+13	-1.201E+13	-1.453E+13
Dimethylsulfoxidl	4.289E+09	4.779E+09	5.296E+09	6.409E+09
Vale-onirile	3.436E+09	3.828E+09	4.242E+09	5.134E+09

References

1. Wibren.Du.,W.Gispen.W., H., (2002). Electron transfer in donor–bridge–acceptor system and derived materials″ Ph. D. Thesis , Debye Institute and University of Utrecht,Chapter 1, p; 1-10.

2. Naheed, K. B., (2002). "heterogeneous electron transfer rate ipyridinium halides" PhD Thesis , Quaidi-Azam University of Islamabad.

3. Thomas Frederiksen, (2007)."Inelastic transport theory for nanoscale systems" Ph.D. Thesis, Department of Micro and Nanotechnology Technical University of Denmark.

4. Hussain K.M. (2012).″Quantum mechanical for electron transfer at metal/semiconductor interface″ MsC. Thesis, University of Baghdad.

5. Kevin T., pavel A.F., and prashant V.K., (2011). "photoInduced electron transfer from quantum dot to metal oxide nano particles "PNAS.Vol.108 , NO.1.

6. Zhu X.-Y., (2002). “electron transfer atmolecule-metal interfaces: a two-photon Photoemission Study” Annu. Rev. Phys. Chem. 53:221–47.

7. Jing H., (2006). "Design, characterization, and electron transfer properties of synthetic metalloproteinase" Ph.D thesis, Graduate College of Bowling Green State University.

8. Gao y Q., and Marcus R. A., (2000). "On the theory of electron transfer reactions at

semiconductor\liquid interface", J. Chem. Phys.Vol 113;No 15.

9. Charles, K. (2005). "Introduction to solid state physics",Book,8th edition, Wiley and Sons publisher.

10. Taif, S. Murdhi, (2013). "Effect of the temperature on the electron transfer at metal/liquid Nanosystem"M.Sc. Thesis, University of Anbar.

11. Kuciauskas H., and Micheal .S., (2001)."Electron transfer in TiO_2 solar cells ", J. Phys .Chem. B ., Vol. 105,No. 2, pp. 394 – 402**.**

12. Al-Agealy H.J,and Hassoni M.A.,(2010)."Atheoretical study of the effect of the solvent tyoe on the reorganization energies of dye /semiconductor system interface"Ibn-ALHaithem .J pure &Appl.Sci.,Vol.23,No.3,pp 51-57.

13. Al-Agealy H. J M. and Hadi A. Z., (2010). "ET between ketone triplets and organic dyes in variety solvent " J. College Basic Education, No. 64, pp.16.

14. PradyotP., (2003). " Handbook of InorganicChemicals" The McGraw-Hill Companies, Inc.

15. Roman Forker, (2010). "Electronic Coupling Effects and Charge Transfer between Organic Molecules and Metal Surfaces"Ph D Thesis TechnischeUniversit¨ at Dresden Naturwissenschaften.

16. Yuval O., Alexander Z. and ShlomoY., (2006). "1,4;5,8-naphthalene-tetracarboxylic diimide derivatives as model compounds for molecular layer epitax"J. Mater. Chem., 16, 2142-2149.

17. Nien H .G., Chung M. W., and Charles H. H., (2000). "Portrait of the potential Femto second studies of Electron pynamics at interface" Acc. Chem. Res .Vol. 33, pp. 111-118.

Implementation of Production Normalize DB based on Functional Dependency Table (FDT)

Maitham Ali Naji

Foundation of Technical Education, College of Electrical and Electronic Techniques, Power Department

ABSTRACT

This paper presents the result of previous papers. It is provides computerized technique to design and create normalize relational database based on Functional Dependency Table (FDT). The system use Data Access Object (DAO) to define tables to the table collection. After the tables and fields have been created, the system will define an index and primary key attributes to the first field of each table, finally the relationships type is created between tables depend on the primary keys and foreign keys.

Keywords Relational Database, DAO Jet Engine, Visual Basic.

تطبيق انتاج قواعد بيانات منسقة استنادا على جدول الوظيفة الاعتمادية

المستخلص

هذه البحث يمثل نتيجة لبحوث سابقة والتي تهدف الى توفير تقنية حاسوبية لتصميم وبناء قواعد بيانات علائقية منسقة من خلال جدول الوظيفة الاعتمادية (FDT). النظام استخدم كائن DAO لتعريف الجداول الى مجموعاتها. بعد تكوين الجداول وحقولها، سوف يعرف النظام الفهرس والمفتاح الرئيسئ للحقل الاول لكل جدول. واخيرا" سوف تنشاء العلاقات بين الجداول اعتمادا" على المفتاح الرئيسي والثانوي.

List of Abbreviations:

RDBMS	Relational Data Base Management System
SQL	Structure Query Language
OODBM	Object Oriented Data Base Management
ERD	Entity Relationship Diagram
ERT	Entity Relationship Table
PK	Primary Key

Introduction

The relational database model focuses on logical representation of the data and its relationships, rather than on the physical storage details. The relational database perceived by the user to be a collection of tables in which data are stored [1]. RDBMS A DBMS that manages relational databases (and no others); equivalently, a DBMS that implements the relational model. Note: SQL DBMSs must be regarded as only approximately relational at best, since SQL involves so many departures from the relational model [2].

Each table is a matrix consisting of a series of row/column intersections. Tables, also called relation, are sharing to each other by sharing a common entity characteristic. The relationship type (1:1, 1: M or M: N) is often shown in relational schema to connect entities [3].

We define object orientation as a set of design and development principles based on conceptually autonomous computer structure known as objects. OODBM is a database management system that integrates the benefits of typical database systems with more powerful modeling and programming characteristics of the object oriented data model [4].

Paper [5] applies normalization rules to ERT to produce FDT. The current system produce normalize database based on FDT.

The DAO Object Hierarchy

The DAO is the name given to the object model for the Jet engine. The DAO have many levels, the top level object of the DAO model, there is a hierarchy of other objects and their collection, each with their own properties and methods, which allow you to access the data in your database [6]. The object hierarchy is shown in figure 1.

1. DBEngine

The top level object in the DAO object hierarchy is the DBEngine. There can be only one DBEngine object; it contains all the other objects in the hierarchy. You do not create the DBEngine object, because it is available by default.

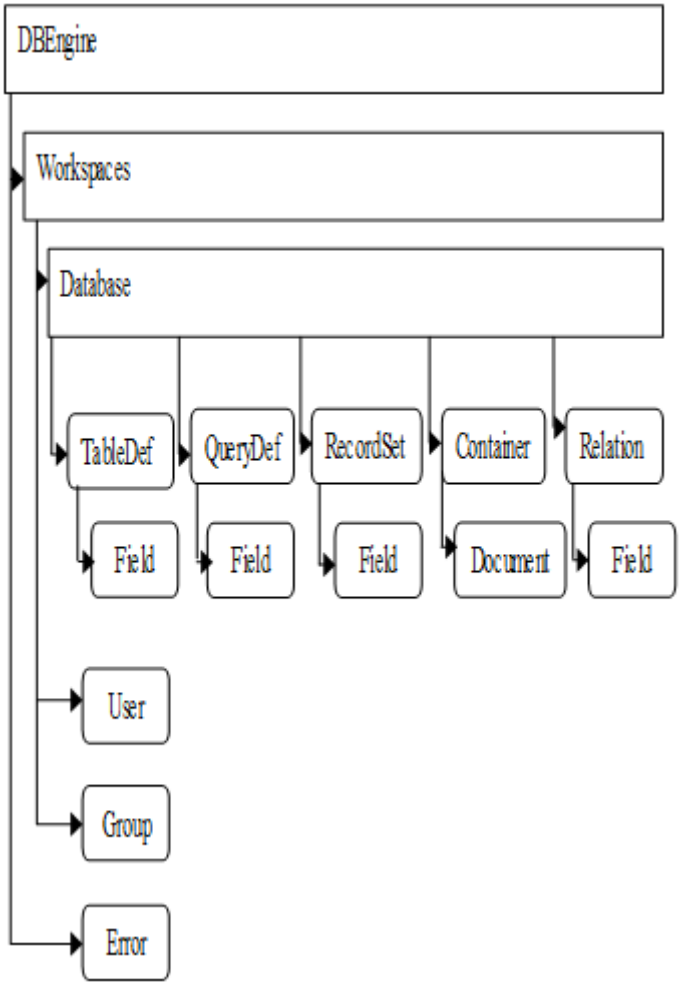

Figure 1. The Data Access Object (DAO) hierarchy [6].

2. Workspaces

Most of the DAO Hierarchy lies under the workspaces collection. A workspace is an organizational structure that allows you to group database connections into a named area or session. You will need more than one workspace if you want to access groups of databases in different ways, such as one group through the jet engine and the other through ODBCDirect.

3. Groups and Users

In a Jet database, such as Microsoft Access, you may define workgroups consisting of Groups and Users, and their

associated permissions for accessing the database.

4.Relation

A Relation object represents a relationship between fields in tables or quires. You can use the Relation object to create new relationships [7].

5. Database

The Database object is the most important object we will be dealing with because it allows us to interface with the database.

To look at the structure of a database, we need first look at the objects, collections, and properties that exist in our DAO hierarchy; figure 2 shows the relevant structure and properties [6].

1.TableDefs

Just as every object under the DBEngine object can be a collection or object, TableDefs is a collection of TableDef objects.

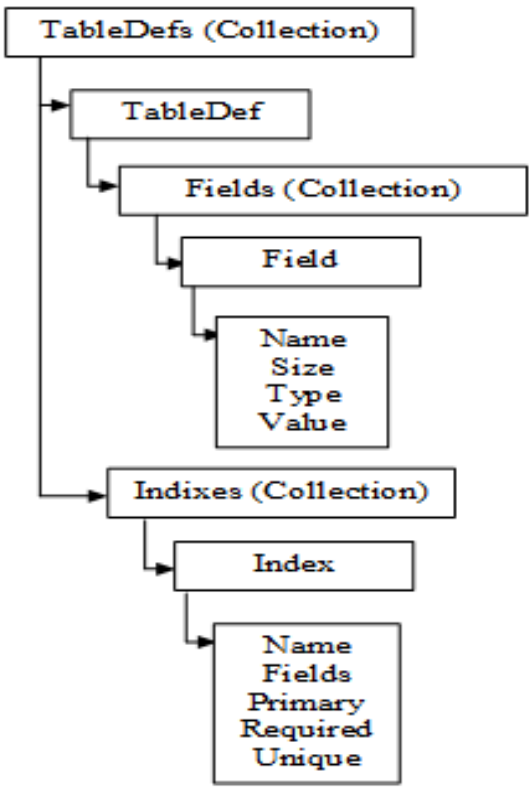

Figure 2. The tabledefs collection hierarchy [6].

2-Fields

Of more interest than the table names are the fields that exist in the table. Each tableDef object contains a Fields collection, which in turn contains one or more Field objects. The most important properties are (name, size, source field, source table, type and value).

3-Indexes

Just as you can look at the various fields you have in a table, you can also view the indexes on it. Each TableDef object can have an associated Indexes collection with one or more Index Object in it. The most important properties are (fields, foreign, name, primary and unique).

2-The System's Flowcharts

In [8], the program divides the entered sentence into three parts, Subject Group, Verb Group and complement group. Subject and complement group are representing the source and destination entities or attributes with its relationship. Verb group is representing the relation name that connects the source and destination entities.

In [9] the system converts the subject, verb, and complement groups to ERT instead of ERD.

In [5] the author applies normalization rules based on primary keys on ERT. The program will split the primary key attributes from non key attributes to build the functional dependency for each table. The Functional Dependency will store in file called FDT that contains Table Name, PK Fields, and Table Fields. As shown in figure 3.

The Functional Dependency Table (FDT) for the following examples shown in figure 3. Employee has Emp ID, Emp name and Dept ID. Department has Dept ID , Dept Name and Dept Location. Skill Master has Skill Code and Skill Name. Employee Skill has Skill Code, Skill Name and Skill level.

FD Table

	Table Name	PK Fields	Table Fields
▶	Employee	Emp ID	Emp Name , Dept ID
	Department	Dept ID	Dept Name , Dept Location
	Skill Master	Skill Code	Skill Name
	Employee Skill	Skill Code	Skill Name , Skill level

Display FD

Figure 3. Functional Dependency Table (FDT).

The FDT will be an input to the current system. The system will pass through six stages to produce relational database. As shown in figure 4.

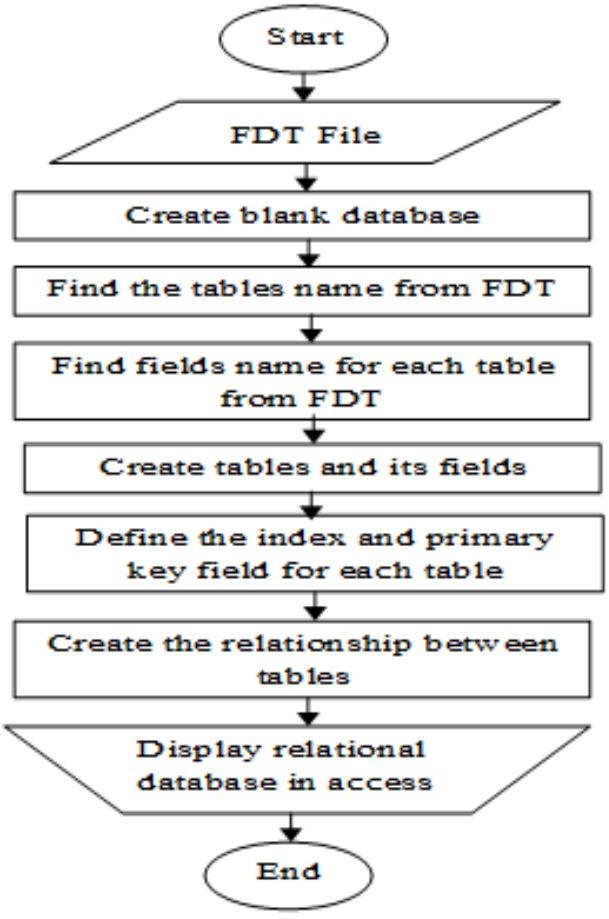

Figure 4. Block diagram of production normalize DB based on FDT.

The first stage, the system will delete the old Database if it's existing; then create new one in first workspace. As shown in figure 5.

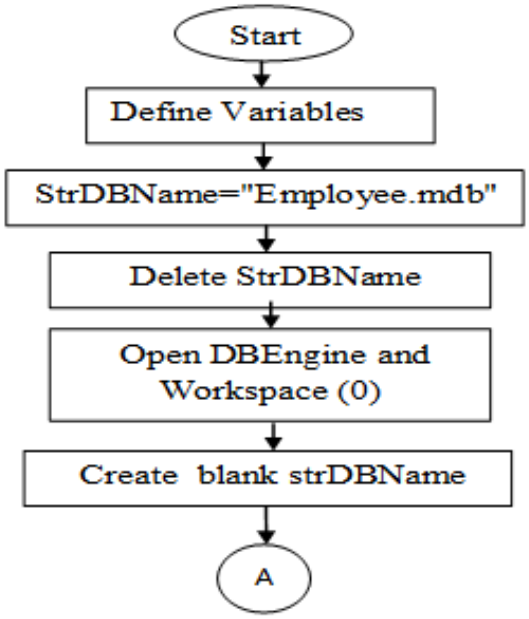

Figure 5. Create new database.

The second stage extraction tables names; the system will store the content of FDT's "Table Name" field that contains tables names in list called "Table List". As shown in figure 6.

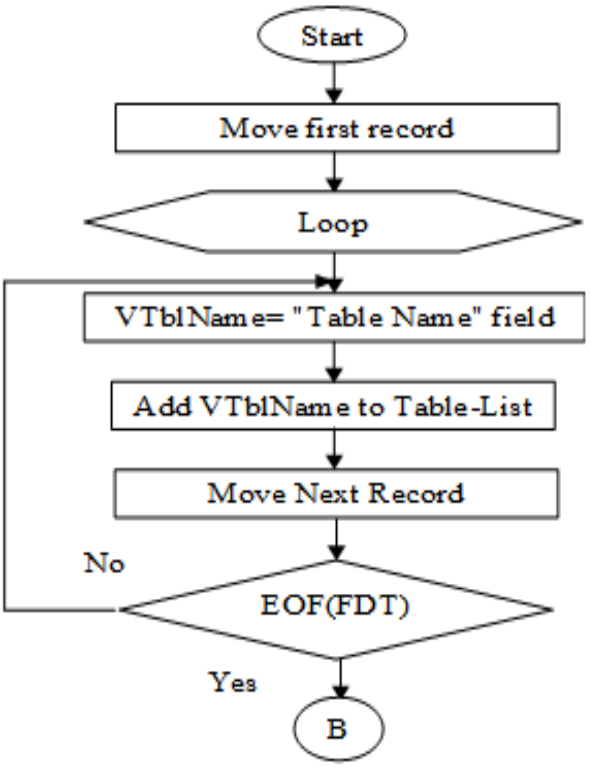

Figure 6. Extracting tables name from FDT.

The output of this stage will pass the table name and its fields to procedure called "Create Table and Fields" to create table in DAO object. This is done by store the primary key attribute and non key attribute in list called "Field List". The primary key attribute will store from PK-Field of FDT in first location of the Field list, while the non key attributes will store from Table Fields to Field List. The Table Fields may contain more than one attributes. These attributes converted to an array by using Split instruction, and then each element in array will be added to Field List. This process is repeated until end of FDT file. As shown in figure 7.

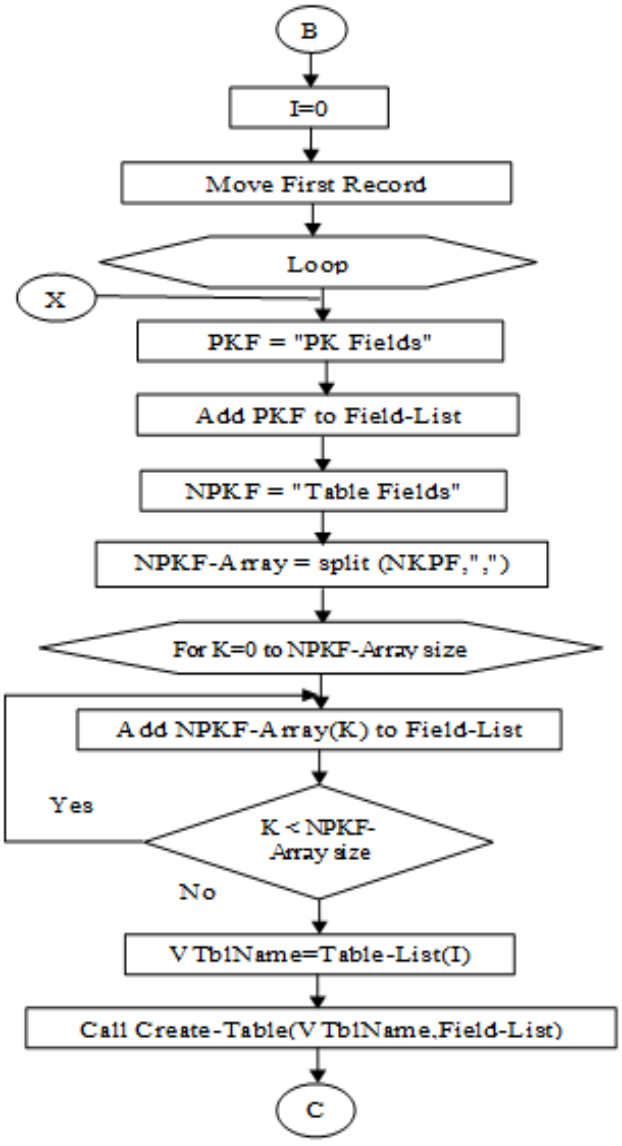

Figure 7. Extracting fields list from FDT.

The output of previous flowchart will be List-Table(0)=Employee

List-Field of Employee =[Emp ID, Emp Name, Dept ID]

List-Table(1)=Department

List-Field of Department =[Dep ID, Dept Name, Dept Location]

List-table(2)=Employee Skills

List-Field of Employee Skill =[Skill Code, Emp ID, Skill Level]

List-table(3)=Skill Master

List-Field of Skill Master =[Skill Code, Skill Name]

The Create Table and fields procedure shown in figure 8 does the following:

1. Create table and added it to the tables collection in DAO object.
2. Create the table's fields after the user define the field type (Text, Number, Date,…, etc) and added it to field collection.
3. Assign index to first field for each table; then added the index to index collection. As illustrated in DAO Object Hierarchy section.

The last stage; the system will establish the relationships between tables. This is done by storing the tables' names and their fields in two dimensional arrays. As shown in figure 9. The result of the flowchart is shown in table 1.

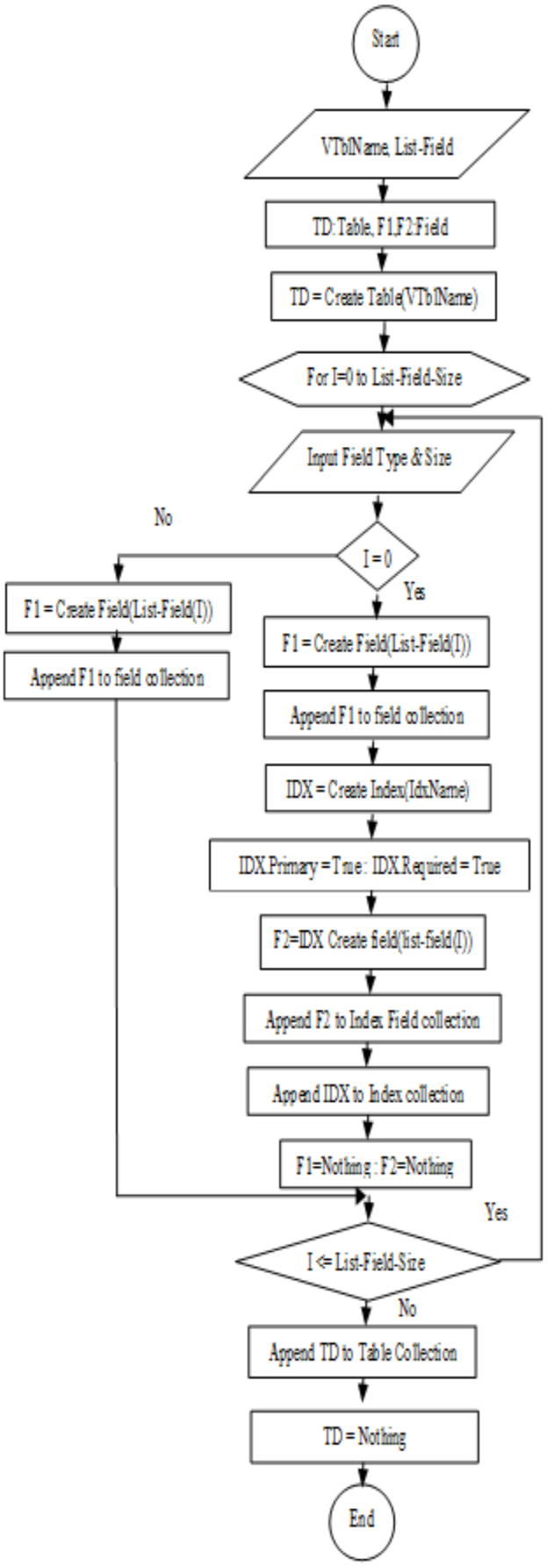

Figure 8.Create table and fields

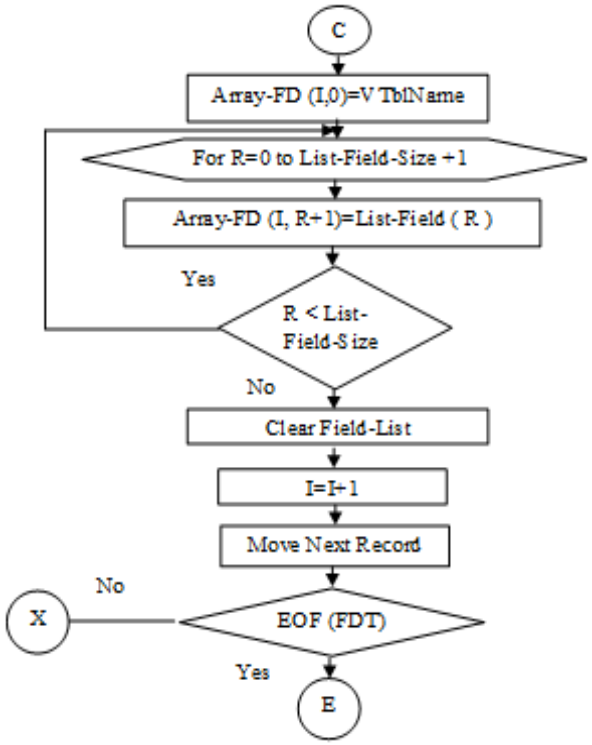

Figure 9. Conversion table into two dimensional arrays.

Table 1. Tables names and their fields.

	Column 0	Column 1	Column 2	Column 3	…	Col 10
1	Employee	Emp ID	Emp Name	Dept ID		
2	Department	Dept ID	Dept Name	Dept Location		
3	Employee Skills	Skill Code	Emp ID	Skills Level		
4	Skill Master	Skill Code	Skill Name			
.						
10						

The system generates two types of relationships; the first type is (1:1). Like the relationship between Employee Skill and Skill Master Tables. The relation called (1:1) if two tables connect via primary key.

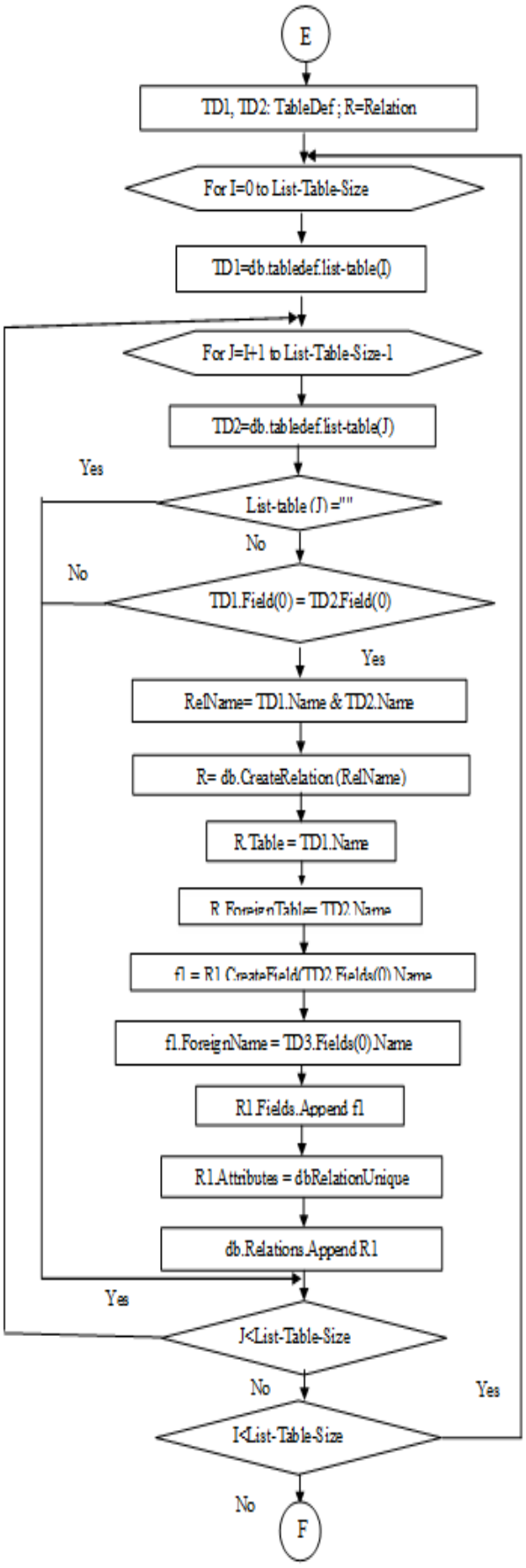

Figure 10. 1:1 Relationship.

The flowchart shown in figure (10) does the following:

1. Add the tables to the collection of tablesdefs.
2. It has two nested loop; will compare the first item of column one (Shaded column) in two dimensional array with all other items in the same column; if the match success the system creates relationship, otherwise will take another item.
3. The program will define relationship name.
4. Create the relationship between tables.
5. Add the relationship to the collection.

The second type is (1: N). Like the relation between Departments and Employee tables. The relation called (1:N) if one tables has primary key and the second table has foreign key.

The flowchart shown in figure 11 does the following:

1. Add the tables to the collection of tablesdefs.
2. It has four nested loop; will take the primary key (item in shaded column) and compare it with all other items in array (except item in shaded column). If the match success the system creates relationship, otherwise will take another item. The steps (3-5) are similar to above steps.

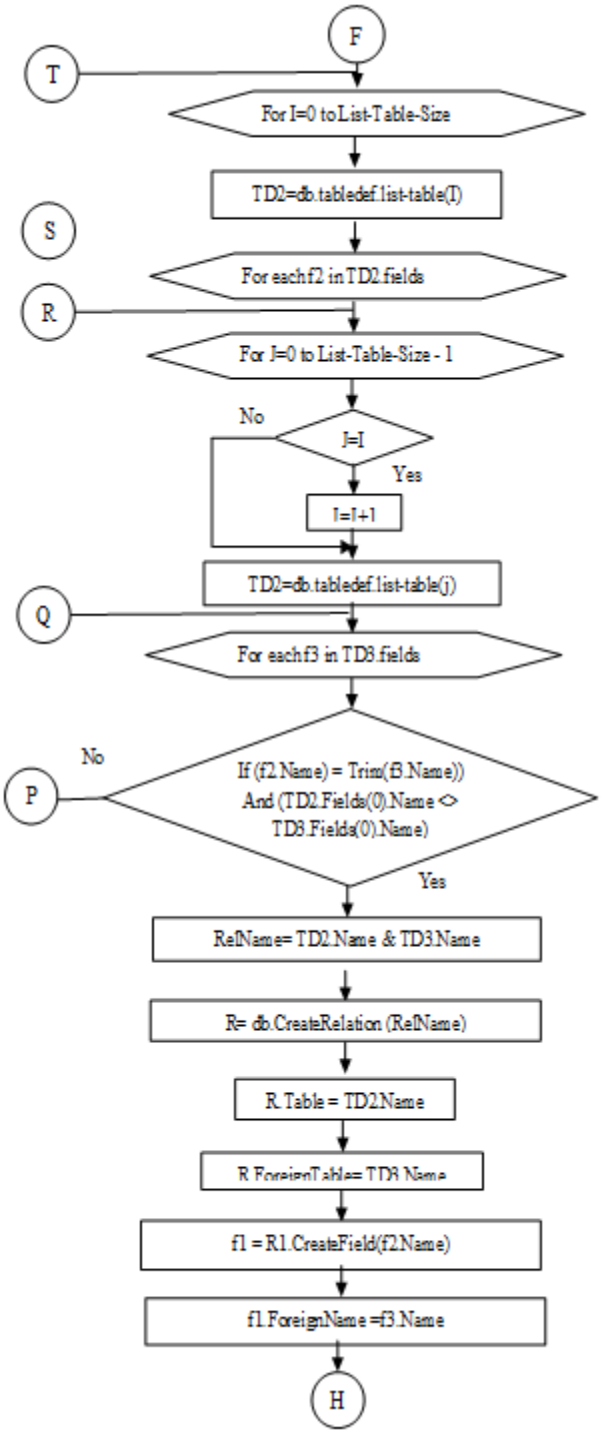

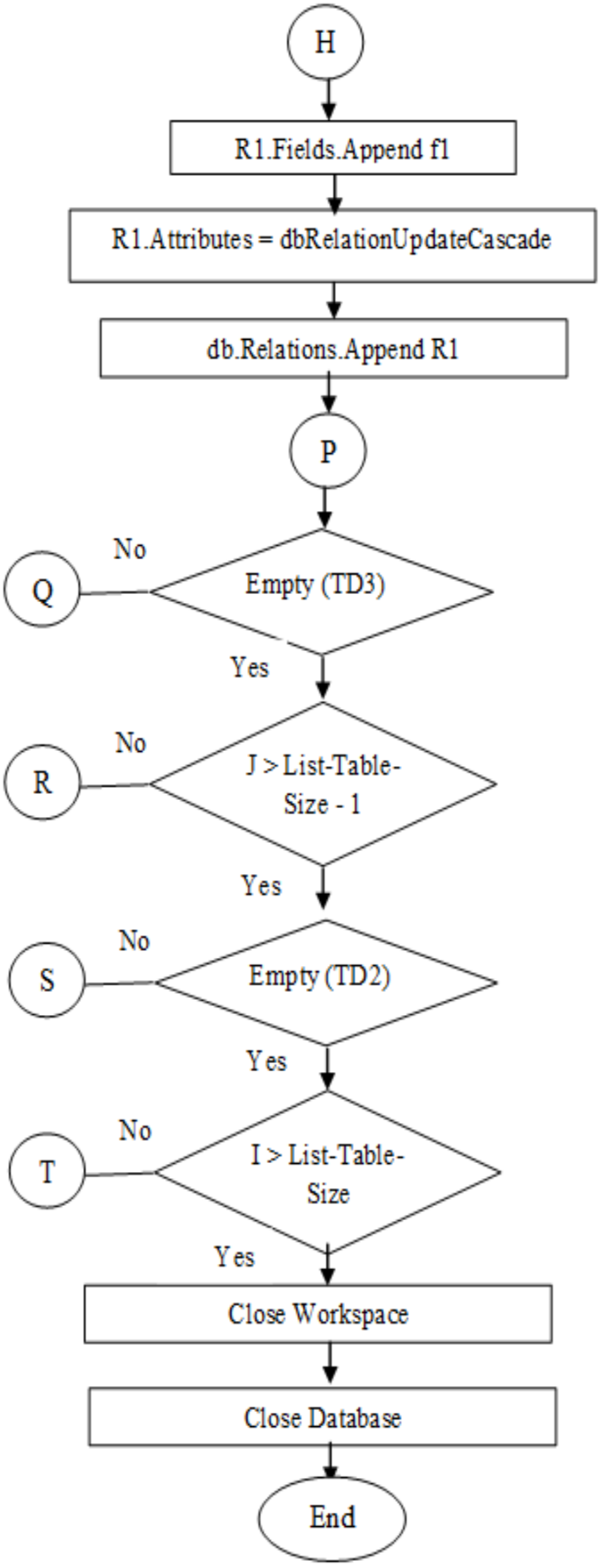

Figure 11. 1: N Relationship.

3-The Implementation

The system has been implemented in Visual Basic language. The program contains the following main windows as shown in figure 12.

Figure 12. Main Form Window.

By click on "Create Database" button, the program will create blank database, and the process will be done on FDT to extract the tables and it is fields, the system will ask from the user to define the data type (Number, Text, Date, etc) for each field before adding the field to the collection. As shown in figure 13.

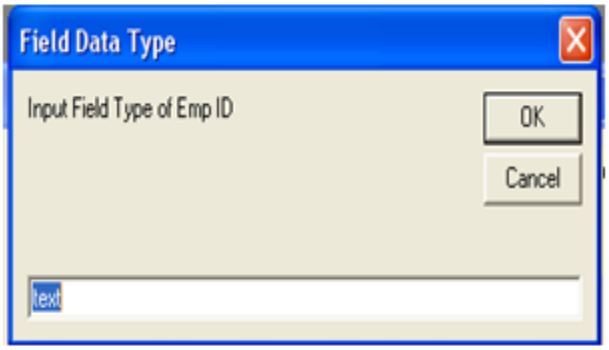

Figure (13): Input Field Data Type.

This process is repeated to give data type to all fields of the tables as shown in Figure (14).

Figure 14. Creating Tables in Access.

Finally the system will establish the relationship between tables shown in figure 15 and displays message "The Relational Database is done" as.

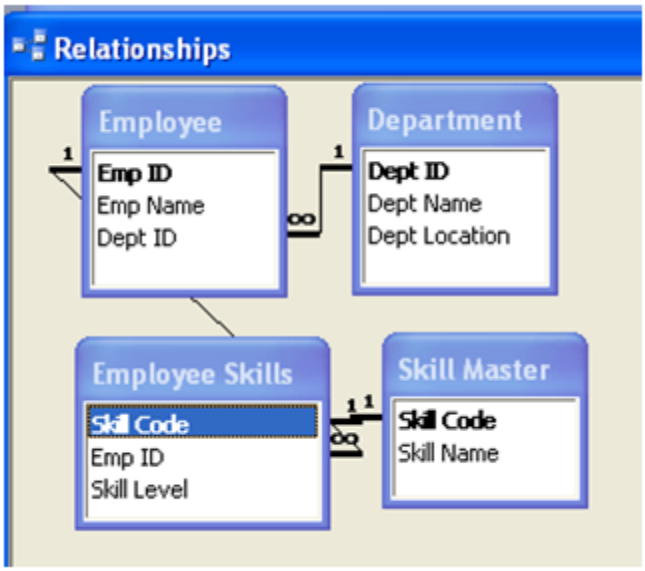

Figure 15. Creating Relationship between Tables.

Conclusion

The majors points can be concluded from this system, the first one the system is easy to use, since the user just enter the business rules (sentences) the output system will be normalize DB.

The second one, some time you find some persons had high skill in DB design but he/she does not like to learn application that help him to apply his/her design, so the system is very useful for this type of people.

The last point the system is very useful to provide secure DB by transmit the DB as a FDT to end user. The end user can convert the FDT to DB by using this program.

References

1. Wisley, Addison; (2010). Fundamentals of Database System. USA, 1172.
2. Date, C.J., (2007). The Relational Database Dictionary. Trafford Publishing, 215.
3. Carter, John, (2000). Database Design and Programming with Access, SQL and Visual Basic. McGraw-Hill Publishing Company, 483.
4. Rob, Morris, Coronel, (2010). Database Systems: Design, Implementation, and Management. McGraw- Hill Edition, USA, 675.
5. Naji, Maitham Ali, (2013). Improve Entity Relationship Table (ERT) by Using Primary Key. Accepted not published in Al-Mustansiriyah Journal of Science.
6. Snowdow, Nick, (2002). Oracle Programming with Visual Basic. SYBEXInc,USA,715.
7. VB Help, (2001). Microsoft Developer Network (MSDN).
8. Naji, Maitham Ali, (2011). Implementation Sentence Analysis via Verb. Foundation of Technical Education, 24(8):83-90.
9. Naji, Maitham Ali, (2011). Proposal of Creating Entity-Relationship Table (ERT) From English Sentence Group. Iraqi Journal of Computers, Communication, Control and Systems Engineering, 11(2): 79-88.

Comparison between Two Types of Electrodes for Electrostatic Quadrupole Lens

Sura A. Obaid

Department of Physiology and Medical Physics, College of Medecine, Al-Nahrain University, Baghdad, Iraq.

E-mail: suraallawi@yahoo.com

Abstract

This work aims to find the optimum design of electrostatic quadrupole lens and make the comparison between two different electrodes shapes which are computed with the aid of transfer matrices. Two types of electrostatic quadrupole lens, cylindrical convex electrodes, and cylindrical concave electrodes were used to find optimum field model, which was close to the field distribution for each design of the proposed lens.

The path of charge-particles beam is traverse the field model has been determined by solving the trajectory equation of motion in Cartesian coordinates. Then, take the comparison of the optimum values of spherical aberration coefficients and resolution limits in both convergence and divergence plans for each proposed type.

Keywords: Electrostatic, quadrupole Lens, spherical aberration, resolution limits, trajectory equation.

الخلاصة

تهدف هذه الدراسة لايجاد التصميم الامثل لعدسة كهروستاتيكية رباعية الاقطاب مع اجراء مقارنة بين نوعين من هذه العدسات بالاستعانة بمفاهيم انتقال المصفوفات ، أحداهما ذات أقطاب اسطوانية بسطوح محدبة والاخرى ذات اقطاب اسطوانية بسطوح مقعرة لإيجاد أنموذج المجال الكهروستاتيكي الأمثل لكل تصميم من العدسات المفترضة أعلاه. يتم حساب مسار حزمة الجسيمات المشحونة المارة خلال أنموذج المجال بواسطة حل معادلة الحركة للأشعة بالإحداثيات الكارتيزيه، وقد تم مقارنة القيم المثلى لمعاملات الزيغ الكروي وحدود التحليل في كلا النموذجين المفترضين.

Introduction

Electron lenses are one of the principle components of the electron optics devices. Both electrostatic lens (electric field) and magnetic lens (magnetic field) are used to focuses charged particles; each type has its advantages and disadvantages. The focusing power of electrostatic lenses independent of the mass of the charged particles and depends only on their energy; therefore to be preferred over magnetic lenses when heavy particles of moderate energy must be focused.

There are numerous types of electrostatic lenses, each one of them classify according to electron-optical properties and domain of application. The first published work on electrostatic fields with rotational symmetry dates back to 1926 [1]. The quadrupole lenses are second in importance only to the axisymmetric electron lenses. Quadrupole lenses began to be used in electron-optical devices in the 1950 s. These lenses have a high focal power and are used to focus the beams in high-energy. They produce fields with two mutually perpendicular planes of symmetry and two planes of asymmetry by means of four identical electrodes arranged symmetrically about the axis. Therefore, if the x-z plane of the lens collects the charged particles, the y-z plane will cause them to diverge, i.e., the quadruple lens is astigmatic [2,3].

Lens Design

This work is concerned with the design of electrostatic quadrupole lens consist of four identical symmetric parts are cut out from cylinder. These four parts represent the concave and convex cylindrical quadrupole lens. The effect of changing the geometrical shape of electrodes for each design like; the angle of gape between electrodes (Γ), where the ratio of cylindrical electrode radius (R) to aperture radius (a) is constant, electrode voltage ratios (V/V_1), electrode thicknesses and spacing between them, as well as the radial and longitudinal dimensions of the electrode. The particular electrode configuration may be found in the value of (K) (electrode shape) and then the excitation parameter of lens as active parameter is changing [4,16].

Quadrupole lens is described as converging lens if the particles moving in x–z plane are deflected toward the z-axis and while described as diverging lens if the particles moving in y-z plane are deflected away from the z-axis [5]. In the current work, the electrodes shapes which taking into consideration are the cylindrical convex and cylindrical concave electrodes that generally used instead of hyperbolic electrodes due to the difficulties of fabricate.

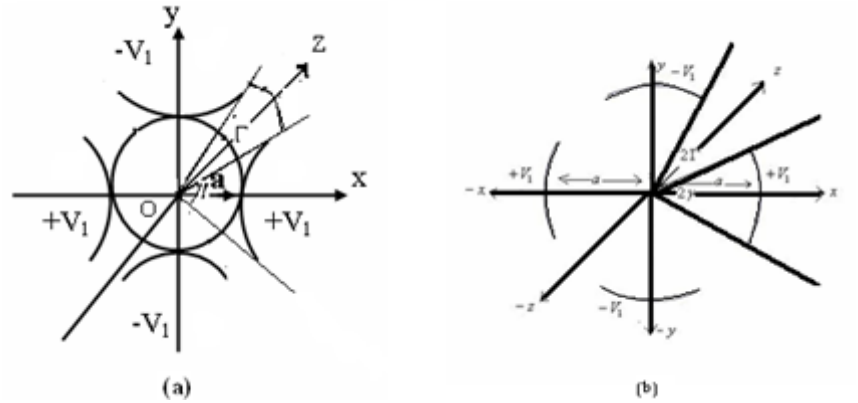

Figure 1. Electrodes of quadrupole lens: (a) cylindrical convex electrodes, (b) cylindrical concave electrodes [12,14].

The Potential Distribution

Variation of the parameter K according to electrode shape gives different modes of potential distribution. In cylindrical coordinates, the potential a long the optical axis is given by the formula;[4].

$$V(r,\theta,z) = D(z)\, V_1\, (r/a)^2 \cos(2\theta) \qquad (1)$$

where V_1 is the electrode potential (take 100 volt in the current study), r is the of the radial displacement of the beam from the optical axis measured in (mm), θ is the angle between electrodes and z-axis measured in degree, and D(z) is the electrodes field (the quadrupole field components) which is equal to; [6].

$$D(z) = K\ f(z) \qquad (2)$$

Thus, $f(z)$ refers to function mode which is normalized to unity at the center $z = 0$.

The parameter K (K1,K2) named the electrode shape, determined by the electrode geometry from K1 and K2 which is represented the coefficients of the electrode shape for cylindrical convex (K1) and cylindrical concave electrodes (K2) respectively are described as equations; [4,6]

$$K1 = 2\sin(\Gamma) / \ln(R/a) \qquad (3)$$

$$K2 = 4\sin(\Gamma) / \pi \qquad (4)$$

Where R is the radius of cylindrical convex electrode equal to [4]

$$R = 1.2\ a \qquad (5)$$

The effective lengths of the electrodes L_1 for convex electrodes, L_2 for concave electrodes are given by relations [1].

$$L_1 = \ell + 0.1056\, a \qquad (6)$$

$$L_2 = \ell + 0.451\, a \qquad (7)$$

Where ℓ is geometrical length of electrodes.

The Trajectory of Electron Beam

In the present work the polarities of each electrode of the x and y axes as shown in figure (1). Since the positive potential (+V_1) is applied on the x–axis electrodes of the lens, then the positively charged particles will be repelled along the x–axis and will be directed towards the z–axis. The positively charged particles will be attracted by the negative potential (–V_1) along the y–axis of the lens.

The trajectory equations in cartesian coordinates for the charged particles beam traversing the field of a quadrupole lens are given by [3]:

$$x'' + \beta^2 f(z)x = 0 \qquad (8)$$

$$y'' - \beta^2 f(z)y = 0 \qquad (9)$$

Where β is the excitation parameter given by the following relation [3].

$$\beta^2 = V_1 K / a^2 V_0 \qquad (10)$$

Where V_0 acceleration voltage, x'' and y'' are the second derivatives with respect to z [7,8].

Where $f(z)$ is the modified bell–shaped field model as in figure (2) represents the intermediate case between the rectangular section of constant maximum value $f(z)_{max} = 1$ in the region $-z_L \le z \le z_L$ and beyond these boundaries it terminates in the form of a half bell - shaped field represented by the following function [3].

$$f(z) = 1/[1+((z-z_L)/d)^2]^2 \text{ when } z > z_L \qquad (11)$$

$$f(z) = 1/[1+((z+z_L)/d)^2]^2 \text{ when } z < -z_L \qquad (12)$$

Where d is the axial extension of the field between the two points.

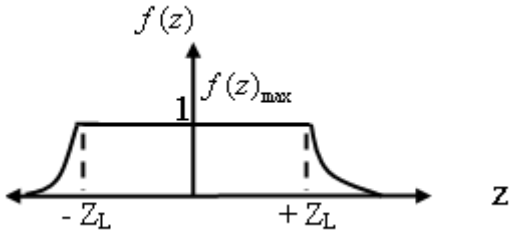

Figure 2. Field distribution of a quadrupole lens (Modified bell–shaped model) [15].

The Spherical aberration

The Spherical aberration is the name given to the effect where the focal length of a lens will vary depending on how far you are from the centre of the lens. What this means in reality is that a parallel rays of light entering the lens near its centre, will be focused less or more than a parallel ray entering near the edges of the lens. In a quadrupole lens, the spherical aberration in

the gaussian image plane can be expressed as [3,9] and [14].

$$\Delta x(zi) = M_x\ (C_s\ \alpha^3 + C_p\ \alpha\ \delta^2) \quad (13)$$

$$\Delta y\ (zi) = M_y\ (D_p\ \alpha^2\ \delta + D_s\ \delta^3) \quad (14)$$

Where α and δ are the image side semi–aperture angles in the x–z and y–z plane, respectively. The coefficients C and D characterize the aberration in the convergence and divergence plane, retrospectively. The coefficient C_s determines the aberration of the real width image in the plane y = 0, and D_s is that for the imaginary image in the plane of x = 0 [10].

The spherical aberration coefficients C and D are given by the forms [7].

$$C_s = \frac{d}{32\sin^4\psi_0}[(w_x^2-1)(w_x^2+3)\frac{\pi}{w_x^5} + \frac{2(7-w_x^2)}{4w_x^2-1}(\sin 2\psi_0 - \sin 2\psi_1) + (2-2n+3n^2)$$
$$(w_x^2-1)[(w_x^2-1)\frac{\pi}{w_x^5} - \frac{2}{4w_x^2-1}(\sin 2\psi_0 - \sin 2\psi_1)]] \quad (15)$$

And [7].

$$C_p = \frac{d}{32\,w_y^2\sin^4(\psi_0)}[[-4[(1-\cos(2\pi\frac{w_y}{w_x}))\ \sin(2\psi)_1 + w_y(1-\cos(2\psi_1)\ \sin(2\pi\frac{w_y}{w_x})]$$
$$+3(w_x^2-1)[-2(w_x^2-1)\frac{\pi}{w_x^3} + \frac{1}{w_x^2-1}[-\frac{w_y{}^2(w_x^2w_y^2+2)}{4w_x^2\,w_y^2-1}\sin(2\psi_0) + (w_y^2+3)$$
$$\sin(2\psi_1) + \frac{3w_y^2+1}{2w_y}\sin(2k\pi\frac{w_y}{w_x})] - \frac{3}{4w_x^2w_y^2-1}[(4w_y^2-1)\sin(2\psi_1)\cos(2\pi\frac{w_y}{w_x}) \quad (16)$$
$$+w_y(2w_y^2+1)\cos(2\psi_1)\ \sin(2\pi\frac{w_y}{w_x})]] + (2+2n-n^2)\ (w_x^2-1)[2(w_x^2-1)\frac{\pi}{w_x^3} -$$
$$\frac{4w_y^2(w_x^2-1)}{4w_x^2w_y^2-1}\sin(2\psi_0) + \sin(2\psi_1) - \frac{1}{2w_y}\sin(2\pi\frac{w_y}{w_x}) - \frac{1}{4w_x^2\,w_y^2-1}[(4w_y^2-1)$$
$$\sin(2\psi_1)\ \cos(2\pi\frac{w_y}{w_x}) + w_y(2w_y^2+1)\cos(2\psi_1)\sin(2\pi\frac{w_y}{w_x})]]]]$$

$$D_s = \frac{d(w_x^2-1)}{32\,w_y^4 \sin^4(\psi_0)}[-\frac{1}{3}[2\ (2+n)\,w_y\,(1-\cos(2\psi_1))\ (1-\cos(2\pi\frac{w_y}{w_x}))\ \sin(2\pi\frac{w_y}{w_x})$$
$$+(4-n)(\cos(4\pi\frac{w_y}{w_x})-4\cos(2\pi\frac{w_y}{w_x})+3)\ \sin 2\psi_1]-(w_y^2+3)\frac{\pi}{w_x}+$$
$$\frac{2w_y^4(5+w_x^2)}{(w_x^2-1)(4w_y^2-1)}\sin(2\psi_0)+\frac{1+w_x^2}{2}\sin(2\psi_1)+\frac{2}{w_y}\sin(2\pi\frac{w_y}{w_x})-\frac{w_x^2-1}{4w_y}$$
$$\sin(4\pi\frac{w_y}{w_x})-\frac{2}{w_x^2-1}[(w_y^2+1)\sin(2\psi_1)\cos(2\pi\frac{w_y}{w_x})+2w_y(\cos 2\psi_1)$$
$$\sin(2\pi\frac{w_y}{w_x})]-\frac{1}{2(4w_y^2-1)}[(5w_y^2+1)\sin(2\psi_1)\cos(4\pi\frac{w_y}{w_x})+2w_y(w_y^2+2)$$
$$\cos(2\psi_1)\sin(4\pi\frac{w_y}{w_x})]+\frac{1}{3}(2-2n+3n^2)\ (w_x^2-1)\ [\frac{3\pi}{w_x}+\frac{6w_y{}^4}{(w_x^2-1)(4w_y^2-1)}$$
$$\sin(2\psi_0)+\frac{2}{3}\sin(2\psi_1)-\frac{2}{w_y}\sin(2\pi\frac{w_y}{w_x})+\frac{1}{4w_y}\sin(4\pi\frac{w_y}{w_x})-\frac{2}{w_x^2-1}(\sin(2\psi_1)$$
$$\cos(2\pi\frac{w_y}{w_x})+w_y\cos(2\psi_1)\sin(2\pi\frac{w_y}{w_x}))-\frac{1}{2(4w_y^2-1)}(\sin(2\psi_1)\cos(4\pi\frac{w_y}{w_x}) \qquad (17)$$
$$+2w_y\cos(2\psi_1)\sin(4\pi\frac{w_y}{w_x})]]$$

Also [7].

$$D_P = C_P - \frac{d}{8\,w_y^2\sin^4(\psi_0)}[(1-\cos(2\pi\frac{w_y}{w_x}))\sin(2\psi_1)+w_y\ (1-\cos(2\psi_1)) \qquad (18)$$
$$\sin 2\pi\frac{w_y}{w_x}]$$

Where ψ_0 is the value corresponds to the position of the object and ψ_1 to that of the image, and $(n=-1)$ for electrostatic quadrupole lens.The properties of the quadrupole lens are characterized by the parameter [7].

$W_x = 1-\beta^2 d^2$ for the convergence plane (19)

$W_y = 1+\beta^2 d^2$ for the divergence plane (20).

The Limiting Resolution

The resolving power of any optical device is the ability to form two separate images of two point objects very close together. The theoretical limit of resolution of microscope is determined by the combined effect of chromatic and spherical aberrations. The practical resolution of any instrument also depends on the supplementary aberrations that arise from constructional defects, or the observer himself, or from mechanism of interaction between the beam

and the object to be observed. The resolution limit is given by equation [11].

$$R = 0.61\,(C\,\lambda^3)^{1/4} \qquad (21)$$

Where λ is the electron wavelength which is given by the form[11].

$$\lambda = \sqrt{\frac{1.5}{V_0}} \qquad (22)$$

Results and Discussion

The axial potential distribution ratio $(V(\theta)/V_1)$ represented in equation (1) is plotted as a function of theta, as shown in figure (3) ,it is found that very close to modified bell-shaped model by use quadrupole lenses of cylindrical convex and cylindrical concave electrodes. This result agrees with the results mentioned in various references such as [6,12,13], and [14].

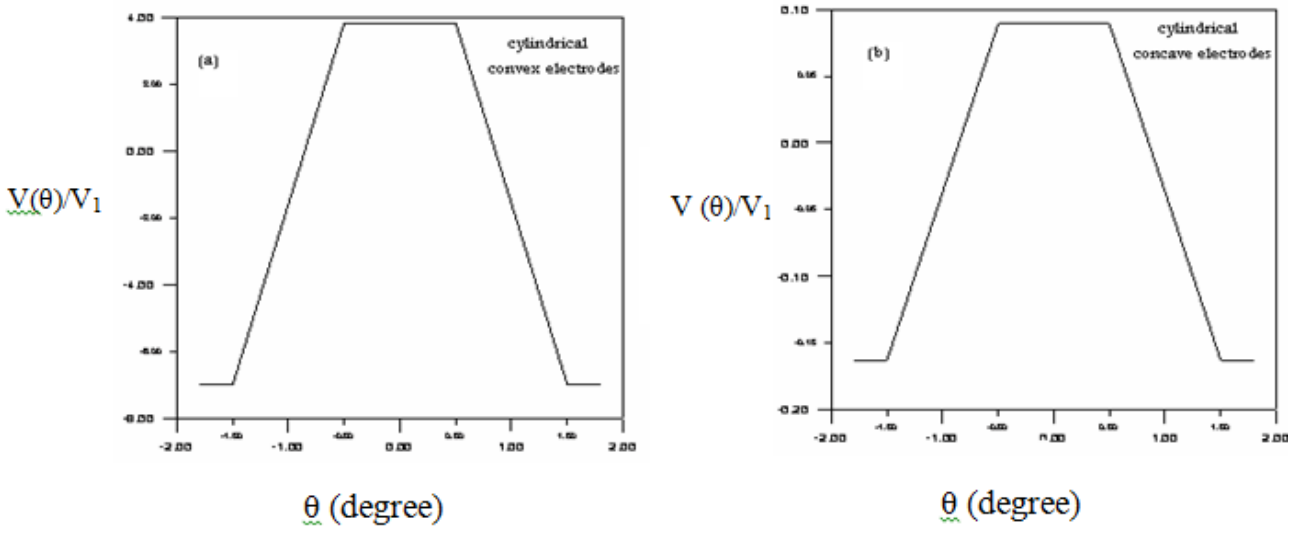

Figure 3. The axial potential distribution ratio $(V(\theta)/V_1)$ as a function of θ for electrostatic quadrupole lens with cylindrical (a)convex and (b) concave electrodes.

The values of K and β computed from equations (3), (4), and (10) are represented as a function of Γ as shown below in figure (4) which is illustrate in the increment in Γ leads to firstly increasing in K and β arriving to maximum values of K_1 =1.097 and $\beta_1 = 0.11$ mm^{-1} at $\Gamma = 45.55^\circ$ for concave electrodes and has the same behavior in convex electrodes with K_2 =1.273 and $\beta_2 = 0.038$ mm^{-1} at $\Gamma = 45.55^\circ$. Then drop to low values (decreases). The excellent agreement shown with other literatures Baranova and Yavor in [1].

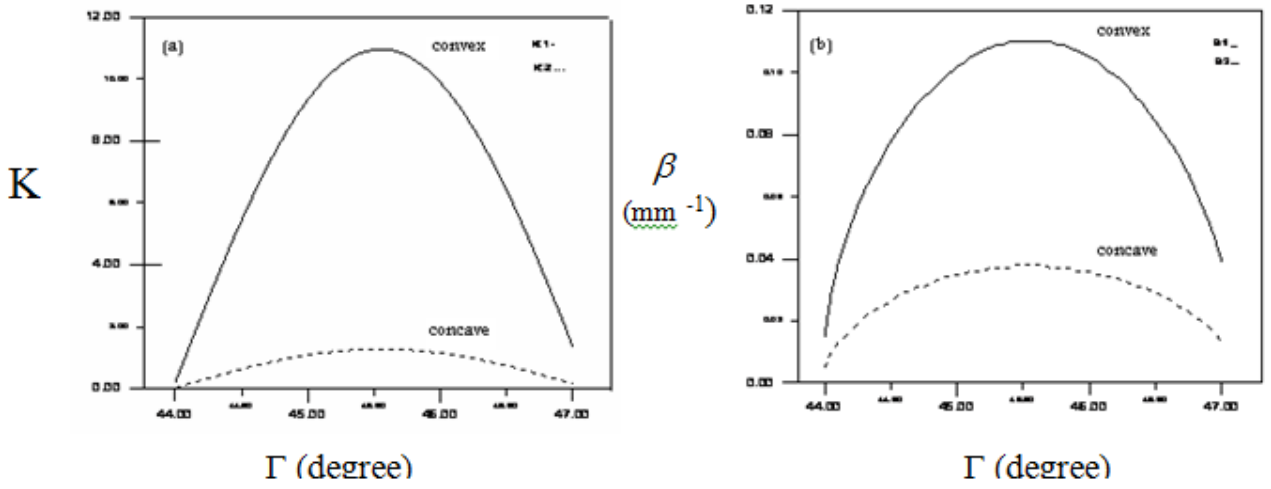

Figure 4. (a) The coefficient of electrode shape K , (b) the excitation parameter β as a function of gap angle Γ.

The trajectory equation of charge particles has been solved for the case of modified bell-shaped model by using simplified transformation for equations (8) and (9). When $\beta_1 = 0.11 mm^{-1}$, $\beta_2 = 0.038\ mm^{-1}$, and z = 5-20 mm in case modified bell-shaped model. These equations describe the paths of charge particles in convergence and divergence plane respectively. In electrostatic quadrupole lens charge particles incident in the (x-z) plane different paths from that in the (y-z) plane, as shown in figure (5). From figure (5) shows the charge particles in the convergence plane (x-z plane) is deflected toward the optical axis (z), while in the divergence plane (y-z plane) is away from the optical axis. i.e. the quadrupole lens is astigmatic, and the results is identify with that published by Baranova and Yavor in [1].

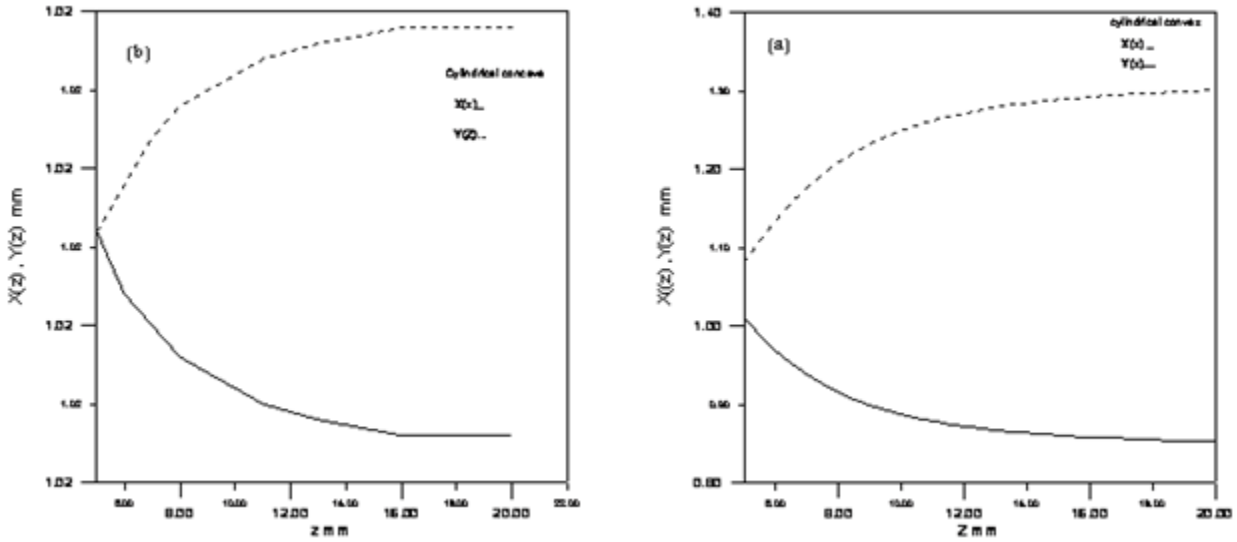

Figure 5. Trajectory of charge particles in electrostatic quadrupole lens with cylindrical (a) convex and(b) concave electrodes for both convergence (x−z) plane and divergence (y−z) plane.

The estimation of optimization for spherical aberration coefficients in both convergence and divergence plane improved the effects of changing the electrode angle and the electrode shape of these lenses on the objective properties (spherical aberration coefficients), as shown in figures 6 and 7, for convergence and divergence plane, respectively.

Figure 6 shows the proportionally relation between spherical aberration coefficient C_{p1}, C_{p2} ,C_{s1},C_{s2} , and Γ for the convergence plane in two electrode shapes, where the spherical aberration coefficient C_{p1} for the electrostatic quadrupole lens of cylindrical convex electrodes and C_{p2} the electrostatic quadrupole lens of cylindrical concave electrodes are decreasing in negative value as Γ is increasing and they have a minimum values $C_{p1} = -69.156$ and $C_{p2} = -14.284$ at $\Gamma = 45.55^{\circ}$.

The lowest absolute value of spherical aberration coefficients C_{p1},and C_{p2} are found after and before these minimum values.

The spherical aberration coefficients C_{s1}, and C_{s2} have the same behavior in all rang of gap angle Γ and the lowest absolute accurate values of these coefficients should be at range $44.5^{\circ} \le \Gamma \le 46.5^{\circ}$. The minimum absolute values of C_{s1} = 4.885 and C_{s2} = 1.885 at $\Gamma = 45.55^{\circ}$.

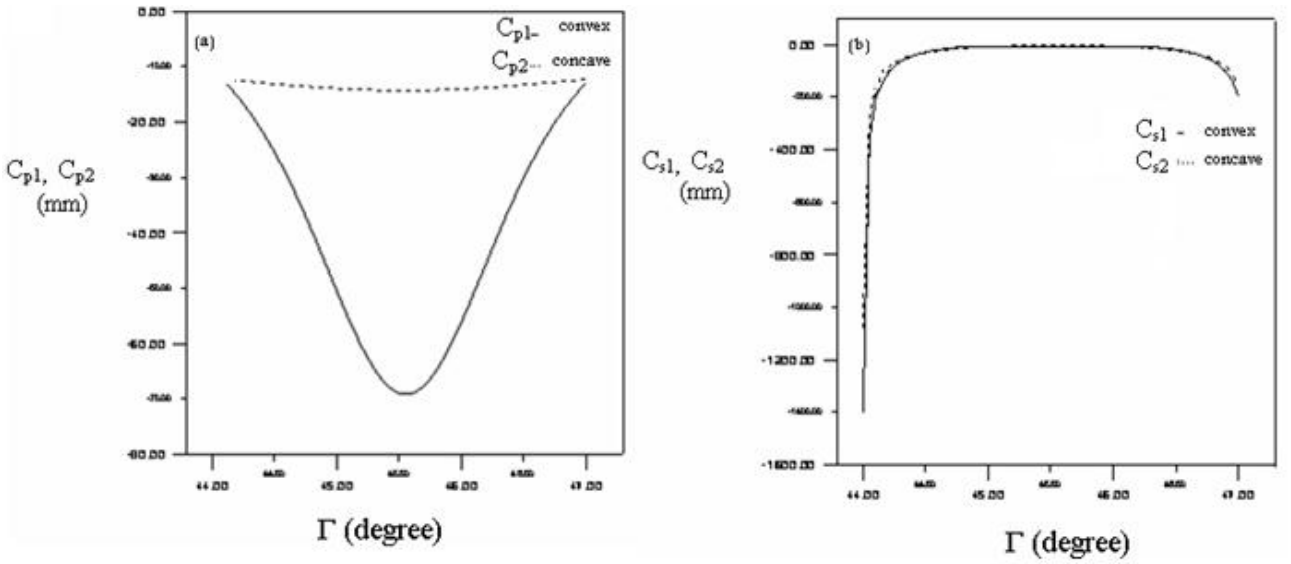

Figure 6. The spherical aberration coefficients (a) C_{p1} and C_{p2}, (b) C_{s1} and C_{s2} as a function of gap angle Γ.

The spherical aberration coefficients D_{p1} and D_{p2} in divergence plane represented as a function of Γ as shown in figure 7-a. According to figure 7-a we notice the values of D_{p1} are always positive and increasing with Γ up to maximum value (13.11) mm at Γ = 45° then happen slow drop then up to the same maximum value at Γ = 46.1°. Therefore drop sharply with increasing Γ. While, the values of D_{p2} are always negative and decreases in its absolute values with increment of Γ until (7.16) mm at Γ= 45.5°.then dropping with increasing Γ.

The last parameter of spherical aberration coefficients are D_{s1} and D_{s2} represented as a function of Γ shown in figure 7-b, which has the same behavior for all values of Γ. The values of D_{s1} and D_{s2} are always negative, and these values increases with Γ increases. These parameters be have as constant values at $\Gamma \geq 44.5^{\circ}$. The D_{s1} give us the better absolute value than D_{s2} which is 1.12 mm at Γ =45.55°.

One can be concluded from figures (6) and (7) that the variation of the four spherical aberration coefficients as a function of Γ, give us the best values for the cylindrical convex electrodes for whole range of Γ.

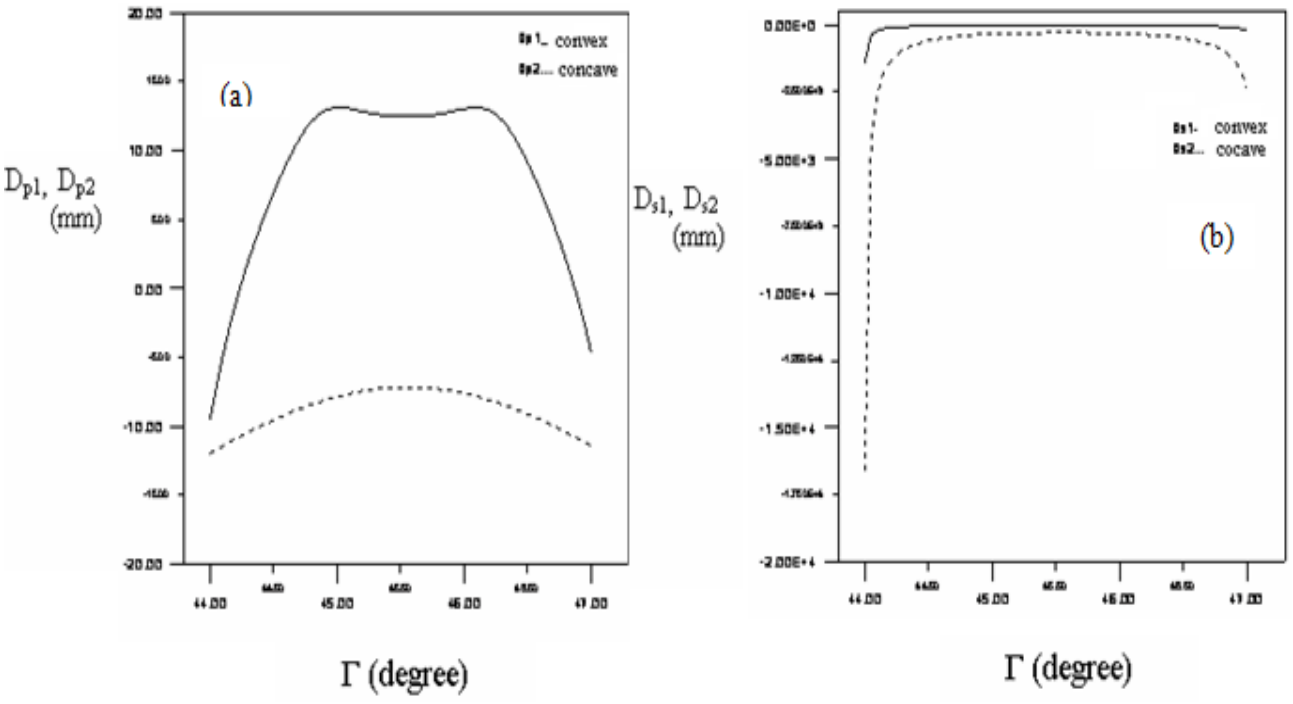

Figure 7. The spherical aberration coefficients of electrostatic quadrupole lens (a) D_{p1}, D_{p2}, and (b) D_{s1}, Ds2 as a function of gap angle Γ.

The resolution limit computes according to equation (21) and (22). Representing the resolution limits R_{cs1} and R_{cs2} as a function of Γ shown in figure (8-a), which has the same curve behavior with minimum values $R_{cs1} = 0.001$ nm at $\Gamma = 45.15^{\circ}$, and $R_{cs2} = 0.0029$ nm at $\Gamma = 45.55^{\circ}$.

While, the resolution limits R_{cp1} and R_{cp2} represented as a function of Γ shown in figure (8-b). The values of R_{cp1} increasing with increment Γ up to maximum values $R_{cp1} = 0.002$ nm, and the values of R_{cp1} increasing slowly with increasing Γ up to maximum values $R_{cp2} = 0.002$ nm, these maximum values happen at $\Gamma = 45.55$ and then drop with increasing Γ.

Representing the resolution limits R_{Ds1} and R_{Ds2} as a function of Γ shown in figure (9-a), which has approximately the same behavior with minimum values $R_{Ds1} = 0.00073$ nm, and $R_{Ds2} = 0.00292$ nm at $\Gamma = 45.55^{\circ}$. While the resolution limits R_{Dp1} and R_{Dp2} represented as a function of Γ shown in figure (9-b). The values of R_{Dp1} increasing with increment Γ up to maximum values $R_{Dp1} = 0.0013$ nm at $\Gamma = 45.05^{\circ}$, then happen slow drop and up to the same maximum value at $\Gamma = 46.05^{\circ}$, therefore, drop sharply with increasing Γ. Thus, the values of $R_{Dp}2$ decreasing with increasing of Γ until minimum values $R_{Dp2} = 0.01162$ nm at $\Gamma = 45.55^{\circ}$, then increasing these values with increasing Γ.

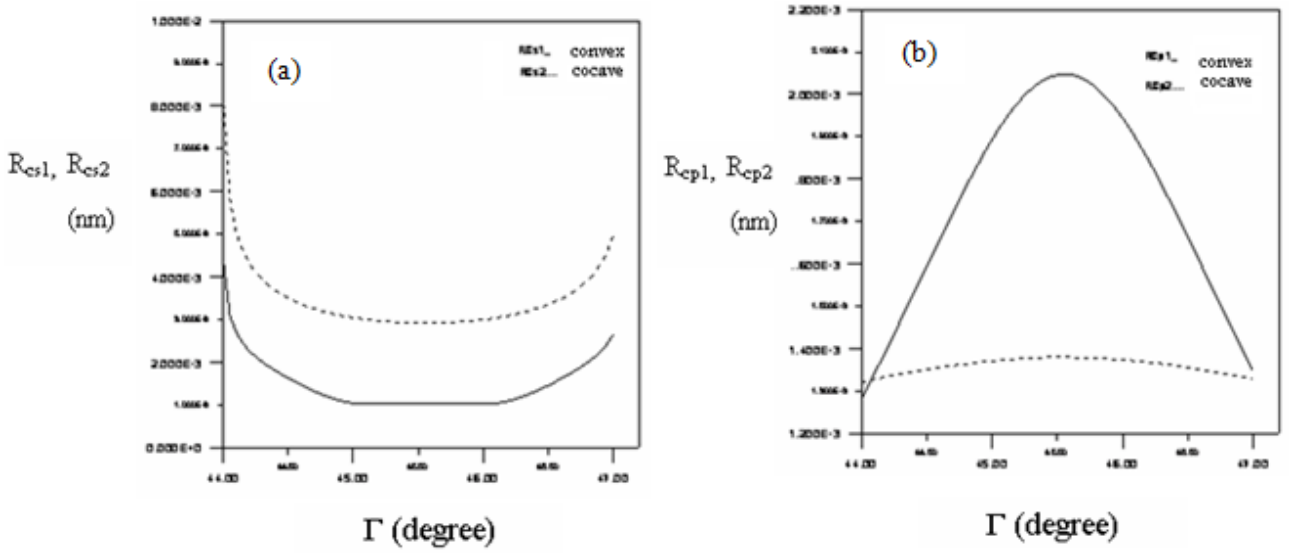

Figure 8. The resolution limit of electrostatic quadrupole lens (a) R_{cs1}, R_{cs2}, and (b) R_{cp1}, R_{cp2} as a function of gap angle Γ.

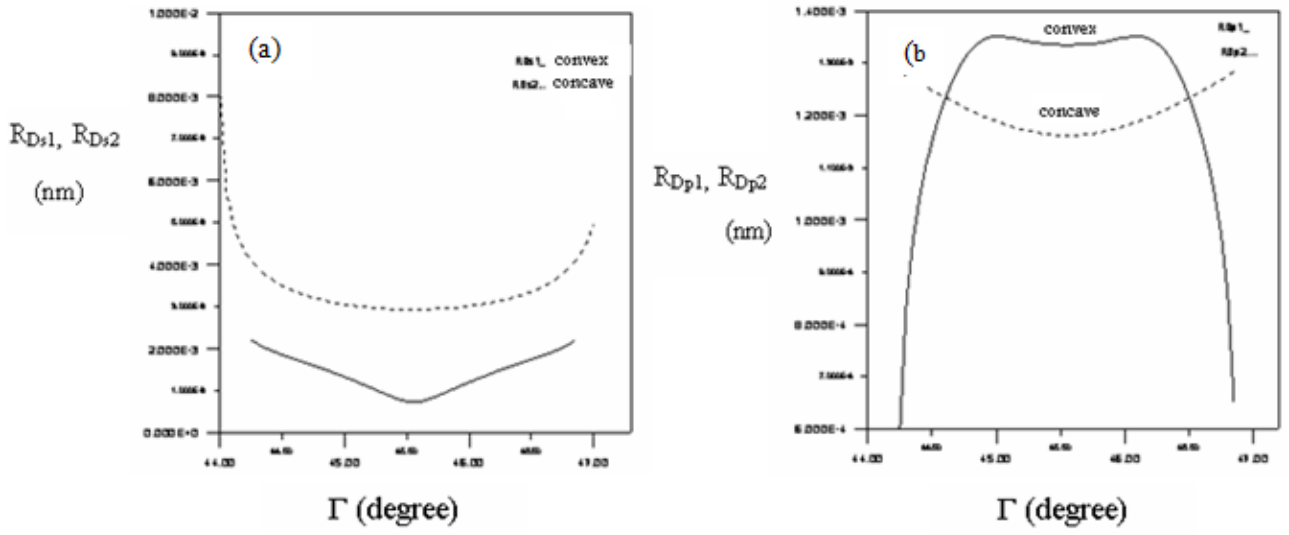

Figure 9. The resolution limit of electrostatic quadrupole lens (a)R_{Ds1}, R_{Ds2}, and (b) R_{Dp1}, R_{Dp2} as a function of gap angle Γ.

Conclusions

The quadrupole lens system has many variable geometrical and operational parameters; thus conclusive result is rather difficult. However, from the present investigation one may conclude the following:

a. It appears that the modified bell-shaped field model very close to the axial field distribution of the electrostatic quadrupole lens of concave and convex electrodes and it gives good properties.

b. In general, the electrostatic quadrupole lens of concave electrodes gives the best result of all spherical aberration parameters and resolution limit (or resolving power) than the electrostatic quadrupole lens of cylindrical convex electrodes.

References

1. Baranova, L. A. and Yavor, S.Ya. (1984), Electrostatic lenses, Sov.Phys.Tech.Phys., **29** (8),827-847.

2. S.Ya. Yavor, (1968) ,p.263 "Focusing of charged particles by Quadruple lenses ".

3. P.W. Hawkes, (1970), "Quadrupoles in electron lens design", Adv.Electronics and Electron Phys.Supplement 7, ed. L. Marton, (Academic Press, New York and London).

4. M. Szilagyi, (1988),"Electron and ion optics", (Plenum Press, New York).

5. Grime, G.W. and Watt, F. (1988),"Focusing protons and light ions to micron and submicron dimensions "Nuclear Instruments and Methods in Physics Research, B30, 227-234.

6. A. Kiss and E. Koltay, (1970),"Investigations on the effective length of asymmetrized quadrupole lenses", Nucl.Instrum. Meth.78, 238-244.

7. A. D. Dymnikov, T. Ya. Fishkova and S.Ya. Yavor, (1965), "Spherical aberration of compound quadrupole lenses and systems ", Nucl. Instrum. Meth., 37, 268-275.

8. P. Grivet, (1972),"Electron Optics", (Pergamon Press, Oxford and New York).

9. Okayama, S. (1989), "Electron beam lithography using a new quadrupole triplet", SPIE, Electron-beam, X-ray, and Ion-beam Tectnology: Submicrometer Lithographies VIII, **1089**, PP 74-83.

10. Fishkova, T. Ya., Baranova, L. A., and Yavor, S. Ya. (1968), "Spherical aberration of stigmatic doublet of quadrupole lenses" (rectangular model).Sov.Phys.Tech.Phys.,13 (4),520-525.

11. P.W. Hawkes, (1972), " Electron optics and electron microscopy", Taylor & Francis LTD, (10-14 Macklin Street London WC2B5NF).

12. T. Hayashi and N. Sakudo, (1968), " Quadrupole field in circular concave electrodes ", Rev. Sci. Instrum., 39 (7),958-961.

13. S. Okayama and H. Kawakatsu, (1978), "Potential distribution and focal properties of electrostatic quadrupole lenses", J. Phys.E: Sci. Instrum., 11, 211-216.

14. Oday A. Hussein, (2009), "Determination of the most favorable shapes for the electrostatic Quadrupole " , J. Al-Nahrain University, Science , 12 (3), 86-93.

15. Hawkes, P.W. (1965/1966), "The electron optics of a quadrupole lens with triangular potential", Optik, 23, 145-168.

16. L.R. Burns et al. (2007), "Evaluation of a novel design for an electrostatic quadrupole triplet ion beam lens", Nucl. Instr. and Meth. B.04.215

Feature Extraction Using Discrimination Power Analysis with Palmprint in Biometric System

Suhiar M. Zeki

Computer Science department, University of Technology

Abstract

There are many methods used to distinguish persons from each other using palmprints, fingerprints, giats, hand geometry, sound waves, shape of the ear, the color of the eyes and the iris, …etc. Discrimination power analysis (DPA) is powerful to extract proper feature for palmprint, after applying (DPA) on the true color image of palmprint, some of the features and coefficients are choosing to construct vectors including these value of features. DPA is a statistical analysis, based on the image coefficients properties after sequence of process on the true color image. The discrimination power of all the coefficients is not the same and some of them are discriminant than others, the higher true of recognition rate depend on feature vectors of Discriminant Coefficient (DCs). It searches for the coefficients which have large power to discriminator different classes better than other, the performance based on (DPA) and selected (DCs) is better with less complexity.

Keywords: Palmprints, Fingerprints, DPA, DCs.

استخراج الميزة باستخدام تحليل قوة التمييز مع بصمة راحة اليد في النظام البيومتري

الخلاصة:

هناك العديد من الطرق المستخدمة للتمييز بين الأشخاص من بعضهم البعض باستخدام النخيل وبصمات الأصابع، المشيات، هندسة اليد، الموجات الصوتية، شكل الأذن، ولون العينين والقزحية، ... الخ. التمييز تحليل السلطة قوية لاستخراج سمة المناسبة للطباعة النخيل، بعد تطبيق (د ب أ) على الصورة اللون الحقيقي للطباعة النخيل، وبعض من ملامح ومعاملات يختارون لبناء ناقلات بما في ذلك هذه القيمة من الميزات. DPA هو التحليل الإحصائي، استنادا إلى خصائص الصورة معاملات بعد سلسلة من عملية على الصورة اللون الحقيقي. قوة التمييز من جميع معاملات ليست هي نفسها وبعضها تميز من غيرها، وارتفاع معدل الحقيقي للاعتراف تعتمد على ناقلات سمة من سمات تميز معامل (DCS). فإنه يبحث عن معاملات التي لها قوة كبيرة لفئات مختلفة الممي أفضل من الأخرى، وعلى أساس الأداء (DPA) واختيار (DCS) هو أفضل مع أقل التعقيد.

Introduction

Biometric is derived from the Greek words "bio" (life) and "metrics" (to measure). It is the science of establishing the identity of an individual based on the physical, chemical or behavioral attributes of the person [1].

The palms of the human hands contain pattern of ridges and valleys much like the fingerprints [10]. In general the biometrics in figure 1 is divided to:

A. Physiological techniques:

It is measure the physiological characteristics of a person example include fingerprint verification, palmprint analysis, iris analysis, facial analysis, hand geometry, vein geometry, DNA (*Deoxyribonucleic acid*) pattern analysis, ear recognition, …etc.

B. Behavioral techniques:

It is cannot be easily transferred between individuals. Further, it represents as unique an identifier as is possible at this time. Voice patterns or speech analysis, handwritten Signature, keystroke sequences analysis, gait (the body movement while walking).

The palmprint system is a hand-based biometric technology. The palmprint is concerned with the inner surface of a hand. Many features in figure (2) of a palmprint can be used to uniquely identify a person, including

a. Geometry Features: According to the palm's shape, such as width, length and area.

b. Principal Line Features: Both location and form of principal lines in a palmprint are very important physiological characteristics for identifying individuals because they vary little over time.

c. **Wrinkle Features**: there are many wrinkles which are different from the principal lines in that they are thinner and more irregular.

d. **Delta Point Features**: it is defined as the center of a delta-like region in the palmprint. Usually, there are delta points located in the finger-root region.

e. **Minutiae Features**: A palmprint is basically composed of the ridges, allowing the minutiae features to be used as another significant measurement.

Biometric system module

Palmprint recognition falls under the general category of pattern recognition problem. There are three stages in palmprint recognition problems, ***palmprint segmentation from an image, feature extraction and classification***.

Palmprint segmentation

We consider number of steps to obtain distinguish all features of palmprint.

Transform True Color to Gray image

The color space in Phase Alternating Line (PAL) TV-Standard System is represented by YUV, where Y represents the luminance and U and V represent the two color components [2]. The luminance Y can be determined from the red-green-blue (RGB) model via the following relation:

For completeness, the transform equation from expression of RGB to YUV are listed below [6]:

$$\begin{pmatrix} Y \\ U \\ V \end{pmatrix} = \begin{pmatrix} 0.299 & 0.587 & 0.114 \\ -0.147 & -0.289 & 0.436 \\ 0.615 & -0.515 & -0.100 \end{pmatrix} \begin{pmatrix} R \\ G \\ B \end{pmatrix} \quad \text{.....(1)}$$

$$Y = 0.299\ R + 0.587\ G + 0.114\ B \text{.....(2)}$$

It is noted that the three weights associated with the three primary colors, R, G, and B, are not the same. There different magnitudes reflect the different responses of the HVS to different primary colors.

Gray-scale images are referred to as monochrome, or one-color, images. They contain brightness information only, no color information. The number of bits used for each pixel determines the number of different brightness levels available. The typical image contains 8 bits/pixel data, which allow us to have 256 (0-255) different brightness (gray) levels [4].

Enhancement Image

It is techniques improve the quality of an image as perceived by a human. There exists a wide variety of techniques for improving image quality [3]. In image processing it is usually necessary to perform a high degree of noise reduction in an image before performing higher-level processing steps, such as edge detection. The median filter is a non-linear digital filtering technique,

often used to remove ***noise*** from images or other signals, the mask of filter is represent in table 1**[5]**.

Edge Detection

Edge detection is a fundamental tool in image processing and computer vision, particularly in the areas of feature detection and feature extraction.

There are three fundamental steps performed in edge detection **[6]**:

- Image smoothing for noise reduction
- Detection of edge points.
- Edge Localization

We using the sobel edge detection mask look for edges in both the horizontal and vertical directions and then combine this information into a single metric. The masks are as follows in figure 3:

These masks are each convolved with the image. At each pixel location we now have two numbers: **d1**, corresponding to the result from the row mask, and **d2**, from the column mask we use these numbers to compute two metrics, the edge magnitude and the edge direction, which are defined as follows **[7]**.

Edge magnitude

$$E = \sqrt{d1^2 + d2^2} \quad \text{.....} \quad (4)$$

Edge direction

$$E1 = \tan^{-1}\left[\frac{d_1}{d_2}\right] \quad \text{.....} \quad (5)$$

Binary Image

The digital image I(x,y) is represented as a two-dimensional array of data, where each pixel value corresponds to the brightness of the image at the point (x,y). Binary images are the simplest type of images and can take on two values, typically black and white, or '0' and '1'. A binary image is referred to as a 1 bit/pixel image because it takes only 1 binary digit to represent each pixel **[5]**.

The basic of intensity thresholding, composed of light object on a dark background, in such a way that object and background pixels have intensity values grouped into two dominant modes. One obvious way to extract the objects from the background is to select a threshold, ***T***, that separates these modes. Then, any point (x, y) in the image at which f(x,y)>**T** is called an object point; otherwise, the point is called a background point. In other words, the segmented image, g(x, y), is given by

$$g(x,y) = \begin{cases} 1 \text{.....} if & f(x,y) > T \\ 0 \text{.....} if & f(x,y) \le T \end{cases} \text{.....} (6)$$

Thinning

Thinning is a morphological operation that is used to remove selected foreground pixels from binary images, somewhat like erosion or opening. It is normally only applied to binary images, and produces another binary image as output. The thinning operation is related to the hit-and-miss transform [8].

An important approach for representing the structural shape of a plane region is to reduce it to a graph. This is often accomplished by obtaining the skeleton of the region via a thinning. (also called Skeltonizing) algorithms **[6]**.

The erosion equation:

$$A \ominus B = \{z | (B)z \cap A^C = \emptyset$$

The set of opening:

$$A \circ B = (A \theta B) \oplus B$$

Thinning procedures play a central role in a broad range of problems in image processing. This algorithm is present for thinning binary regions. In the following discussion it is assumed that region points have value **1** and background points have value **0**. The method consists of successive passes of two basic steps applied to the contour points of the given region. Where a contour point is any pixel with value **1** and have at least one 8- neighbor valued **0 [9]**.

P_0	P_2	P_3
P_8	P_1	P_4
P_7	P_6	P_5

Figure 4. Neighborhood arrangement used by the thinning algorithm.

The first step flags a contour point P for deletion if the following conditions are satisfied:

a) $2 \leq N(P_1) \leq 6,$

b) $S(P_1) = 1,$

c) $P_2 \cdot P_4 \cdot P_6 = 0,$ .....(7)

d) $P_4 \cdot P_6 \cdot P_8 = 0,$

Where $N(P_1)$ is the number of nonzero neighbors of P_1 :that is:-

$$N(P_1) = P_2 + P_3 + \ldots + P_8 + P_9 \quad \ldots\ldots (8)$$

And S (P_1) is the number of 0-1 transitions in the ordered sequence of P_2, P_3, ..., P_8,P_9.

In the second step, conditions a and b remain the same, but conditions c and d are changed to

c') $P_2 \cdot P_4 \cdot P_8 = 0,$ .....(9)

d') $P_2 \cdot P_6 \cdot P_8 = 0.$

Feature extraction

The stage of feature extraction is very important as it ultimately determines the performance of a recognition system.

After first stage, we obtain matrix in form two dimensional of data has been obtained, it is represent active data in palmprint image. We applied Discrimination Power Analysis (DPA) algorithm has been applied on the image to find feature extraction.

Discrimination power analysis (DPA)

The coefficient of DP depends on two properties:

1. Large variation between the classes.
2. Small variation within the classes.

The coefficient matrix for the image size of i×j

$$I = \begin{bmatrix} I_{11}\ I_{12} \dots\dots I_{1j} \\ I_{21}\ I_{22} \dots\dots I_{2j} \\ \dots\dots\dots\dots\dots\dots \\ \dots\dots\dots\dots\dots\dots \\ I_{M1}\ I_{M2} \dots\dots I_{ij} \end{bmatrix} \dots 10$$

To find discrimination power having C classes and S training images for each class, totally C × S training images are present. DP of each coefficient (I_{ij})

i=1, 2, 3,….M , j=1, 2, 3 ,…N can be estimated as follows:

1. Construct the train set matrix A_{ij}.

$$A_{ij} = \begin{bmatrix} I_{ij}(1,1)\ I_{ij}(1,2) \dots\dots I_{ij}(1,C) \\ I_{ij}(2,1)\ I_{ij}(2,2) \dots\dots I_{ij}(2,C) \\ \dots\dots\dots\dots\dots\dots\dots\dots \\ I_{ij}(S,1)\ I_{ij}(S,2) \dots\dots I_{ij}(S,C) \end{bmatrix}_{S\times C} \dots\dots\dots 11$$

C: No of Class.

S: No of Samples

2. Calculate the mean value of each class:

$$M_{ij}^{c} = \frac{1}{S}\sum_{d=1}^{S} A_{ij}(d,C), \quad c = 1,2,\dots.C \quad \dots\dots.12$$

3. Calculate variance of each class:

$$V_{ij}^{c} = \sum_{d=1}^{S}(A_{ij}(d,C) - M_{ij}^{c})^2, \ c = 1,2,\dots\dots C \quad \dots 13$$

4. Average the variance of all the classes:

$$V_{ij}^{w} = \frac{1}{C}\sum_{e=1}^{C} V_{ij}^{e} \quad \dots\dots 14$$

5. Calculate the mean value of the all training samples:

$$M_{ij} = \frac{1}{S*C}\sum_{d=1}^{C}\sum_{e=1}^{S} A_{ij}(d,e) \dots\dots\dots\dots 15$$

6. Calculate the variance of all the training samples:

$$V_{ij}^{B} = \sum_{d=1}^{C}\sum_{e=1}^{S}\left(A_{ij}(e,d) - M_{ij}\right)^2 \dots\dots\dots 16$$

7. Estimate the DP for location (I, j):

$$D(i,j) = \frac{V_{ij}^{B}}{V_{ij}^{W}}, \quad 1 \le i \le M, \ 1 \le j \le N \dots\dots 17$$

8. The maximum recognition rate by using the coefficient that has the maximum discrimination power and take 32 of maximum values of

discriminator power in figure (9), to save and compression in DB.

System Model (block diagram)

Classification

For classification the extracted features of the palmprint image has been compared with the ones stored in a palmprint database. After doing this comparison, palmprint image is classified as either known or unknown.

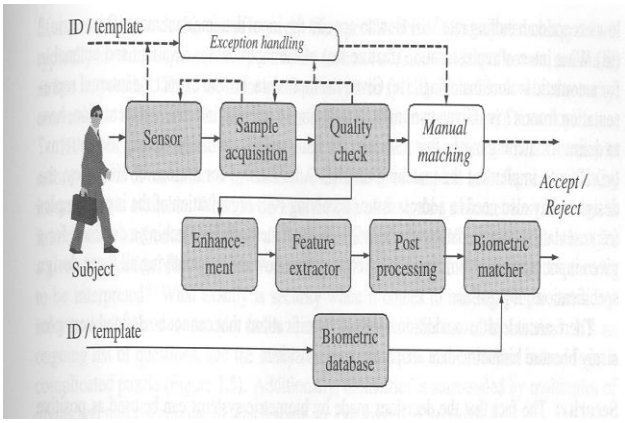

Figure 1. A generalized diagram of a biometric system [1].

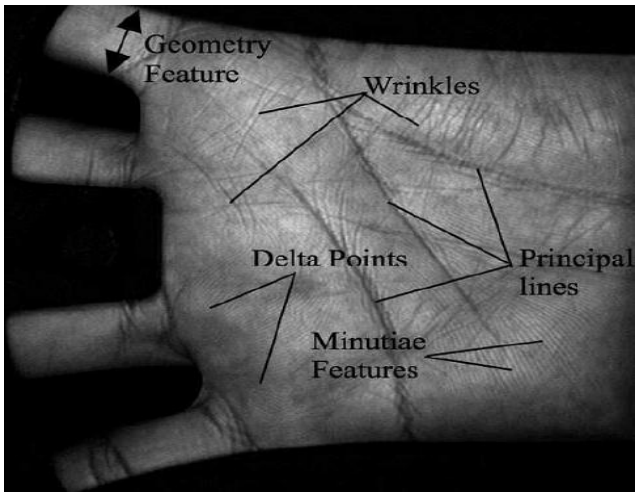

Figure 2. Illustrates some major features that can be observed on a palm [11].

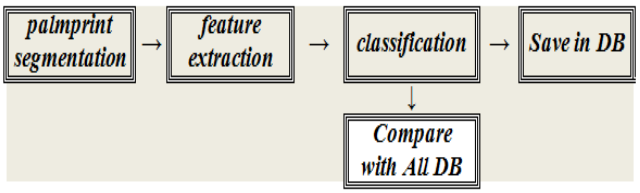

Figure 4. Block diagram of biometric system module.

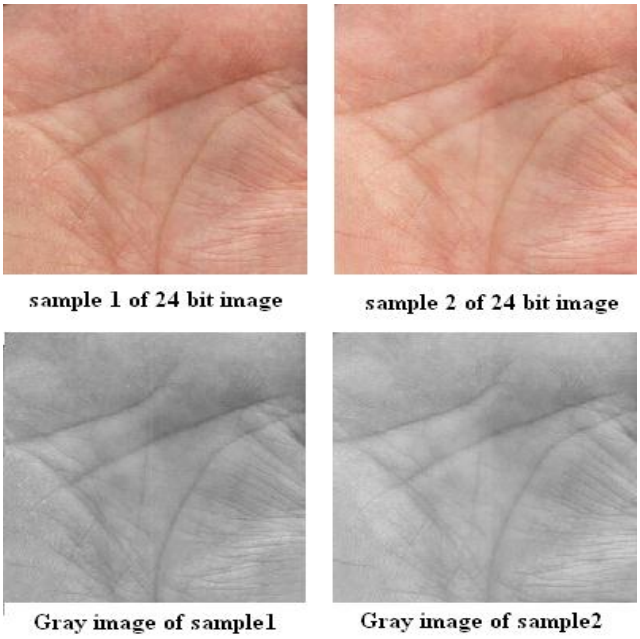

Figure 5. Transform true color to gray image

Table 1. It is mask of median filter.

1	1	1
1	8	1
1	1	1

Row mask

$$\begin{pmatrix} -1 & -2 & -1 \\ 0 & 0 & 0 \\ 1 & 2 & 1 \end{pmatrix}$$

Column mask

$$\begin{pmatrix} -1 & 0 & 1 \\ -2 & 0 & 2 \\ -1 & 0 & 1 \end{pmatrix} \quad \text{.....(3)}$$

Figure 6. Edge detection mask.

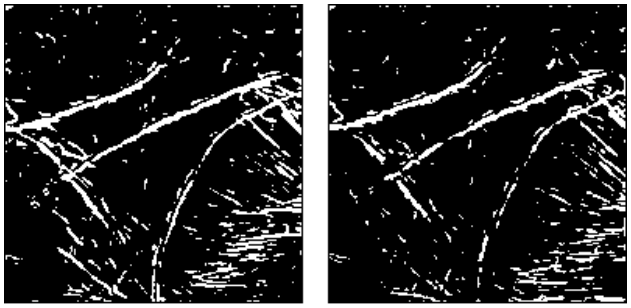

Edge detection of sample 1 Edge detection of sample 2

Figure 7: Edge detection and binarization of two samples.

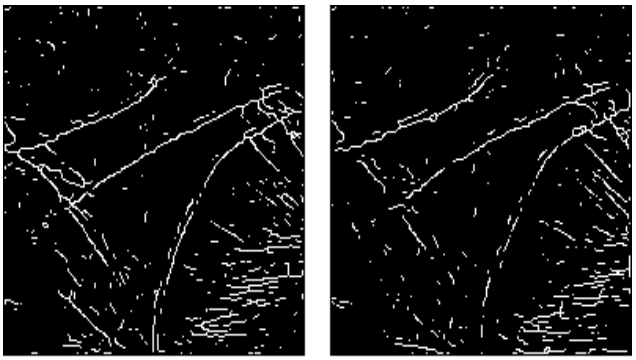

Thinning of sample 1 Thinning of sample 2

Figure 8. Thinning of two samples.

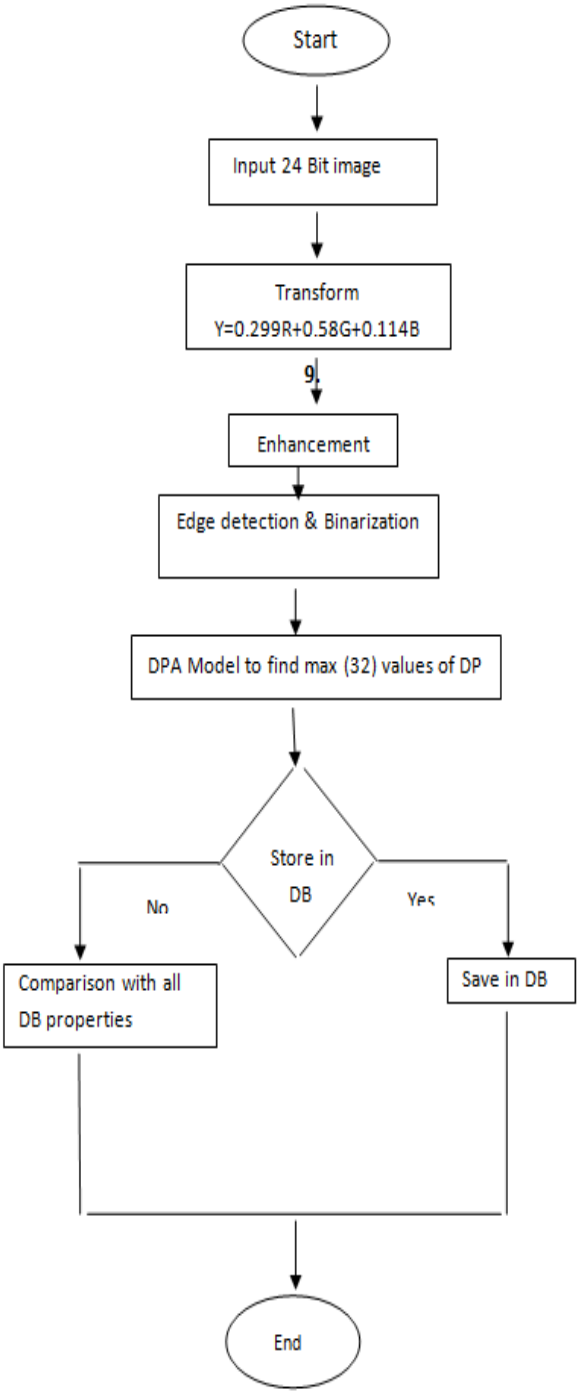

Figure 3. Flowchart of Process.

.91	.2	.08	.66	.87	.78	.65	.22	.74	.12	.34	.89	.1	.74	.23	.02
.12	.8	.65	.87	.7	.77	.32	.34	.55	.77	.74	.88	.34	.55	.65	.35
.74	.88	.98	.33	.65	.66	.44	.21	.84	.32	.55	.44	.36	.84	.65	.75
.55	.24	.44	.78	.23	.44	.32	.17	.23	.65	.84	.23	.35	.89	.76	.32
.84	.04	.23	.89	.34	.45	.08	.43	.12	.32	.22	.23	.54	.46	.22	.43
.77	.76	.23	.44	.9	.24	.32	.17	.23	.45	.23	.55	.66	.98	.21	.9
.93	.56	.33	.43	.19	.12	.87	.66	.56	.23	.54	.12	.76	.78	.32	.04
.98	.46	.22	.87	.54	.23	.7	.89	.66	.87	.67	.08	.33	.44	.45	.04
.56	.98	.21	.7	.65	.92	.65	.44	.87	.7	.77	.44	.22	.23	.66	.76
.87	.34	.67	.65	.32	.76	.66	.78	.3	.65	.88	.32	.17	.23	.33	.55
.45	.42	.08	.44	.94	.01	.44	.75	.55	.12	.65	.21	.74	.76	.43	.44
.12	.67	.90	.65	.02	.33	.32	.17	.23	.92	.55	.34	.95	.66	.65	.32
.78	.21	.12	.32	.32	.44	.12	.6	.45	.34	.46	.22	.84	.54	.32	.54
.98	.32	.55	.67	.89	.44	.34	.22	.83	.11	.98	.21	.32	.22	.12	.78

Figure 9. (32) Max value of discrimination power.

References

1. Anil K. Jain, Arun A. Ross and Patrick Flynn,(2004) “Hand Book of Biometrics”, USA.
2. Ghanbari, M.;(2003) "Standard Codecs: Image Compression to Advanced Video Coding"; Magazine of the Institution of Electrical Engineers; London United Kingdom.
3. Jensen. J.R. (1996). Introduction To Digital Image processing: A Remote Sensing Perspective Practice Hall, New Jersey, 1996.
4. Pitas. I and A.N.vent sanopoulos(1990) "Digital image processing: Principle & Applications" KLuwer Academic.
5. A Zriel Rosenfeld,(1969) Picture Processing by computer, New York: Academic Press, available at: http://en.wikipedia.org/wiki/Digital – image – processing # history.
6. Gonzalez, R., and Woods, R.(2008) "Digital Image Processing"; Pearson Education International; Prentice Hall; Inc.; 3rd Edition; New Jersey.
7. Unbaugh, S.E.(1998) "Computer Vision and Image Processing: A practical Approach using CVIP tools", Prentice Hall PTR.
8. Jain. A. Fundamentals of Digital Image Processing, Prentice-Hall, 1989, Chap. 9.
9. Zhang, T.Y. and Suen, C.Y.1984. "A Fast Parallel Algorithm for Thinning Digital Patterns," Comm. ACM, vol. 27, no.3, pp. 236-239.
10. Zunkel. D.,(1999) Hand Geometry Based Authentication. In A. K. Jain, R. Bolle, and S, Pankanti, editors, Biometrics: Personal Identification in Networked Society, page 87-102, Kluwer Academic Publishers, London, UK.

11. Im S. K., Park H. M., Kim. Y. W, Han. S, C, Kim S. W., and Kang. C, H.,(2001) An biometric identification system by extracting hand vein pattern, Journal of the Korean Physical Society, 38(3):268−272.

Study of Lipids Disorder in sera of Patients with Type II Diabetes Mellitus in Diyala

Zuhair Maroof Hussien[1], Yasmine Sami Nassir[1], Dawood Salman Al-Azzawi[2]

[1]Department of Biochemistry, College of Medicine, University of Diyala.

[2]Department of Pediatric, College of Medicine, University of Diyala.

Abstract:

Diabetes mellitus has been known to associate with lipid disorders and cardiovascular complication. This study was carried out to determine the changes in serum lipid profile in type 2 diabetic patients. Lipid profile was measured in sera of thirty males and females type-2 diabetic patients who attend Baqubah Educational Hospital in Diayla province and compared with thirty healthy of matched age and sex, as control group. The result indicate the presence of significant increase in serum TG ($p < 0.0001$), TC ($p < 0.0001$), LDL-C ($p < 0.0001$), and VLDL-C ($P < 0.0001$). Serum HDL-C levels were significantly decreased ($p < 0.0001$) in type 2 diabetic patients. In conclusion several lipid abnormalities were found in type 2 diabetes mellitus.

Key words: Diabetes Mellitus type 2, lipid profile, lipid abnormalities, hyperlipidaemia.

دراسة اضطراب الدهون في مصول دم المرضى المصابين بداء السكري(النوع الثاني) في محافظه ديالى

زهير معروف حسين ، ياسمين سامي ناصر ، داود سلمان العزاوي

الخلاصة:

من المعروف ان مرض السكري يقترن مع عدم انتظام الدهون ومشاكل امراض القلب. تم في الدراسة الحالية تعيين التغيرات في مستوى الدهون في مصول المرضى المصابين بمرض السكري الذين تتراوح اعمارهم من (45-65) سنة .

وقد تم قياس مستوى الدهون في مصل 30 مريض بداء السكري(النوع الثاني) من كلا الجنسين في مستشفى بعقوبة التعليمي في محافظة ديالى وتم مقارنتها مع 30 من عينات السيطرة الاصحاء من كلا الجنسين وباعمار مقاربة.

اشارت النتائج الى وجود زيادة معنوية في مستوى الكولسترول ، الدهون الثلاثية ، البروتين VLDL(P<0.0001) والبروتين الدهني منخفض الكثافة جداLDL الدهني منخفض الكثافة

HDL(P<0.0001) في حين ان هناك انخفاض معنوي في مستوى البروتين الدهني عالي الكثافة

في مصل الدم للمرضى المصابين بداء السكري(النوع الثاني).

Introduction

Diabetes Mellitus is a metabolic disorder characterized by chronic hyperglycemia and disturbances of carbohydrate, fat and protein metabolism associated with absolute or relative insulin deficiency. Diabetes Mellitus is two types: Type I and Type II [1].

Type II Diabetes Mellitus is a heterogeneous condition characterized by the presence of both impaired insulin secretion and insulin resistance [2]. It is one of the most common chronic diseases in the world, and the number of patients with Diabetes Mellitus has risen sharply in recent years [3].

Diabetes Mellitus may be associated with a number of complications including diabetic nephropathy, neuropathy, retinopathy, diabetic foot, macrovascular and microvascular diseases [4]. Type II Diabetes Mellitus considered as independent risk factor for coronary artery disease and risk of coronary disease is three to four fold increases in patients with Diabetes compared with non-diabetic population and

60-80% of Type II diabetics are obese [5]. The lipid abnormalities in patients with diabetes are probably playing important role in the development of atherogenesis. These lipid disorders include not only quantitative but also qualitative abnormality of lipoproteins which are potentially atherogenic [6]. Quantitative abnormalities include increased levels of total plasma cholesterol, triglyceride and low-density lipoprotein (LDL) cholesterol, and decreased level of high density lipoprotein (HDL) cholesterol. Qualitative abnormalities include change in the composition of LDL-cholesterol (small dense LDL-cholesterol, increase triglyceride content and increase electronegativity of LDL-cholesterol). These changes make LDL-cholesterol susceptible to oxidation and glycation with consequential foam cell formation, endothelial dysfunction and atherosclerosis [7]. Triglyceridemia has been associated with increased risk of coronary heart disease both in non-diabetic and Type II diabetic subjects. Remnants of triglyceride rich lipoproteins seem to be extremely atherogenic. LDL-cholesterol is related to life style factors such as diet and exercise. It has associated with metabolic syndrome [8]. The determination of the serum lipid levels in people with diabetes is now considered as a standered of the diabetes care and the measurement of the lipid profile of diabetic patients is needed to investigate how there lipid metabolism is affected by diabetes, as they have different genetic composition and life styles [9]. This study was carried out to compare between the lipid profile of patients with Type II Diabetes Mellitus and healthy peoples.

Materials and Methods

Patients with Type II Diabetes Mellitus were included in this study. Thirty diabetic patients (15 males and 15 females) treated with diabetic medication which does not have any side effects on lipid profile and thirty healthy controls (15 males and 15 females) were randomly selected and they examined for lipids abnormality. The patients who were enrolled in this study were selected from Type II diabetic patients who were attending Baqubah Educational Hospital in Diayla provinc. The age group selected was 45 to 65 years for both diabetic patients and healthy control.

Five to ten milliliters of blood were collected in tubes without anticoagulants. The blood samples allowed to clot at room temperature for one hour and were obtained by centrifugation at (3000xg) for 10 minutes and the collected serum was transferred into plain tube for lipid profile measurement.

Parameters that were measured include: Cholesterol, Triglyceride (TG), High density lipoprotein (HDL), Low density lipoprotein (LDL) and Very low density lipoprotein (VLDL).

Total cholesterol and triglyceride (TG) were determined by an enzymatic colorimetric method (Linear Chemicals. S. L.) [10,11]. HDL-cholesterol was measured enzymatically in the supernatant after the selective precipitation of apoliprotein B-containing lipoproteins (VLDL , LDL and (a) Lpa) by phosphotungstic acid /magnesium chloride solution and centrifugation (Linear Chemicals. S.L.) [12].

Low density lipoprotein (LDL) cholesterol was calculated by using Friedewald formula [13]:

LDL-cholesterol (mmol/L) = total cholesterol-HDL-cholesterol-TG/2.2 (mmol/L)

VLDL concentration is calculated by Fiancis formula:

VLDL (mmol/L) = TG/2.2

The values of all the parameters were given in mmol/L and they were described in terms of mean ± SD .The statistical significance of the deference between the control and study groups were evaluated by the t-test; a level of $p<0.0001$ was considered as statistically significant.

Results and Discussion

The mean ± SD of total cholesterol, TG, HDL-C, LDL-C, and VLDL-C of diabetic patients and control subject are shown in table 1.

Type 2 diabetic males and females showed statistically significant increase in the levels of serum TC, serum TG, serum LDL-C, VLDL-C ($P < 0.0001$) when compared to control subject, while serum HDL-C levels showed statistically significant reduced ($p < 0.0001$).

Table 1. Level of cholesterol, triglyceride, HDL, LDL and VLDL in sera of type 2 diabetes mellitus patients and control.

Parameters	Control subject	Type 2 diabetes mellitus patients treated with diabetic medication	P value
No.	30 (15male+15 female)	30 (15male+15 female)	
Age(years)	45-65	45-65	
Total cholesterol mmol/L mean±SD	5.30±0.43	7.68±0.15	P<0.0001
Triglyceride mmol/L mean±SD	1.08±0.24	2.64±0.20	P<0.0001
HDL-C mmol/L mean±SD	1.22±0.18	0.70±0.18	P<0.0001
LDL-C mmol/L mean±SD	3.59±0.49	5.78±0.122	P<0.0001
VLDL-C mmol/L mean±SD	0.49±0.11	1.20±0.09	P<0.0001

In the present study, the results showed that the lipid and the lipoprotein profiles were significant different ($p < 0.0001$) in type 2 diabetes mellitus patients. Total serum cholesterol, serum triglyceride, LDL-C and VLDL-C were significantly increased in the patients group and HDL-C was significantly decreased as compared to the control group. This variation in prevalence may be due to differences in BMI and possibly genetic variation and the results were in agreement with the findings of many similar study [4,18].

However, khan et al [16] reported no significant differences were observed in the levels of serum TC, LDL, HDL, and the LDL/HDL ratio. The most common abnormality found in diabetes is high triglycerides with Low high density lipoprotein (HDL), and although if low density lipoprotein (LDL) might not be higher, its metabolism is abnormal [14]. There is also an inverse relationship between serum levels of HDL-C and triglycerides in diabetic patients; with low serum HDL-C levels possible representing an independent risk factor for cardiovascular disease. Insulin resistance, which is central to the metabolic syndrome and type 2 diabetes mellitus, leads to high levels of very low-density lipoprotein (VLDL),which contain a high concentration of triglycerides, resulting in high serum triglyceride level and low serum HDL-C levels [15]. Although, in another study low triglyceride concentration was found in type 2 diabetic patients in African Americans [4]. Lipid abnormalities in diabetic patients with type 2 are described as increased serum triglycerides, very low density lipoproteins, low density lipoproteins and lowering of high of high density lipoproteins [17]. Early detection and treatment of hyperlipidemia in diabetes mellitus can prevent the progression of lipid abnormalities and minimize the risk for atherogenic cardiovascular disorder and cerebrovascular accident [18]. Out of this work, we conclude that there is several lipid abnormalities occur in our type 2 diabetic patients. Common lipid abnormalities in diabetes are increased triglyceride, LDL-C, serum cholesterol, VLDL-C and low HDL-C.

References

1. Surajeet K.P., Kshitish K.K., Nagendra K. (2011).Lipid ratios in Type 2 Diabetes Mellitus.RJPBCS; 2:397-402.

2. Nasir A., Jahangir K., Tahir S.S.(2008) .Frequency of dyslipidaemia in type 2 Diabetes Mellitus in patients of Hazara Division.J Ayub Med Coll Abbottabad;20 (2): 51-54.

3. Gordon L,Ragoobirsingh D, Morrison E. (2010). Dyslipidaemia in hypertensive obese type 2 Diabetic patients in Jamaica. Arch. Med. Sci.; 6(5): 701-8.

4. Amin-ul-Haq,Jamil ur Rehman,Rashid M.(2006) Pattern Of Lipid Profile in Type

2 Diabetes Milletus patients. JPMI, 20 (4): 366-369.

5. Yadav NK, Thanpari C, Shrewastwa MK. (2012) Comparision of lipid profile in Type 2 obese Diabetics and obese non – diabetic individual. A hospital based study from western Nepal. Kathmandu Univ Med J. 10 (39) : 44-7.

6. H.O. Otamere, C.P.Aloamaka ,P.O. Okokhere (2011). Lipid profile in diabetes mellitus;What impact has age and duration.British Journal of Pharmacology and Toxicology, 2(3):135-137.

7. S.A. Isezuo, MBBS, FMCP. (2003) Comparative analysis of lipid profile among patients with type 2 diabetes mellitus, hypertension and concurrent type 2 diabetes and hypertension: A view of metabolic syndrome. Journal of the National Medical Association.,95(5)328-334.

8. Riffat Sultana. (2010) Impact of duration of Type 2 Diabetes Mellitus on lipid profile. Gomal Journal of Medical Sciences.; 8 (1): 57-59.

9. Samatha P., Venkateswarlu M., Siva Prabodh v (2012). Lipid profile level in Type 2 Diabetes Mellitus from the Tribal population of Adilabad in Andhra Pradesh, India.Journal of Clinical and Diagnostic Research.,6(4):590-592.

10. Allain C.C.,Poon LS.,Clau C.S.G,Richmond W and Fu P.D. (1992)Enzymatic determination of total serum cholesterol. Clin. Chem. 1974,20:470, and Richmond W.,Ann. Analytical Reviews in Clinical Biochemistry: The Quantitative Analysis of Cholesterol. Clin. Biochem.,29: 577.

11. Bucolo G and David H.(1982) Quantitative determination of serum triglycerides by the use of enzymes. Clin. Chem. 1973,19:476, and Fossati R. and Prencipe L.Serum triglycerides determined colorimetrically with an enzyme that produces hydrogen peroxide.Clin. Chem.,28:2077.

12. Burstein M., Scholnick H.R. and Morfin R. (1980)Scand. **Rapid method for the isolation of lipoproteins from human serum by precipitation with polyanions.** J. Clin. Lab. Invest., 40: 560.

13. Friedewald W, Levy RI, Fredrickson DS. (1972). Estimation of the concentration of low density lipoprotein cholesterol in plasma, without use of the preparative ultracentrifuge. Clin. Chem.,18: 499-502.

14. Lukshmy M.H., Sudari W.G., Sudheera S.J. (2007). Lipid abnormalities in type 2 diabetes mellitus patients in SriLanka. Galle Medical Journal.,12 (1):1-4.

15. Nesto RW. (2005). Beyond low-density lipoprotein: addressing the atherogenic lipid triad in type 2 diabetes mellitus and the metabolic syndrome. Am J Cardiovasc Drugs.,5 (6): 379-87.

16. Khan SR, Ayub N, Nawab S,Shamsi TS. (2008) Triglyceride profile in dyslipidaemia of type 2 diabetes mellitus. J Coll Physicians Surg Pak.,18(5):270-3.

17. Mumtaz A. S., Santosh K., Rafi A. G. (2010) Type 2 diabetes mellitus and lipid abnormalities. JLUMHS.,9 (3): 145-147.

18. Khursheed M. U., Bikha R. D., Syed Zulfiquar A. S. (2011). Lipid profile of patients with diabetes mellitus (A multidisciplinary study).World Applied Sciences Journal.,12 (9): 1382-1384.

Cinnamic Acid Activity on Complete Blood Count Tests Against Trichlorfon Residues in Mice

Niba,Kh.Mousa[1]; Jabbar,F. Al-maadhidi[2]; Abrar, N.Mohammd[1]; Eman, H. Qatia[1]; Amal, Ab. Halub[1]; Duha, B. Mohammed[1]; Alaa,D. Kadhum[1]; Azhar,S. Abd-alkharem[1]; Mohamed, Ab. Ayyash[1]; Ishrak, Ab. Ahmed[3]

[1]Environmental-Water Research and Technology Directorate, Ministry of Science and Technology.

[2]Madenat Alelem University College.

[3]The National Center for Drug Control and Research, Ministry of Health.

Abstract:

The current study aimed to evaluate the role of cinnamic acid and its activity on complete blood count (RBC, WBC, HG, HCV, MCH, MCHC and Platelets) and protective effect against the trichlorfon which is a chemical compound that damage hepatic cells and has mutagenic effects. Two concentrations of pure cinnamic acid (30 & 60 mg/kg) were used in the first step to choice the perfect concentration in comparison with negative and positive controls of trichlorfon. The comparison group represent vitamin C. The second step was carried out to understand cinnamic acid mechanism activity towards trichlorfon by used pre-trichlorfon and post – trichlorfon in interaction with perfect concentration of cinnamic acid dose (30 mg / kg).The analysis showed that cinnamic acid removed kinds of anemia ,leukemia,bone marrow failure, hypoxia, cancer chemotherapy, hemolytic anemia and hormone erythropoietin from kidney failure in post-trichlorfon than pre-trichlorfon perfectly. Therefore, cinnamic acid has cure ability and removed trichlorfon damage and it can be given to patient whom used trichlorfon in transplanting body part surgeries to a void refused the part for 6 days after transplanting surgeries.

Keywords: Cinnamic acid, Trichlorfon, Complete Blood Count, Mice.

فعالية حامض السينامك على اختبار مجاميع الدم تجاه بقايا مبيد التررايكلورفان في الفئران البيض

نبال خليل موسى[1]،جبار فرحان المعاضيدي[2] ،ابرار ناطق محمد [1]،ايمان هندي كاطع [1]،امل عبد النبي حالوب[1]،ضحى بهاء محمد[1]،الاء داغر كاظم [1]،ازهر سالم عبد الكريم[1]،محمد عبود عياش[1]،إشراق عبد الأمير احمد [3]

1. دائرة تكنولوجيا وبحوث البيئة والمياه– وزارة العلوم والتكنولوجيا.بغداد–العراق

2. كلية مدينة العلم الجامعة.

3. المركز الوطني للرقابة والبحوث الدوائية،وزارة الصحة.بغداد–العراق.

الخلاصة

هدفت الدراسة تقييم ومعرفة مدى فعالية حامض السينامك على نشاط تعداد الدم الكامل (RBC,WBC,HG,HCV,MCH,MCHC and Platelets)وازالة الاضرار التي تنجم عن بقايامبيد الترايكلورفان والذي يعد مركب كيمائي يسبب تلف خلايا الكبد .انتخب تركيزين من حامض السينامك (30 & 60 ملغم ⁄كغم)في المرحلة الاولى لاختيار التركيز الامثل بالمقا نة مع كل من السيطرة السالبة ، السيطرة الموجبة للسايتوكسان ومجموعة المقارنة لفيتامين سي اما الخطوة الثانية فقد تضمنت دراسة الية عمل حامض السينامك تجاه السايتوكسان بطريقة قبل– السايتوكسان وبعد السايتوكسان بالتداخل مع التركيز الامثل للحامض (30 ملغم ⁄كغم)واظهرت التحاليل ان لحامض السينامك اثر في فقر الدم ، سرطان الدم ،الفشل النخاعي ،نقص الاوكسجين ،العلاج الكيميائي للسرطان ،فقر الدم الانحلالي والفشل الكلوي في مرحلة مابعدالمبيد تماما لهذا فان لحامض السينامك صفة علاجية واعطائه لمدة 6 ايام لازالة ضرر المبيد.

Introduction

In the last decades, the development industry and growing human action in discovery many chemical components that use in difference sides, some of them, pesticides industry, drugs and nutrition industry, which increasing environmental pollution and reflected on the health of human body [1]. These compounds have the ability to cause damage in different tissues and systems of human body, whether the expose directly or indirect albeit little concentrations because most of them can accumulation in cells and tissue, then conversion to derivatives rich in electrons [2]. The frequently cell exposed execute to making changes in DNA that finally caused cancer. The statistics assure that near 85% from mutation components are carcinogenic components [3].

Trichlorfon is an organophosphate insecticide used for control cockroaches, crickets, silverfish, bedbugs, fleas, cattle grubs, flies, ticks, leaf miners and leaf-hoppers [4]. It is applied to vegetable, fruit and field crops; livestock; ornamental and forestry plantings; in agricultural premises and domestic settings; in greenhouses, and for control of parasites of fish in designated aquatic environments [5]. It is also used for treating domestic animals for control of internal parasite [6,7]. It is available in dust, emulsifiable concentrate, granular, fly bait, and soluble powder formulations [8].

Trichlorfon is a selective insecticide, meaning that it kills selected insects, but spares many or most other organisms. Trichlorfon is toxic to target insects through direct applications and by ingestion. In other words, it works both by contact and stomach poison action [5]. Trichlorfon is one of organophosphates family of insecticide. These chemicals act by interfering with an essential nervous system enzyme, cholinesterase.

Plants have the role in inhibition cancered components and protective effects. The primary studies show that the cancer less rate in societies that vegetarianism habitat in compare with societies least used plants in their daily food [9]. The natural vegetarianism components, nutrition and non-nutrition due to their important role in keeper the human health and improvement his life.

The bioaviabilities of plant polyphenol and their ability to inhibit and prevent tumor after entering blood circulation and absorbing by bowel belong to their affection on protein or control factors and the role in repairing cells [10], in addition to motivate immunology system,increasing natural killer cells (NK) and effect on the enzymes which responsible for process and complete the cell cycle by hyper-expression arrangement [11].

Complete blood count (CBC) gives important information about kinds and numbers of cells in the blood, especially red

blood cells (RBCs), white blood cells (WBCs) and platelets. A complete blood count (CBC) helps in diagnosing conditions, such as anemia, infection, and many other disorders. To quantify the toxicity of trichlorfon, the next important step is to assess the various hematological parameters such as hematocrit (HCT), hemoglobin (HB), red blood cells (RBCs), white blood cells (WBCs) and platelets (PLTs) count [12].

In the last years, the consumption of cinnamon increasing widely in many countries, because of the ability to prevent some kinds of cancer due to their components and its effect on mutation and cancer by interacting in metabolism reactions and bio-pathways of these components in body [13]. Searcher interesting increased in finding methods express the components characters of cinnamon such as cinnamic acid and invention of activity to know if they are oxidant or antioxidant, cancered or protective. Many of organizations and science corporations recommended to apply and use the biosystem to detect the toxicity of manufacture components or natural whether are *in vitro* or *in vivo*, some of them the mammalian systems that use the animals of laboratory mice with all different organisms, blood cells and bone marrow in additional the sexual cells like spermatic.

The study aimed to evaluate the role of cinnamic acid in removing the trichlorfon effect that reflect on complete blood count and documenting the ability of cinnamic acid in removed bone marrow failure and leukemia due to trichlorfon, which had no reported before.

Materials and Methods

Material

- Phosphate Buffer Solution (PBS) [13].
- Colchicine solution: 1 mg of colchicines (one tablet) was dissolved in 1 ml sterile distilled water. The solution was used immediately after preparing (2.5 to 3 hours post the timed of preparation) [15].

Doses

Two doses from the pure cinnamic acid which were (30, 60) mg/mice weight and vitamin C (180 mg/kg) [16] as comparative groups and trichlorfon compound in (50 mg/kg) [13] as a positive control and the PBS as a negative control [18].

The experiment

To study the oxidant effect and the antioxidant in laboratory animals:

- 1 ml of cinnamic acid solution was given orally by syringe.
- The Trichlorfon solution was injected Intraperitonially [14].

Fifty –five mice, weighing 20-25 g were divided into three groups: choice perfect cinnamic acid concentration (negative control (PBS),positive control (Trichlorfon)

comparative group vitamin C. and two cinnamic acid concentration (30.60) mg/kg , pre-Trichlorfon and post -Trichlorfon figure 1.

Collection of Blood and Serum

The blood was collected from the heart of mice (*Mus musculus*) and collected for experiment using Heparin (10 units/ml) as the anticoagulant from all animals on the seventh day after experiment [19].

Hematological analysis

The hematological autoanalyzer (Orphee Mythic 22 Hematological Analyzer; Diamond Diagnostic; USA) was used to determine different hematological parameters, such as Red Blood Cells (RBC), White Blood Cells (WBCs), Hemoglobin (HB), Hematocrit (HCT), Mean Corpuscular Volume (MCV), Mean Corpuscular Hemoglobin (MCH), Mean Corpuscular Hemoglobin Concentration (MCHC), Red blood cell Distribution Width (RDW), Platelet Distribution Width (PDW)%, Platelet crit (PCT)% and Platelets (PLTs) [20].

Statistical analysis

The statistical analysis has been used to study the effects of treatments in different trails. The least significant difference (LSD) test was used to signify a comparison between the means [21].

Results and Discussion

Perfect cinnamic acid concentration compared with Trichlorfon.

The effect of the perfect concentration of cinnamic acid extract (30 mg/kg) for 7 days treatment in mice were showed lack of influence, other denoted like changes in color and thickness of mice hair, eyes shape, change in weight, change in liver function enzymes and the antioxidant enzyme, while concentration (60 mg/kg) showed changes in color of mice hair as it became light yellow, lowing in thickness and losing hair in some parts of the body, beside that changes in the eyes shape and lose their bright, in addition to increase in LFTs and antioxidant enzymes [19] when compared with the negative, positive treated and Vit.C because high dose of vitamins and minerals can be toxic [20].

The concentration (30 mg/kg) of cinnamic acid extract showed excellent results in increasing weight table 1, active in moving, increasing the ability to eat more, increasing in mice hair thickness to be more white than the normal and the eyes were bright with no changes in shape. In the other side the LFTs and the antioxidant were a good results (when compared with the negative, positive treated and Vit.C).

Trichlorfon was injected Intraperitonially member because gulping caused losing within 3-12 hours [21].

Trichlorfon was caused inactive in moving of mice, losing the hair in the back, legs, shoulders [14], because trichlorfon is a chemotherapy, which makes cells grow slow or block the cell growth [21]. Cytochrome P-450 was group of enzymes in endoplasmic reticulum known as the most important family of metabolizing enzymes in liver and the terminal electron transport chain of oxidase [22].

The main effect of trichlorfon by metabolizing several pathways. The two major reactions include: hydrolysis of the methoxylmoiety [23] with the methyl group being incorporated byalkylation or methyl transfer into proteins in liver and various organs [24] and hydrolysis of the phosphonate (P-C) bond [25] yielding trichloroethanol which is subsequently conjugated. Others have suggested that conjugated metabolites from rabbits contain molecule that has an altered trichloroethyl moiety and an intact phosphorus atom. This alteration product has not been further defined. In most instances the metabolism in plants and animals appears to follow the same route [26].

The lymphocytes (WBC) represent the first line against the different infections in body [27]. Trichlorfon (medicine that can decrease the immune response) [21] has been showed lower than normal white blood cell counts which called leucopenia, which may be due to autoimmune disease, bone marrow failure (4) tumor, fibrosis and disease of liver [14,19], when compared with negative control (PBS) and vitamin C., while the cinnamic acid (60mg /kg) showed increased than normal of numbers of WBCs, which called leukocytosis when compared among PBS vitamin C and trichlorfon treatment, results from leukemia and tissue damage [28].

Red blood count showed decreased in both trichlorfon and cinnamic acid (60 mg/kg) when compared with PBS and vitamin C. The reduce in RBCs count means increased destruction of red blood cells or layses of red blood cells. Lack of iron, vitamin B12, folic acid in diet as well as certain chronic diseases [19]. Lower the number of red blood cells produced by bone marrow failure, chronic kidney disease, hemolysis, leukemia, long term infections (hepatitis) and other blood cancers due to tumor or fibrosis [29]. trichlorfon caused red blood cells to break down earlier than normal which called immune hemolytic anemia secondary to drugs. In the same time cinnamic acid (30 mg /kg) showed increased with normal when compared with vitamin C and BPS and trichlorfon.

Hematocrit (HCT) is a blood measures the percentage of whole blood volume that is made up of red blood cells. This measured

depend on the number of red blood cells and the size of RBCs. Trichlorfon figure 2 showed lower than normal in hematocrite may due to anemia, bleeding, overhydration, nutrition deficiencies of iron, floate, vitamin B12, B6, malnutrition, destruction of red blood cells [30] in compared with PBS and vitamin C. Cinnamic acid (60 mg/kg) showed high hematocrite may be due to congenital heart diseases, corpulmonale, dehydration, erthyocytosis, low blood oxygen levels (hypixia) [30], while cinnamic acid (30 mg/kg) showed normal increased incompared with PBS and vitamin.

Hemoglobin is a protein in red blood cells that carried oxygen [30]. In figure 2 trichlorfon showed lower than normal may be due to various types of anemia such as chronic disease and leukemia [31], while cinnamic acid (60 mg/kg) showed higher than normal may be due to heart diseases, erthyocytosis and hypoxia but cinnamic acid (30 mg/kg) showed increased with normal when compared with each PBS and vitamin C.

Red blood cells (RBCs) are part of the complete blood count (CBC) test. They are used to help diagnose the cause of anemia a condition in which there are too few red blood cells. RBCs include: Average red blood cell size (MCV), hemoglobin amount red blood cell (MCH) and MCHC referred to the amount of hemoglobin relation to the size of the cell (hemoglobin concentration)per red blood cell. In figure 2 trichlorfon showed decreased in MCV which means microcytic anemia [30] and increased in MCH mean normochronic anemia and decreased in MCHC mean different types of anemia when each one compared with PBS and vitamin C. Microcytic anemia / normochronic anemia results from adeficiency of the hormone erthyropoietin from kidney failure [31]while cinnamic acid (30 mg / kg) showed normal levels in MCH, MCV and MCHC when compared with BPS, vitamin C and trichlorfon.

Platelets count helps the blood clot. They are smaller than red and white blood cells. In figure 2 trichlorfon showed lower than normal levels of platelets numbers when has been compared with PBS and vitamin C which due to cancer chemotherapy [21], hemolytic anemia hyperspleism, leukemia and heart valve [30], while cinnamic acid (30mg/kg) showed increased with normal numbers when has been compared with PBS ,vitamin C and trichlorfon treatment.

Interaction Trichlorfon and Perfect concentration of cinnamic acid (30 mg/kg)

The interaction among trichlorfon and PBS, vitamin C and perfect concentration of

cinnamic acid dose (30 mg/kg) in post-trichlorfon showed in figure 3 the best results in comparison with pre-trichlorfon treatment. Cinnamic acid dose (30mg /kg) showed high reaction in remove trichlorfon effects and increased each of WBC, RBC, MCH, MCHC, MCV, HCT, Hb and platelets count, mechanisms of cinnamic acid to repair removed were:

- Phenolic hydroxyl groups are good hydrogen donors [29]. Hydrogen donating antioxidants can react with react oxygen and reactive nitrogen species and breaks the cycle of generation of new radicals [31].
- Following interaction with the initial reactive species, a radical form of the antioxidant was produced and had a greater chemical stability than the initial radical [32].
- Interaction of phenol hydroxyl groups with π-electrons of benzene ring gave molecules with special properties, the ability to generate free radicals where stabilized by delocalization. Formation of these long-lived free radicals is able to modify radical-mediated oxidation processes [31].
- Antioxidant capacity of phenolic compounds is also attributed to ability chelate metal ions involved in production of free radicals. However, phenolic compounds can acts as pro-oxidants by chelating metals in manner that maintains or increases their catalytic activity or by reducing metals, thus increasing their ability to form free radicals [32].
- Hydrophobic benzenoid rings and hydrogen bonding potential of phenolic hydroxyl groups interact with protein and gave cinnamic acid capacity to inhibit some enzymes involved in radical generation [31, 32].
- Avoid and prevent hydroxyl radical as a product of hydrogen peroxide and gave the first spark for start the chemical interaction such as lipid peroxidation [32].
- Avoid or prevent or repair oxidation of DNA and protein, which depend on the hydroxyl groups of cinnamic acid [33, 34].
- Cinnamic acid was suppressed hepatic fibrosis and protected liver against damage [35].
- Cinnamic acid has anti-hyperlipidemic action [36].
- Release of inflammatory mediators such as cytokines, histamine, prostaglandins and leukotrenes to protect hepatocyte [36].

Conclusion

1. Cinnamic acid has no side effect in dose 30 mg/kg.
2. Leukopenia, bone marrow failure and fibrosis which reflected from decreased WBC due to trichlorfon removed by pure cinnamic acid in post-trichlorfon perfectly.
3. All kinds of anemia which reflected from hemoglobin (Hb) analysis removed when used cinnamic acid dose (30 mg/kg) perfectly in post-trichlorfon treatment.
4. Anemia bleeding, heart disease and low blood oxygen levels (hypoxia), which reflect from hematocrit (HCT) removed due to cinnamic acid dose (30 mg/kg) perfectly in post-trichlorfon treatment.
5. The ratio between MCHC/MCH showed microcytic anemia /normochronic anemia due to deficiency of hormone erythropoietin from kidney failure which reflected from trichlorfon treatment in each perfect concentration pre-trichlorfon and post-trichlorfon and removed perfectly in post-trichlorfon due to cinnamic acid dose (30mg/kg).
6. The ratio of ratio platelets count (RWD/CV, RDW/SD) showed increased in normal could remove (cancer chemotherapy, hemolytic anemia and leukemia) trichlorfon effects perfectly by cinnamic acid dose (30 mg/kg) in post-trichlorfon treatment.

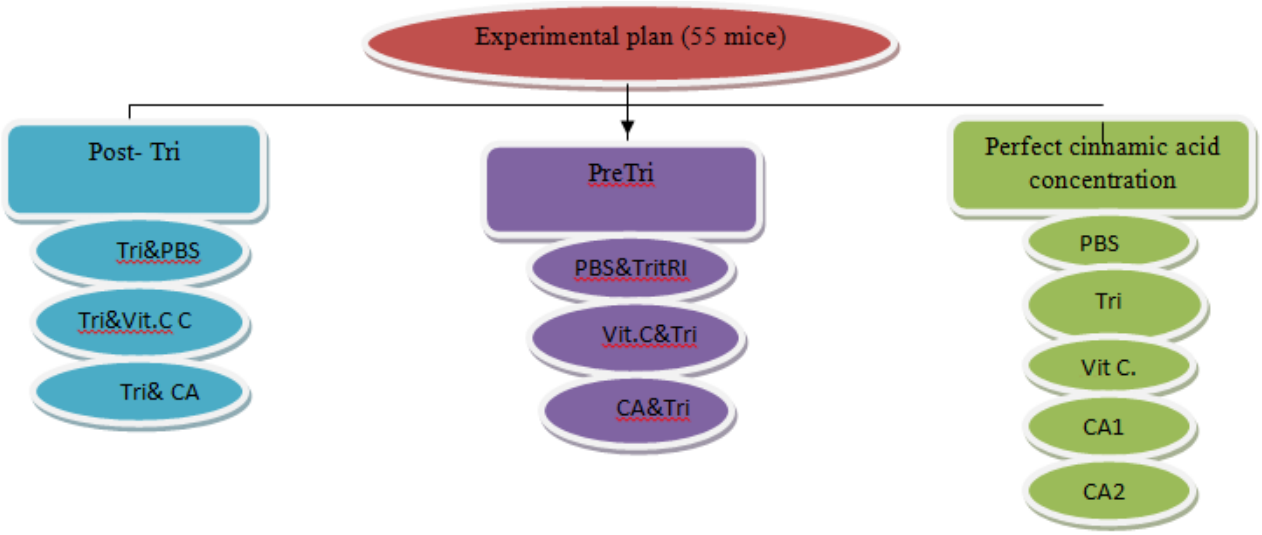

Figure 1. Experimental plan. *Tri =Trichlorfon, CA= cinnamic acid,PBS=phosphate buffer solution, Vit C=vitamin C.

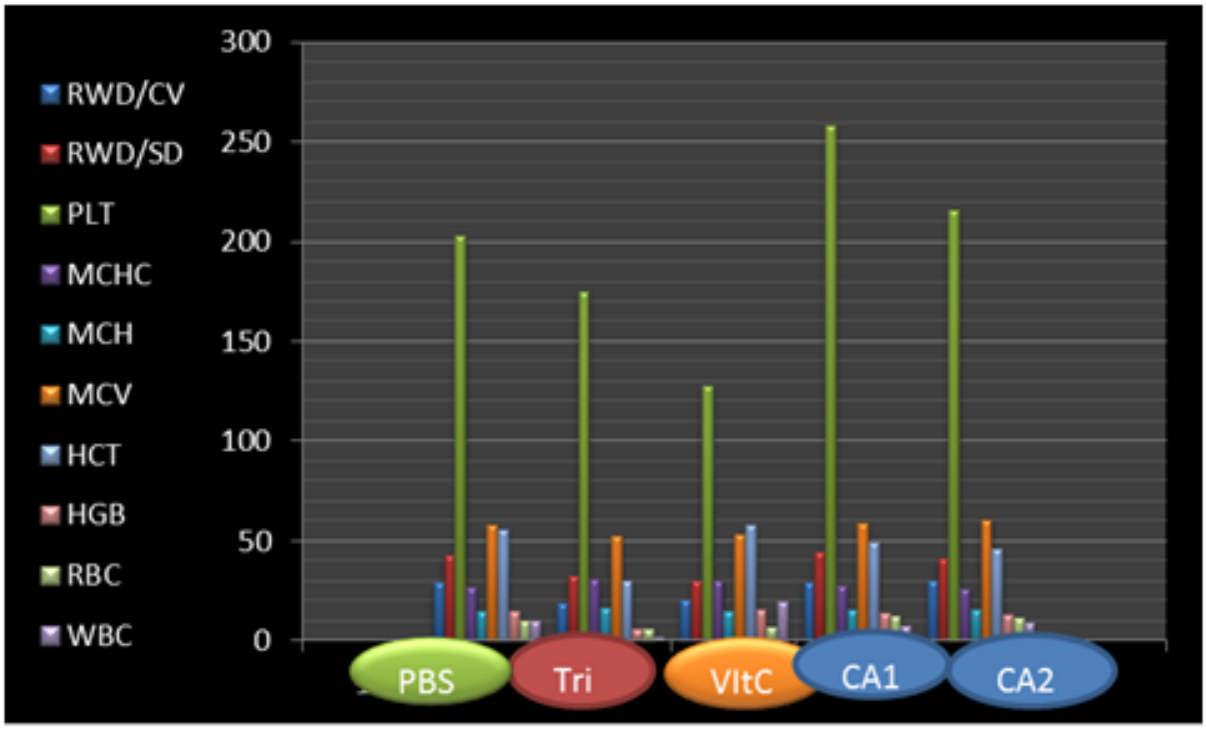

Figure 2. Complete blood count and perfect concentration of cinnamic acid. PBS: phosphate buffer solution, Tri: trichlorfon, CA: CA1: cinnamic acid dose (60 mg /kg), CA2: cinnamic acid dose (30mg / kg).

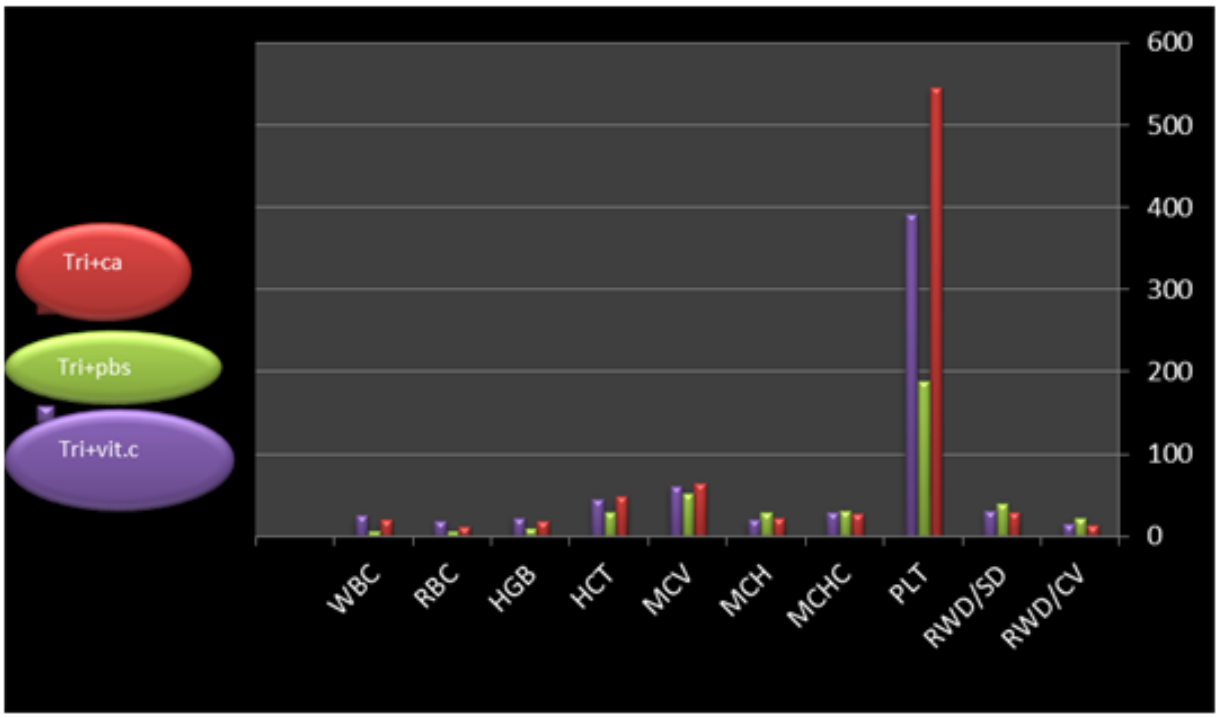

Figure 3. Complete blood cell and post-trichlorfon treatment. PBS: phosphate buffer solution, Tri: trichlorfon, CA: CA1: cinnamic acid dose (60 mg/kg), CA2: cinnamic acid dose (30 mg/kg).

References

1. FAO. (2004). Biotechnology applications in food processing .Electronic forum on Biotechnology in Food and Agriculture. Conference11. United Nation.
2. Kohlmeier, L.; Simonsen, N. and Mottus, K. (1995). Environmental Health Issues. Environ. Health Perspect, 103 : 1-11.
3. Kier, L. D.; Brusick, D. J.; Auletta, A. E.; Halle, E. S.; Brown, M. M. and Simmon, V. F. (1986). The *Salmonella typhimurium*/ mammalian microsomal assay : A report of the U.S. Environmental Protection Agency Gen-Tox Program. Mut. Res. 168 : 240-269.
4. Klein,T. E.; Chang, J.T.; Cho, M. K.; Easton, K. L.; Fergerson, R.; Hewett, M.; Lin, Z.; Liu, Y.; Liu, S.; Oliver, D. E.; Rubin, D. L.; Shafa, F.; Stuart, J. M. andAltman, R. B. (2001) "Integrating Genotype and Phenotype Information: An Overview of the Pharm GKB Project" , The Pharmacogenomics Journal 1, 167-170.
5. Doull, J., Vesselinovitch, D., Root; M., Cowan, J., Meskauskas, J. and Fitch, F.(1962) Chronic oral toxicity of Dylox to male and female Rats .Unpublished report by Department of Pharmacology, University of Chicago.
6. 6.Morgan, D. P.(1982). Recognition and management of pesticide poisonings.Third edition. U. S. Environmental Protection Agency. Washington, DC: U. S. Government Printing Office.
7. Cheminova Agro A/S.(1991).Material Safety Data Sheet: Dimethoate. Cheminova, Lemvig, Denmark.
8. Witt, J. M. (1985). Chemistry, biochemistry, and toxicology of pesticides. Proceedings of an Extension Service Short Course at Oregon State University. Pest control education program. Eugene, OR.
9. Kotake-Nara, E. ; Kushiro, M. ; Zhang, H. ; Sugawara, T. ; Miyashita, K. and Nagao, A. (2001). Carotenoids affect proliferation of human prostate cancer cells. J. Nutr. 131: 3303-3306.
10. Tsuda, H. ; Ohshima, Y. ; Nomoto, H. ; Fujita, K. ; Matsuda, E. ; Iigo, M. ; Takasuka, N. and Moore, M. A. (2004). Cancer prevention by natural compounds.Drug Metab.Pharmacokinet, 19: 245-263.
11. Roomi, M.W.; Ivanov, V.; Kalinovsky, T. ; Niedzwiecki, A. and Rath, M. (2005). In vitro and in vivo antitumorigenic activity of a mixture of lysine, proline, ascorbic acid, and green tea extract on human breast cancer lines MDA-MB-231 and MCF-7. Med. Oncol. 22 : 129-138.
12. Powers A, Silberstein LE. Autoimmune hemolytic anemias. In: Hoffman R, Benz EJ Jr., Shattil SJ.(2008).*Hoffman Hematology: Basic Principles and Practice*. 5th ed. Philadelphia, Pa: Churchill Livingstone Elsevier; 2008: chap 47.

13. Al-Zubaidi,L.Ah. (2005). Inhibition activity of bark cinnamon extracts against some microorganisms to be used in ground meat preservation, MS.C, Genetic Engineering and Biotechnology Institute for Postgraduate Studies, Baghdad, Iraq.

14. WHO. (1993). Research Guidelines for Evaluating the Safety and Efficacy of Herbal Medicines. Regional Office for the Western Pacific, Manila.

15. Jwad, B. M. (2010). Toxicopathological and Mutagenic effects of fluoride given in drinking water to male mice University of Baghdad College of Veterinary Medicine.

16. Al-Rubaie,El.,Ab.(2005).The Antimutagenic Effects of Eruca sativa and Daucus carota in Bacteria and Mammalian system. M.Sc. Genetic Engineering and Biotechnology Institute for Post Graduate Studies.

17. Mc-Donald,G.B.;Slattery, J.T. and Bouvier M.E. (2003). Cyclophosphamide metabolism, liver toxicity, and mortality following hematopoietic stem cell transplantation, *Blood*, vol. 101, (5): 2043-2048.

18. Mousa,N.,Kh.; Labeeb,Ah.,Al-Zubaidi and Ishrak, Ab,Ahmed. (2011). Evaluation Toxic oxidant activity for pure cinnamic acid in albino mice,Journal of Madenat Alelem College ,3(2):34-4.

19. Marks PW, Glader B. Approach to Anemia in the Adult and Child. In: Hoffman R, Benz EJ, Shattil SS,(2008).*Hematology: Basic Principles and Practice*. 5th ed. Philadelphia, Pa: Elsevier Churchill Livingstone:chap 34.

20. Marks PW, and Glader B.(2008) Approach to Anemia in the Adult and Child. In: Hoffman R, Benz EJ, Shattil SS,.*Hematology: Basic Principles and Practice*. 5th ed. Philadelphia, Elsevier Churchill Livingstone:chap 34.

21. SAS. (2001). SAS/STAT user's guide for personel computers release. 6.12. SAS. Inst. Inc. Cary. NC. USA.

22. Mousa,N.,Kh.; Labeeb, Ah., Al-Zubaidi, Iman, I., Qatia and Ishrak, Ab,Ahmed. (2011). Biochemical, Hepatoprotective Effects of pure cinnamic acid Against Cyclophosphamide in white mice, Journal of MadenatAlelem College ,3(2):45-65.

23. Dedek,W. and Lohs, K. (1970a) Zuralkylierenden Wirkung vonTrichlorphoninWarmblütern I. Untersuchungen *in vitro* in Humanserummit^{14}C-Trichlorphon. Z. Naturforsch., 25b: 94-96.

24. Dedek,W. and Lohs, K. (1970b). Zuralkylierenden Wirkungvon Trichlorphon in Warmblütern II. Verteilung von ^{14}C in Organen undLeberproteinenbeiRattennachApplikation von ^{14}C-Trichlorphon. Z. Naturforsch., 25b: 1110-1113.

25. Bull, D. L. and Ridgway, R. L. (1969) Metabolism of trichlorfon in animal and

plants. J. Agr. Food Chem., 17: 837–841.

26. Miyamoto, J. (1961) Studies on the mode of action of Dipterex Part II. New glucorunides obtained from the urine of rabbit followingadministration of Dipterex. Agr. Biol. Chem., 25: 566–572.

27. Moss Ralph, W. (2000). Antioxidants Against Cancer .Brookly .NY;Equinox press ,Inc.

28. Takimoto, CH.; Calvo, E. ; Pazdur, R.; Wagman , LD. ; Camphausen, KA. and Hoskins, WJ.(2008)."Principles of Oncologic Pharmacotherapy" in (Eds) Cancer Management: A Multidisciplinary Approach. 11 ed.

29. Brock,N.(1989)."Oxazaphosphorinecyto statics:past–present–future.Seventh Cain Memorial Award lecture". Cancer Res. Vol. 49, No. 1. Page: 1–7.

30. Bull, D. L. and Ridgway, R. L. (1969) Metabolism of trichlorfon inAnimal and plants. J. Agr. Food Chem., 17: 837-841.

31. Abdelhalim, M. A. and Moussa, Sh. (2012). The Dimensional Hematological Alterations Induced in Blood of Rats *invivo* by Intraperitoneal Administration of Gold Nanoparticles, Nanomed Nanotecho, (l3): 4.

32. Schmaier AH. Laboratory evaluation of hemostatic and thrombotic disorders. In: Hoffman R, Benz EJ Jr, Shattil SJ.(2008) *Hoffman Hematology: Basic Principles and Practice*. 5th ed. Philadelphia, Pa: Churchill Livingstone Elsevier; chap 122.

33. Lertlakana, B. ;Somdet, S. ; Duangta, K. ; TTawat, T. ; Hathairat, Th. and Tanin, B. (2011). Hepatoprotective effects olychee (Litchi ChinensisSonn) : A combination of Antioxidant and anti-apoptotic activities .Journal Ethnopharmacol, Thailand. 8 :49-54.

34. Valko, M. ;Izakovic, M. ; Mazur, M. ; Rhodes, C. and Telser, J. (2004). Role of oxygen radicals in DNA damage and cancer incidence.Mol. Cell Biochem.266 : 37–56.

35. Nakabeppu, Y.; Sakumi, K. ; Sakamoto, K. ; Tsuchimoto, D. ; Tsuzuki, T. and Nakatsu, Y. (2006). Mutagenesis and carcinogenesis caused by the oxidation of nucleic acids. Biol. Chem. 387: 373–379.

36. Yamamoto,J.; Yamada, K.; Naemura, A.; Yamashita,T. and Arai, R. (2005). Testing various herbs for antithrobotic effect.Nutrition,21:580-587.

Morphological and Histological Study of The Tongue in Rock Pigeon *Columba livia gaddi* Gemlin, 1789

Iman S. Al-Jumaily; Entidhar .M.Mnati; Baydaa .H. Mutlak and Hussain A.M. Dauod

Department of Biology, College of Education (Ib-Al-Haitham), Al Adhamia , Baghdad ,Iraq

Abstract

The present study aimed to recognize the morphological description and histological structure of the tongue in rock pigeon *Columba livia gaddi* using light microscope. Ten adult rock pigeon of both sexes were used in this study. Results of the present study showed that the tongue is characterized by an elongated triangular format. Three parts are distinguished in the dorsal surface: the apex the body and the root. On the dorsal surface of the apex and body a median groove is found. Large conical papillae are located symmetrically in the form of the letter V at the median line between the body and the root, also there is one large papillae at each half was observed behind the main row of papillae. The mucosa of the tongue is covered by a thick stratified squamous epithelium which is cornified only on the ventral surface. The desquamate cells were observed on the dorsal surface in the lingual apex and body. The tongue was supported by a hyaline cartilage , which extended from the lingual root to the apex. The lingual glands (branched tubulo-alveolar gland) were embedded in the connective tissue of lamina propria of the dorsal surface and extended laterally from the apex to the laryngeal clefts, while the ventral surface devoid of any glandular structure.

Key words: Morphology, Histological structure, Tongue, Rock pigeon

دراسة مظهرية ونسجية للسان في الحمام الطوراني
Columba livia gaddi Gemlin 1789

ايمان سامي الجميلي و انتظار محمد مناتي وبيداء حسين مطلك وحسين عبد المنعم داود

قسم علوم الحياة ،كلية التربية (ابن الهيثم)، الاعظمية ،بغداد، العراق

الخلاصة

هدفت الدراسة الحالية التعرف على الوصف المظهري والتركيب النسجي للسان في الحمام الطوراني *Colomda livia gaddi* بأستخدام المجهر الضوئي.

استخدمت في الدراسة الحالية عشرة طيور بالغة من كلا الجنسين . اظهرت نتائج الدراسة الحالية ان اللسان في الحمام الطوراني البالغ يتميز بشكله المثلث المتطاول والمقسم الى ثلاثة اجزاء متميزة هي القمة والجسم والجذر ، ويلاحظ وجود اخدود وسطي على السطح الظهري لمقدمة وجسم اللسان تترتب الحليمات المخروطية الكبيرة بشكل حرف V على طول الخط الوسطي الظهري الواقع بين جسم وجذر اللسان، كذلك يلاحظ وجود الحليمات الجانبية التي تكون كبيرة وتقع ا خلف الصف الرئيسي من الحليمات المخروطية. يغطى السطح الظهري والبطني لقمة اللسان بنسيج ظهاري حرشفي مطبق، ويكون متقرناً في السطح البطني منه كما يمكن ملاحظة خلايا غير حرشفية في السطح الظهري لقمة وجسم اللسان ويدعم اللسان بتركيب مكون من الغضروف الزجاجي والذي يمتد من الجذر الى قمة اللسان. تكون الغدد اللعابية اللسانية (غدد نبيبية – سنخية متفرعة) وتظهر في النسيج الضام للصفيحة الاصيلة للسطح الظهري والتي تمتد جانبياً من القمة الى الشق الحنجري البلعومي ،بينما لم يلاحظ وجود اي تركيب غدي على السطح البطني.

الكلمات المفتاحية :الشكل المظهري،التركيب النسجي، اللسان ، الحمام الطوراني

Introduction

The cross anatomy and histology of the adult tongue of domestic animals and its papillae is described in numerous text books of histology [1,2]. All birds are adapted to their different environments with respect to food sources, reflecting their different life styles; birds have different feeding habits, leading differences in the structures of their tongues. Anatomy of the tongue, revealed that are three distinguished parts: apex, body and root [3,4]. The tongue is a highly muscular organ covered with squamous epithelium and situated at oropharyngeal region [5].

Studies on the morphology of the tongue, especially the structure of the dorsal surface have been conducted on a small number of avian species such as golden eagle [6], wood pecker [7], cormorants [8], ostrich [9], owl [10], domestic goose [11] and little tern [12].

In the literature, almost the morphological data characterizing the surface structure of the tongue in pigeon are very scanty. Thus, this study described the morphological and histological features of the tongue of rock pigeon.

Material and Methods

Ten adult pigeons (5 males and 5 females) donated from a local abattoir were used to study the morphology and the histology of the tongue.

Samples were fixed in the 10% neutral formaldehyde for 48 hour or Bouin's fluid for 24 hours at room temperature and later submitted to the dehydration process in a series of ethanol at increasing concentration (70-100%) and embedded in paraffin wax. Histological slides of thickness of about 5 µm were stained routinely with haematoxylin-eosin in order to determination the type of the lingual epithelium [13].

Selected sections were examined with light microscope (Kruss-Germany) and photographed with digital camera (Sony 14.1 MP).

Results

Tongue of the rock pigeon is characterized by an elongated triangular format for both sex. Neither the morphology nor the dimensions of the tongue show sex-specific differences. Three parts were distinguished in the dorsal surface of the tongue: apex, body and root. On the dorsal surface of the apex and the body of the tongue a median groove is found, this groove divides the apex and body into two symmetrical halves .Large conical papillae are located symmetrically in the form of the letter V in the median line between the body and the root of the tongue .An additional row, composed only one large papillae in each half was observed behind the main row of papillae (Figure 1).

The mucosa of the dorsal surface of the lingual apex is covered with a thick stratified squamous epithelium which is cornified only on the ventral surface of the tongue, whereas lingual body and root are covered with non keratinized stratified squamous epithelium, on the dorsal surface of the epithelium of the lingual apex the desquamate cells are present in the lingual mucosa (Figure 2). Penetration of many capillaries was observed on the superficial part of the epithelium .The connective tissue of the lamina propria penetrated deeply into the epithelium, forming connective tissue papillae (Figure 3), the lamina propria and submucosa are dense irregular connective tissue, which contain collagen fibers, adipose cells and many blood vessels.

In the multilayered epithelium of the lingual mucosa, a basal, intermediate and superficial layer could be distinguished .In all parts of the tongue, the cells of the basal layer were found to be round or elliptical, their nuclei occupying two third parts of the cell size and showing 1 or 2 nucleoli (Figure 4), the cells were flatted towards the surface of the epithelium and created the intermediated layer, the cells of this layer type appeared polygonal with round nuclei (Figure 5). The structure of the superficial epithelial layer was very diverse containing highly condensed nuclei (Figure 6).

The lingual salivary glands of the rock pigeon composed of two laterally situated single strands, are located in the lamina propria of the dorsal lingual surface and extended from the apex to both sides of the laryngeal cleft (Figure 7). The glands are branched tubulo-acinar type and consist of mucous secretory units composed of tall columnar cells with extensive vesicular cytoplasm. The ventral surface of the tongue is devoid of any glandular structure (Figure 8).

There are muscles in the lamina propria of the dorsal surface of the tongue. The muscles are arranged thin and striated in the form of circular in the apex, but oriented in the form of circular and longitudinal in different direction in the body and root of the tongue (Figure 9).

Gustatory papillae are not found in the epithelium covering the tongue in the rock pigeon .The tongue is supported by cartilage hyoid apparatus revealed on entoglossal bone as skeletal element of the tongue which extending from the lingual root to lingual apex (Figure 2).

Discussion

Previous studies on the avian tongue has shown that the shape, mucosal epithelium, supportive elements and papillary localization are closely correlated with the type of food, method of feeding as well as the habitat [14]. In many avian species, the tongue has a triangular shape and fully fits the shape of the lower part of the beak [15]. In the case in rock pigeon which is the subject of the present study. In some other species including emu, the tongue body occupied the middle third of the floor of the oropharynx and was appeared as a triangular structure with the apex pointing rostral [16], while the tongue in male ostrich is semicircular, short and quite thick, and it contains the unpaired broad intra glossal bone which articulates with the basihyoid bone, a blunt round apex, base and body [9]. Elongated flat tongue can be found in bean goose [17].

Results obtained from the present study showed that the tongue of rock pigeon is a well developed triangular organ with three distinct anatomical parts: apex, body and root. These morphological features resemble those of common quail, domestic pigeon and chuker partridge [13, 14, 15].

Data obtained from the present study also showed that distinct median groove

divides the apex and body of the tongue into two symmetrical halves, this result resemble of those found on the tongue of white tailed eagle and domestic goose [18,11], whereas it is absent on the tongue of chickens [19].

Results of the present study showed that a main row of large conical papillae are located symmetrically in the form of the letter V in the marginal region between the body and the root of the tongue. This results is similar to those the documented by Parchami *et al.*,[15] and Parchami and Dehkordi, [13] in common quail and domestic pigeon. In the chucker partridge and common quail, the caudal region of the tongue bears conical papillae with the pointed a pieces directed posteriorly arranged in the letter V, behind this row there is additional row composed of laterally located large papillae[14, 15], while in the Middendroff's bean goose there are giant conical papillae located between the anterior and posterior region ,on both of the lateral sides of the anterior region .There are lingual hairs are compactly distributed and small number of large cylindrical papillae are arranged between these lingual hairs [17], that doesn't note in the present study. On the contrary, Pasand *et al.,* [9] reported the large conical papillae in ostrich were not observed between the lingual body and root.

Distribution of these lingual papillae have been considered to be related to species feeding habits of birds, the conical papillae found in the lingual body was sits aiding in the transfer of swallowed food towards the esophagus and at the same time preventing its regurgitation [18].

Based on the findings of this study, we showed that the mucosa of the dorsal surface of the lingual apex is covered with a thick stratified squamous epithelium which is keratinized only on the ventral surface, whereas the lingual body and root are covered with non- keratinized stratified squamous epithelium, this finding is similar to that described by Jacckowiak and Godyniki, [18] in the white tailed eagle and by Parchami and Dehkcrdi, [13] in the domestic pigeon. Contrary to reports in the chucker partridge that the dorsal lingual surface was covered by keratinized stratified squamous epithelium with layer of keratin being rather thick [14], whereas in the ostrich , the dorsal and ventral surfaces of the tongue are covered by non keratinized stratified squamous epithelium [9].

The differences in the degree of keratinization of the lingual epithelium between different species seem to be related to the differences in habitat, this differences clearly appear in chicken live in habitat much drier than that of the water Middendroff's bean goose and the little tern. Even clearer example are provided by reptiles, for example the lingual epithelium of snakes which are adapted to dry terrestrial life is strongly keratinized [20], whereas that of fresh water turtles which are adapted to aquatic life ,is non- keratinized [21]. In birds, the degree of keratinization of lingual

epithelium seems to be a certain extent to reflect differences in life style [17].

Results of the present study showed that the lamina propria is dense irregular connective tissue, which contain adipose cells and many blood vessels. This connective tissue is supported by the strong layer of striated muscle fibers which are oriented in longitudinal and circular direction in the body and base of the tongue, also it has been observed that the tongue contains hyaline cartilage, which extending from the lingual apex to the lingual root and enclosed by lingual muscle fibers. These observations are similar to that of Pasand *et al.*, [9] in male ostrich and by Parchami and Dehkrochi, [13] in domestic pigeon.

In the rock pigeon which is the subject of the present study we showed that the lingual glands are simply branched tublo-acinar glands with mucous secretion, there is no any serous cells, the morphology of the lingual salivary glands and the kind of secretion in the white tailed eagle [18]. In the domestic pigeon [13] were similar to the rock pigeon. In the ostrich, the lingual glands in which the lamina propria of the lingual mucosa is filled with mucous glands whose openings were found on both the dorsal and ventral surfaces of the tongue [22], but in the Japanese quail ,salivary lingual glands are in pairs and are located in the right and left side of the entoglossal cartilage [15]. In the common vampire, the salivary glands are elongated tubular with both mucous and sero mucous secretions [23]. Contrary to report in the cormorant phalacrocorax, there is no any salivary gland [24].

In conclusion, results of the present study showed that the unique features of the tongue in the rock pigeon were the presence of conical papillae with V-shaped arrangement an also presence of one large papillae in each half behind the main papillae.

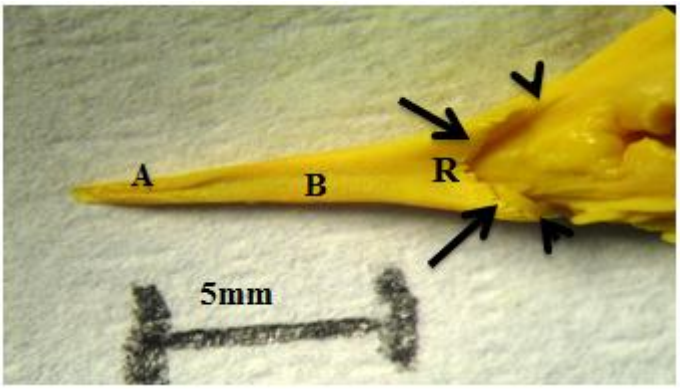

Figure 1. Morphological feature of the tongue showed: three parts of the dorsal surface: Apex(A) Body (B) Root(R) ,Conical papillae (arrows), large lateral papillae (head of arrows).

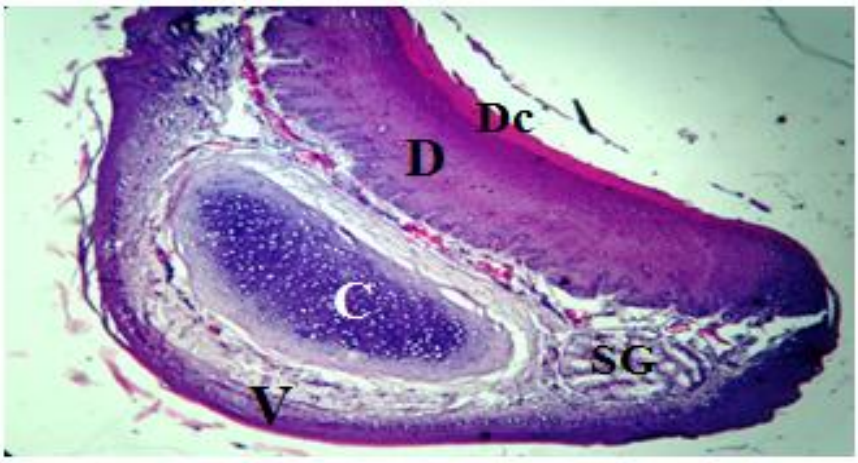

Figure 2. Cross section of the lingual apex in the rock pigeon showed: dorsal (D) and ventral surface (V), lingual salivary glands (SG), desquamate cells (Dc), cartilage (C), H&E (40 X).

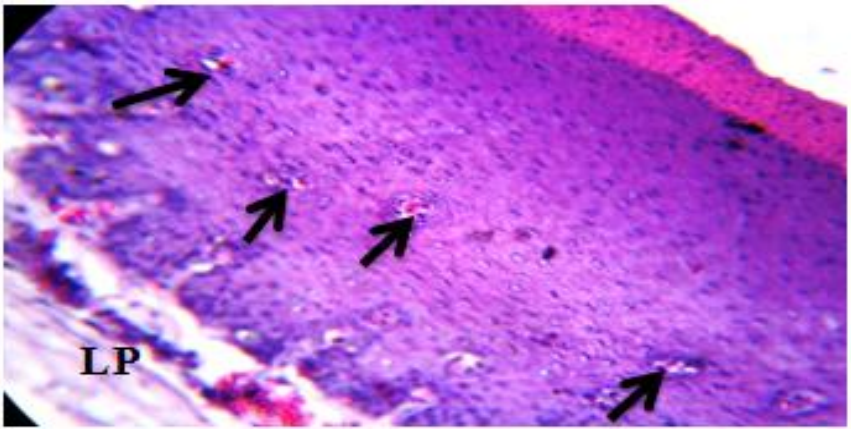

Figure 3. The penetration of the blood capillaries in the epithelium of the dorsal surface of the tongue (arrows) and lamina propria (LP). H&E (100X).

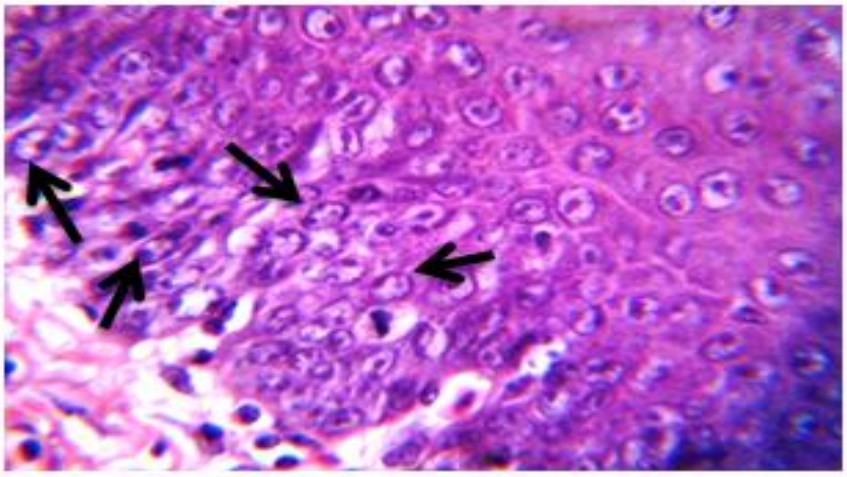

Figure 4. Higher magnification of the basal layer of the epithelium of the Lingual body showed: a rounded cells nucleus with nucleoli (arrows). H&E (400X).

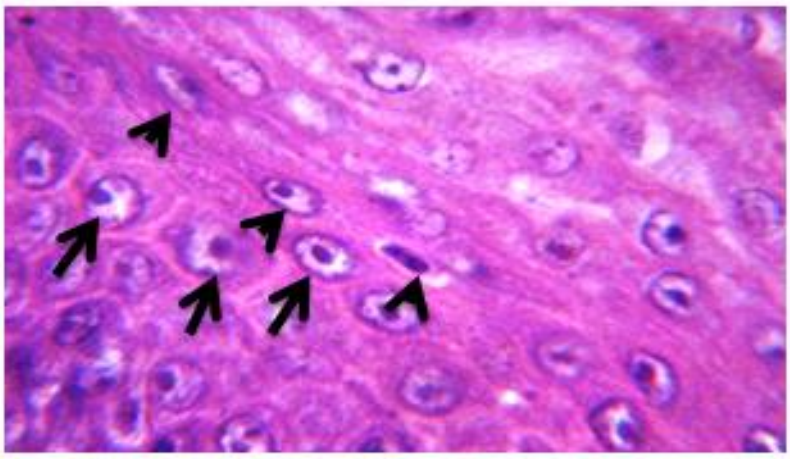

Figure 5. Higher magnification of the intermediate layer of the lingual body showed: the polygonal cell with rounded and flatted nuclei (arrows and head of arrows) H&E (1000 X).

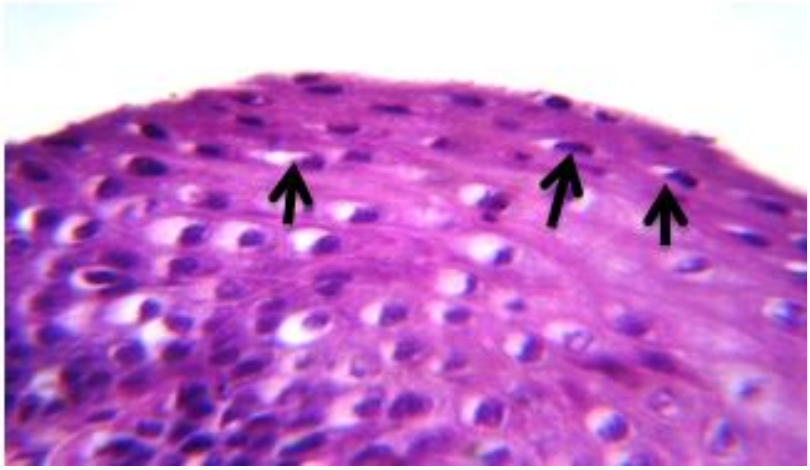

Figure 6. Higher magnification of the superficial layer of the lingual body showed: the cells have light cytoplasm and flat nucleolus (arrows), H&E (1000X).

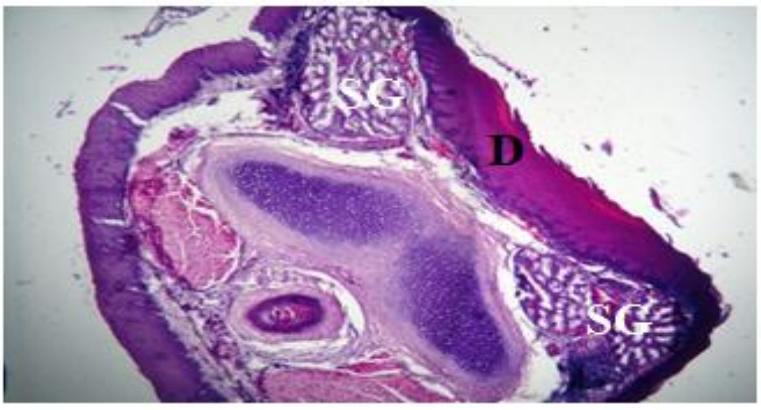

Figure 7. Cross section of the lingual root showed: the salivary glands (SG) on the both side of the dorsal surface (D).H&E (40 X).

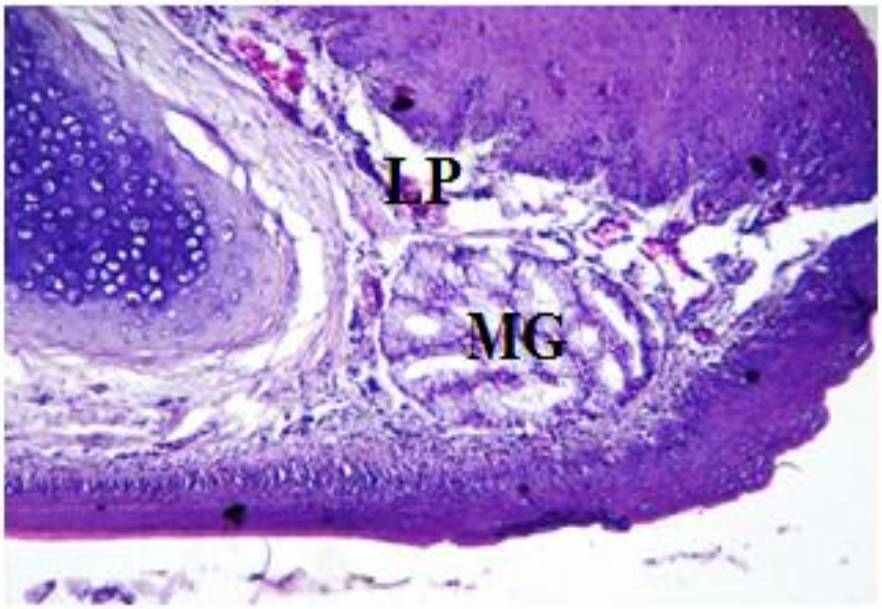

Figure 8. Cross section of the lingual apex showed: the secretory units of mucous glands (MG) in the lamina propria (LP) in the dorsal surface. H&E (100X).

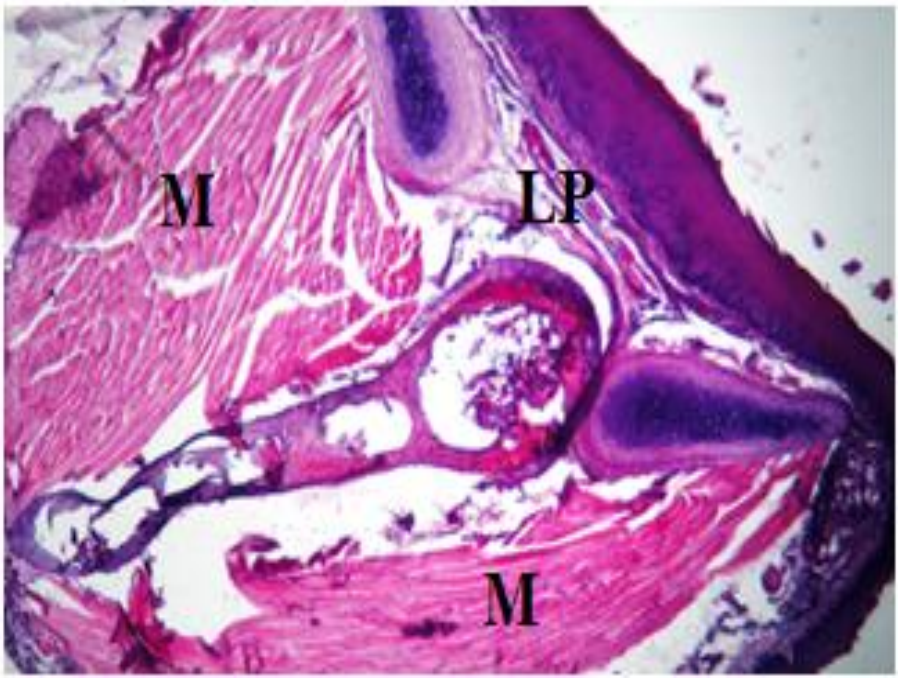

Figure 9. Cross section of the lingual root showed: bundles of muscles (M) in the lamina propria (LP) of dorsal surface, H&E (40 X).

References

1. Gali, M.A. and Dauod, H.A.M. (2002). Comparative anatomy of chordates. Baghdad University Press: 799pp (in Arabic).
2. Kent, G. C. and Carr, R.K. (2001). Comparative anatomy of the vertebrates, 9th ed.McGraw-Hill Co.,New York:XV11+524 PP.
3. Komarek, K.V., Malinovesky, L. and Lemez,L. (1986). Anatomia avium domesticarum et embryology galli. Priroda vedavatel'stvo Knihacasposov ,Bratyslava. (Abstract).
4. Iwasaki ,S.I. (2002). Evolution of the structure and function of the vertebrate tongue.J.Anat.201:1-13.
5. Stevens,A. and Lowe, J.S. (2005). Human histology (3rd ed.). Elsevier limited, USA: 190-194.
6. Parchami, A., Dehkordio, F.R.A. and Bahadoran,S. (2010). Scanning electron microscopy of the tongue in the golden eagle *Aquila chrysaetos* (Aves: Falconiformes Accipitridae). World. J. Zool.,5(4): 257-263.
7. Emura,S., Okumura, T. and Chen, H. (2009). Scanning electron microscopic study of the tongue in the Japanese pygmis woodpecker (*Dendrocopos kizuki*). okajimas Folia Anat. Jpn., 86(1): 31-35.
8. Jackowiak, H., Andrzejewski, W. and Codynicki, S. (2006). Light and scanning electron microscopic study of the tongue in the cormorant *phalacrocorax carbo* (phalacroracidae,aves). Zool. Sci., 23: 161-167.
9. Pasand, A. P., Tadjalli, M. and Mansouri, H. (2010). Microscopic study on the tongue of male ostrich. Eur. J. Bio.Sci., 2(2): 24-31.
10. Emura,S. and Chen,H. (2008). Scanning electron microscopic study of the tongue in the owl (*Strix uralensis*). Anat. Histol. Emberyol., 37: 475-478.
11. Jackowiak,H., Skieresz-szwczyk, K., Iwasaki, S.I. and Meyer,W. (2O11). Functional morphology of the tongue in the domestic goose (*Anser anser domestica*). Anat. Rec., 294: 1574-1584.
12. Iwasaki, S.I. (1992). Fine structure of the dorsal lingual epithelium of the little tern, *sterna albifrons* (Aves, Lari). J. Morphol., 212: 13-26.
13. Parchami, A. and Dehkordio, F.R.A. (2011). Lingual structure of the domestic pigeon (*Columba livia domestica*). A light and scanning electron microscopic studies. Mid. Eas. J. Sci, Res., 7(1): 81-86.
14. Erdogan, S., Sagsoz, H. and Akbalik, M.E. (2012). Anatomical and histological structure of the tongue and histochemical characteristics of the lingual salivary glands in the chukar partridge (*Alectoris chukar*, Gray 1830). Brit. Poul. Sci., 53(3): 307-315.
15. Parchami, A., Fatahian, R. A. and Bahadoran,S. (2010). Fine structure of the dorsal lingual epithelium of the

common quail (*Coturinx coturnix*) Worl. Appl. Sci. J. 10(10): 1185-1189.

16. Crole, M. R. and Soley, J.T. (2009). Morphology of the tongue of the emu (*Dromaius novaehollandae*). Histological features .Onderst. J.Veter. Res. 76: 347-361.

17. Iwasaki, S.I., Asami, T. and Chiba, A. (1997). Ultra structural study of the keratinization of the dorsal epithelium of the tongue of Middendorff's bean goose ,*Anser fabalis middendorffi* (Anseres,Antidae) .Anat.Rec. , 247:149-163.

18. Jackowiak,H. and Godyicki, S. (2005). Light and scanning electron microscopic study study of the tongue in the white tailed eagle(*Haeliaeetus albicilla*, Accitripidae, Aves). Anna. Anat.,1 87: 197-222.

19. Grant, V. and Temeles, E.J. (1992). Faraging ability of Rufus humming birds on humming bird flowers and how kmoth flowers. Proc. Noit. Acad. Sci. USA, 89: 9400-9404.

20. Iwasaki, S.I. and Kumakura, M. (1994). An ultrastructural study of the dorsal lingual epithelium of the rat snake *Elaphe quadrivirgata*.Acta. Anat.,176:455-462.

21. Mutlak, B.H., Dauod, H.A.M. and Al-Dori,T.Y. (2000). Morphological and Histological study of fresh water turtle *Cleymms caspica caspica.* J. Dyalla, 8(1): 115-126.

22. Jackowiak, H. and Ludwing, M. (2008). Light and scanning microscopic study of the structure of the ostrich (*Strutio camelus)* tongue. Zool. Sci., 25(2): 188-194.

23. Bernard, T., Kuniaki, T., Yuji, S., and Carleton, J. (1997). Ultrastructure of the salivary glands in the mid tongue of the common vampire bat,*Domodus rotundus*. Anat. Rec.,246: 196-205.

24. Jackowiak, H. and Andrz, W. (2006). Light and scanning electron microscopic study of the tongue in the cormorant *phacrocorax carbo* (Phalacoracidae, Aves). Zool. Sci., 23(2): 161-167.